

Control of Lateral Vibration of an Axially Moving Cantilever Beam Using Piezoelectric Actuators

Quincy Gnananathan

Supervised by Dr.Kefu Liu

Date : 26th October 2005

A Thesis Submitted In Partial Fulfillment Of The Requirements
Of The MScEngi Degree In Control Engineering

Faculty of Engineering

Lakehead University

Thunder Bay, Ontario



Library and
Archives Canada

Bibliothèque et
Archives Canada

Published Heritage
Branch

Direction du
Patrimoine de l'édition

395 Wellington Street
Ottawa ON K1A 0N4
Canada

395, rue Wellington
Ottawa ON K1A 0N4
Canada

Your file *Votre référence*
ISBN: 978-0-494-15617-9
Our file *Notre référence*
ISBN: 978-0-494-15617-9

NOTICE:

The author has granted a non-exclusive license allowing Library and Archives Canada to reproduce, publish, archive, preserve, conserve, communicate to the public by telecommunication or on the Internet, loan, distribute and sell theses worldwide, for commercial or non-commercial purposes, in microform, paper, electronic and/or any other formats.

The author retains copyright ownership and moral rights in this thesis. Neither the thesis nor substantial extracts from it may be printed or otherwise reproduced without the author's permission.

AVIS:

L'auteur a accordé une licence non exclusive permettant à la Bibliothèque et Archives Canada de reproduire, publier, archiver, sauvegarder, conserver, transmettre au public par télécommunication ou par l'Internet, prêter, distribuer et vendre des thèses partout dans le monde, à des fins commerciales ou autres, sur support microforme, papier, électronique et/ou autres formats.

L'auteur conserve la propriété du droit d'auteur et des droits moraux qui protègent cette thèse. Ni la thèse ni des extraits substantiels de celle-ci ne doivent être imprimés ou autrement reproduits sans son autorisation.

In compliance with the Canadian Privacy Act some supporting forms may have been removed from this thesis.

Conformément à la loi canadienne sur la protection de la vie privée, quelques formulaires secondaires ont été enlevés de cette thèse.

While these forms may be included in the document page count, their removal does not represent any loss of content from the thesis.

Bien que ces formulaires aient inclus dans la pagination, il n'y aura aucun contenu manquant.


Canada

Abstract

A typical example of an axially moving cantilever beam is flexible robotic manipulators with prismatic joints. The model governing lateral vibration of such system is time-varying. Time-varying systems pose significant challenges in modelling and control. The objective of this research is to control the lateral vibration of an axially moving cantilever beam.

In this research, first an analytical model of an axially moving cantilever beam is developed. Second, the effect of an end mass is investigated. Third, piezoelectric actuators (PZT) are considered to design a direct velocity feedback controller to suppress the lateral vibration of the system. The presence of higher modes in the system and the spillover instability are investigated. Fourth, an active control design based on the gradient algorithm is developed. The controllability, observability and the stability of the system are investigated.

Acknowledgement

I would like to express my gratitude to my supervisor Dr.Kefu Liu for his support and guidance during my graduate studies at Lakehead University. I would like to thank my co-supervisor Dr.Henry Saliba for his support. Also I would like to thank Dr.X.Liu and Dr.K.Natarajan for their suggestions in different areas of this work.

I dedicate this work to my parents Mr & Mrs Gnananathan, and to my fiance Jude Alexander for their love, guidance and support.

Contents

1	Introduction	1
1.1	Overview of the Previous Studies on Axially Moving Cantilever Beams	1
1.2	Overview of the Previous Studies of Control Applications on Linear Time-Varying Systems (LTV)	2
1.3	Application of Piezoelectric Actuators	3
1.4	Objectives of the Research	3
1.5	Outline of the Thesis	4
2	Dynamics of an Axially Moving Cantilever Beam	5
2.1	Dynamic Model	5
2.2	The Effect of an End Mass on the Model	9
2.3	State-Space Representation	11
2.4	Vibration Energy of the System	12
2.5	Stability of a LTV System	13
2.6	Computer Simulation	17
2.7	Summary	28
3	Direct Velocity Feedback Control of Lateral Vibration of an Axially Moving Cantilever Beam	29
3.1	Velocity Feedback Control	29
3.2	Constant Gain Feedback	33
3.3	Spillover Instability	41
3.4	Stability of a Slowly-Varying System	41

3.5	Eigenvalues of the Frozen System	42
3.6	Control Strategies	47
3.7	Computer Simulation	50
3.8	Conclusion	58
4	Active Control Design for the Axially Moving Cantilever Beam Based on the Gradient Algorithm	59
4.1	Introduction	59
4.2	Transition Matrix and Stability of Closed-loop System	60
4.3	Controllability	63
4.4	Observability	64
4.5	Gradient Algorithm	67
4.6	State Feedback Control	68
4.7	Observer Based State Feedback Control	74
4.8	Summary	77
5	Summary and Future Work	78
5.1	Summary	78
5.2	Future Work	79
A	Proofs of Theorems and Other Calculations	86
A.1	Proof of Theorem 1	86
A.2	Uniform Exponential Stability	87
A.3	Determining The Initial Conditions Through Deflection Curve	88
A.4	Theorem: Stability of Slowly-Varying System	89
A.5	First Order Runge-Kutta Method	91

List of Figures

2.1	Axially moving cantilever beam system	6
2.2	Axial motion profiles of Scenario A and Scenario B. (a) Axial displacement. (b) Axial velocity. (c) Axial acceleration.	17
2.3	State response for axial extension without the end mass ($m_e = 0$). (a),(b),(c) generalized coordinates. (d),(e),(f) generalized velocities.	19
2.4	State response for axial retraction without the end mass ($m_e = 0$). (a),(b),(c) generalized coordinates. (d),(e),(f) generalized velocities.	19
2.5	State response for axial extension with the end mass ($m_e = 0.4$ Kg). (a),(b),(c) generalized coordinates. (d),(e),(f) generalized velocities.	20
2.6	State response for axial retraction with the end mass ($m_e = 0.4$ Kg). (a),(b),(c) generalized coordinates. (d),(e),(f) generalized velocities.	20
2.7	Displacement responses without the end mass. (a) Output at $r_1 = 0$ m, (b) Output at $r_1 = 0.3$ m, (c) Output at $r_1 = 0.6$ m.	22
2.8	Displacement output responses with the end mass ($m_e = 0.4$ Kg). (a) Output at $r_1 = 0$ m, (b) Output at $r_1 = 0.3$ m, (c) Output at $r_1 = 0.6$ m.	22
2.9	Velocity responses without the end mass. (a) Output at $r_1 = 0$ m, (b) Output at $r_1 = 0.3$ m, (c) Output at $r_1 = 0.6$ m.	23
2.10	Velocity responses with the end mass ($m_e = 0.4$ Kg). (a) Output at $r_1 = 0$ m, (b) Output at $r_1 = 0.3$ m, (c) Output at $r_1 = 0.6$ m.	23

2.11	The vibration energies. (a) Axial extension, (b) Axial retraction. broken line represents the energy without end mass. Solid line represents the energy with end mass.	25
2.12	The energies. T -kinetic energy of the beam. U -potential energy of the beam T_e -kinetic energy of the end mass. (a) Energies when $m_e = 0$, (b) Energies when $m_e = 0.4$	25
2.13	Lyapunov function $V = x^T Q x$. (a) Axial extension, (b) Axial retraction. Dotted line represents the energy without the end mass. Solid line represents the energy with the end mass.	26
2.14	Eigenvalues of the Lyapunov stability condition $A^T(t)Q(t) + Q(t)A(t) + \dot{Q}(t)$. (a) Axial extension, (b) Axial retraction.	27
3.1	Axially moving cantilever beam system with PZT actuators	30
3.2	Deflection responses for Scenario A and Scenario B with one output feedback. (a) noncollocated $r_1 = 0$ m, (b) noncollocated $r_1 = 0.3$ m, (c) collocated $r_1 = 0.66$ m.	36
3.3	Damping ratios ζ_i and damping index J of one output feedback system for Scenario A and Scenario B. (a) noncollocated $r_1 = 0$ m, (b) noncollocated $r_1 = 0.3$ m, (c) collocated $r_1 = 0.66$ m.	36
3.4	State responses of one output feedback system for Scenario A and Scenario B when $r_1 = 0$ m. (a) q_1 , (b) q_2 , (c) q_3	37
3.5	State responses of one output feedback system for Scenario A and Scenario B when $r_1 = 0.3$ m. (a) q_1 , (b) q_2 , (c) q_3	37
3.6	State responses of one output feedback system for Scenario A and Scenario B when $r_1 = 0.66$ m. (a) q_1 , (b) q_2 , (c) q_3	38
3.7	Deflection responses for Scenario A and Scenario B with two noncollocated outputs feedback. (a) $r_1 = 0$ m, (b) $r_2 = 0.3$ m.	38

3.8	Deflection responses for Scenario A and Scenario B with one collocated and the other noncollocated outputs feedback. (a) $r_1 = 0.3$ m. (b) collocated $r_2 = 0.66$ m.	39
3.9	State responses of the two output feedback system for Scenario A and Scenario B when $r_1 = 0$ m and $r_2 = 0.3$ m. (a) q_1 , (b) q_2 , (c) q_3 .	39
3.10	State responses of the two output feedback system for Scenario A and Scenario B when $r_1 = 0.3$ m and $r_2 = 0.66$ m. (a) q_1 , (b) q_2 , (c) q_3 .	40
3.11	Damping ratios ζ_i and damping index J of two output feedback system for Scenario A and Scenario B. (a) $r_1 = 0$ m and $r_2 = 0.3$ m. (b) $r_1 = 0.3$ m $r_2 = 0.66$ m.	40
3.12	\tilde{D}_{ii} and $\tilde{\zeta}_i$ of the frozen system with $r_1 = 0.66$ m a collocated output feedback. (a),(d) $i = 1$. (b),(e) $i = 2$. (c),(f) $i = 3$.	45
3.13	\tilde{D}_{ii} and $\tilde{\zeta}_i$ of the frozen system with a non-collocated output feedback $r_1 = 0.17$ m. (a),(d) $i = 1$. (b),(e) $i = 2$. (c),(f) $i = 3$.	45
3.14	\tilde{D}_{ii} of the frozen system. Two sensors, Collocated $r_1 = 0.66$ m and non-collocated $r_1 = 0.17$ m. (a) $i = 1$. (b) $i = 2$. (c) $i = 3$.	46
3.15	\tilde{D}_{ii} of the frozen system. Two non-collocated outputs at $r_1 = 0.4$ m and $r_1 = 0.17$ m. (a) $i = 1$. (b) $i = 2$. (c) $i = 3$.	46
3.16	On-off gain scheduling scheme for the axially moving beam. Collocated $r_1 = 0.66$ m and $r_2 = 0.17$ m. (a) Displacement response. (b) Damping index J .	51
3.17	On-off gain scheduling scheme for the axially moving beam. $r_1 = 0.4$ m and $r_2 = 0.17$ m. (a) Displacement response. (b) Damping index J .	51
3.18	Deflection responses using the second control method. One collocated and one non-collocated feedback system. (a) Displacement response at $r_1 = 0.3$ m. (b) Displacement response at collocated sensor $r_2 = 0.65$ m.	54

3.19	Gains and damping using the second control method. One collocated and one non-collocated feedback system. (a) Gains g_{v1} and g_{v2} for $r_1 = 0.3$ m and $r_2 = 0.65$ m. (b) Damping ratios ζ_i and damping index J	54
3.20	As Figure 3.18. Two non-collocated outputs feedback system. (a) Displacement response at $r_1 = 0.2$ m. (b) Displacement response at collocated sensor $r_2 = 0.4$ m.	55
3.21	As Figure 3.19. Two non-collocated outputs feedback system. (a) Gains g_{v1} and g_{v2} for $r_1 = 0.2$ m and $r_2 = 0.4$ m. (b) Damping ratios ζ_i and damping index J	55
3.22	Deflection responses using the third control method. Two non-collocated and one collocated outputs feedback system. (a) $r_1 = 0.2$ m, (b) $r_2 = 0.4$ m, (c) $r_3 = 0.65$ m.	56
3.23	Gains and damping using the third control method. Two non-collocated and one collocated outputs feedback system. (a) Gains g_{v1} , g_{v2} and g_{v3} for $r_1 = 0.2$ m, $r_2 = 0.4$ m and $r_3 = 0.65$ m respectively. (b) Damping ratios ζ_i and damping index J	56
3.24	As Figure 3.22. Three non-collocated outputs feedback system. (a) $r_1 = 0.1$ m, (b) $r_2 = 0.3$ m, (c) $r_3 = 0.5$ m.	57
3.25	As Figure 3.23. Three non-collocated outputs feedback system. (a) Gains g_{v1} , g_{v2} and g_{v3} for $r_1 = 0.1$ m, $r_2 = 0.3$ m and $r_3 = 0.5$ m respectively. (b) Damping ratios ζ_i and damping index J	57
4.1	(a) Maximum singular values, (b) minimum singular values of the transition matrices for Scenario A and Scenario B.	61
4.2	Same as Figure 4.1 (b). $\sigma_{min}[\Phi(t, kT)]$ axis is magnified.	62
4.3	Controllability testing using the grammian for extension and retraction. (a) maximum singular values of $P_c(t)$, (b) minimum singular values of $P_c(t)$	64

4.4	Observability testing using grammian for extension and retraction. The deflection output is observed at $r_1 = 0.1$ m. (a) maximum singular values of $P_o(t)$, (b) minimum singular values of $P_o(t)$	65
4.5	Observability testing using the grammian for extension and retraction. The deflection output is observed at the collocated sensor location $r_1 = 0.66$ m. (a) maximum singular values of $P_o(t)$, (b) minimum singular values of $P_o(t)$	65
4.6	Observability testing using the grammian for extension and retraction. The velocity output is observed at $r_1 = 0.1$ m. (a) maximum singular values of $P_o(t)$, (b) minimum singular values of $P_o(t)$	66
4.7	Observability testing using the grammian for extension and retraction. The velocity output is observed at the collocated sensor location $r_1 = 0.66$ m. (a) maximum singular values of $P_o(t)$, (b) minimum singular values of $P_o(t)$	66
4.8	State feedback displacement responses at $r_1 = 0.1$ m. (a) Output response with controller ($\gamma_c = 2$) and without controller ($\gamma_c = 0$). (b) Control input $u(t)$ when $\gamma_c = 2$	70
4.9	State feedback displacement responses at $r_1 = 0.1$ m. (a) Output response with controller ($\gamma_c = 12$) and without controller ($\gamma_c = 0$). (b) Control input $u(t)$ when $\gamma_c = 12$	71
4.10	State feedback displacement responses at $r_1 = 0.1$ m. (a) Output response with controller ($\gamma_c = 16$) and without controller ($\gamma_c = 0$). (b) Control input $u(t)$ when $\gamma_c = 16$	71
4.11	Maximum values of control input $u(t)$ for γ_c ranging from 0-16 when $r_1 = 0.1$ m. (a) Scenario A, (b) Scenario B.	72
4.12	R for γ_c 's ranging from 0-16 when $r_1 = 0.1$ m. (a) Scenario A, (b) Scenario B.	72

4.13	Observer based feedback control responses at $r_1 = 0.1$ m. $\gamma_c = 5$ and $\gamma_o = 5$. (a) True output y and estimated output \hat{y} , (b) Estimation error \tilde{y} , (c) control output u	76
5.1	Schematic diagram of the axially moving cantilever beam and PZT actuator system	80
A.1	Deflection Curve	88

List of Tables

2.1	$\beta_j L$ and σ_j of the first three modes of a cantilever beam	7
2.2	Natural frequencies of the beam with the shortest length and longest length . . .	18

Notations

LTV	Linear time-varying
L	length of the beam (m)
\dot{L}	velocity of the beam (m/s)
\ddot{L}	acceleration of the beam (m/s ²)
w	deflection of the beam (m)
m_e	end mass attached to the tip of the beam (kg)
s	axial location of the output sensor (m)
E	modulus of elasticity (N/m ²)
I	moment of inertia (m ⁴)
q_n	generalized coordinate (m)
ϕ_j	mode shape function
μ	length density of the beam (kg/m)
T_b	kinetic energy of the beam
U_b	potential energy of the beam
F_a	axial force
U_{F_a}	strain energy of the beam
T_e	kinetic energy of the end mass
E_v	vibration energy
f_n	natural frequency (Hz)
PZT	Piezoelectric actuator
s_{in}	axial location of the actuator(m)
Q_F	virtual work
g_p	PZT constant
$H(\cdot)$	Heaviside step function

V	voltage applied to PZT
g_{v_n}	feedback gain
λ_i	eigenvalue
J	stability index
ζ_i	damping ratio
σ_{max}	maximum singular value of the transition matrix
σ_{min}	minimum singular value of the transition matrix
P_c	controllability grammian
P_o	observability grammian
Z	parameter error
w	regressor vector
K	feedback gain vector
R	measure of the output response
L	observer feedback gain

Chapter 1

Introduction

A typical example of an axially moving cantilever beam is flexible robotic manipulators with prismatic joints. The model governing lateral vibration of the beam is time-varying. Time-varying systems pose significant challenges in modelling and control. This research is motivated to develop an analytical model of an axially moving cantilever beam system, and to use piezoelectric actuators to suppress the lateral vibration of an axially moving cantilever beam.

1.1 Overview of the Previous Studies on Axially Moving Cantilever Beams

Studies dealing with mathematical modelling of axially moving cantilever beams are reported in [1-7]. The models are derived by the energy method that employs Lagrangian formulation based on the assumption that the deflection gradients of the beam are small and the beam is axially rigid. The axial motion influences the dynamics of the axially moving cantilever beam. The extending and retracting motions of the beam have destabilizing and stabilizing effects on the lateral vibration based on the fact that the deflection at the tip of the beam becomes large during the axial extension and small during the axial retraction. The axial extension increases the amplitude of the deflection due to a reduced stiffness while the axial retraction reduces the deflection of the beam due to an increased stiffness. Also the axial extension decreases the amplitude of the lateral velocity because of dissipation of vibration energy while the axial retraction increases the amplitude of the lateral velocity because of absorption of vibration

energy [3].

In the previous studies, little effort has been made in analyzing the contribution of generalized coordinates, generalized velocities and vibratory modes to the transient responses including strain, displacement, velocity and acceleration in the axially moving cantilever beam system.

1.2 Overview of the Previous Studies of Control Applications on Linear Time-Varying Systems (LTV)

To design a high performance active control system, an accurate system model is a prerequisite. It is difficult to obtain an accurate mathematical model due to the fact that irregularities, including physical damping effect and nonlinear factors, exist in the system.

Many control designs for linear time-varying systems are reported in [8 - 28]. The development of modal control algorithms for axially moving systems were pioneered in [8]. In the study, the control design was based on a discretized model of the infinite dimensional axially moving system and spillover instabilities were demonstrated. To avoid spillover instabilities, the study reported in [9] used transfer function approaches to develop a class of asymptotically stabilizing controllers for distributed parameter models of axially moving strings and beams. A pointwise controller was designed to ensure that all the eigenvalues of the controlled system remain strictly in the left-half plane. The stability margin of the controlled translating string and beam was subsequently investigated in [10 - 11]. The optimal control location leading to the maximum stability margin for all the modes of vibration, was determined for the controlled translation beam through a combined numerical analysis for eigenvalues of low modes and analytical prediction of them for all the high modes [10].

The active vibration control of systems with periodic parametric excitations also has been studied by several researchers. The most conventional approach is to use the optimal control theory, where the system is stabilized by state feedback control with periodically time-varying state feedback gain [12]. For linear systems with non-stationary parametric excitations, the

controllability-grammian based control [13] can suppress the state oscillation effectively. Unfortunately this control design imposes a strict assumption that one must be able to predict how the non-stationary excitation varies in future in order to calculate the desired control input [12]. To control the vibration of an axially moving cantilever beam, one of the methods applied in this study is the new approach given in [12] to the active control design for parametrically excited systems. The approach is based on the gradient algorithm in adaptive identification [14].

1.3 Application of Piezoelectric Actuators

The principles of piezoelectric actuators and their applications to control vibration on beams are reported in [29-36]. There are many piezoelectric materials that are currently being used. One of them is poly-vinylidene fluoride (PVDF), which is a semicrystalline polymer film and lead zirconate titanate (PZT), which is a piezoelectric ceramic material. These materials strain when exposed to a voltage and, conversely, produce a voltage when strained. This is due to the permanent dipole nature of these materials [31]. A single piezoceramic element bonded to the base of the beam functioned both as distributed moment actuator and strain sensor [36]. In the past applications of these piezoelectric actuators are commonly done on stationary structures. In this research the piezoelectric actuators are applied on an axially moving beam.

1.4 Objectives of the Research

1. The first objective of the research is to develop an analytical model and conduct a computer simulation in order to understand the dynamics of the system.
2. The second objective of the research is to use piezoelectric actuators to control the lateral vibration of the axially moving cantilever beam.
3. The third objective of the research is to apply different control algorithms to suppress the lateral vibration of the axially moving cantilever beam system and to analyze the stability

of the system.

1.5 Outline of the Thesis

The following chapters of the thesis are organized as follows: Chapter 2 describes the dynamics of an axially moving cantilever beam, develops an analytical model for the system and presents some computer simulation results. Chapter 3 gives the design of the direct velocity feedback control of the system and the computer simulations results. Chapter 4 gives an active control design for the system based on the gradient algorithm and the computer simulation results. Chapter 5 draws the conclusion of the study and gives recommendations for the future work.

Chapter 2

Dynamics of an Axially Moving Cantilever Beam

The objective of this chapter is to derive the equation of motion of an axially moving cantilever beam and to perform the simulation to study the dynamics of the system.

This chapter is organized as follows: Section 2.1 describes the modelling and develops a dynamic model of an axially moving cantilever beam. Section 2.2 includes an end mass in the model. Section 2.3 shows the state-space representation of the system. Section 2.4 presents the derivations for the vibration energy of the system. Section 2.5 conducts the stability analysis of the system. Section 2.6 shows the computer simulation and the observations. Section 2.7 is a brief summary and conclusion of the chapter.

2.1 Dynamic Model

Figure 2.1 shows the model of an axially moving cantilever beam, where s and t represent the axial location or the location of an output sensor and time, respectively, $L(t)$ represents the length of the beam, $w(s, t)$ represents the lateral deflection of the beam, and m_e denotes the end mass attached to the tip of the beam.

The following assumptions are made:

1. The beam is Euler-Bernoulli beam.
 - The beam is uniform along its longitudinal direction, both in mass distribution and

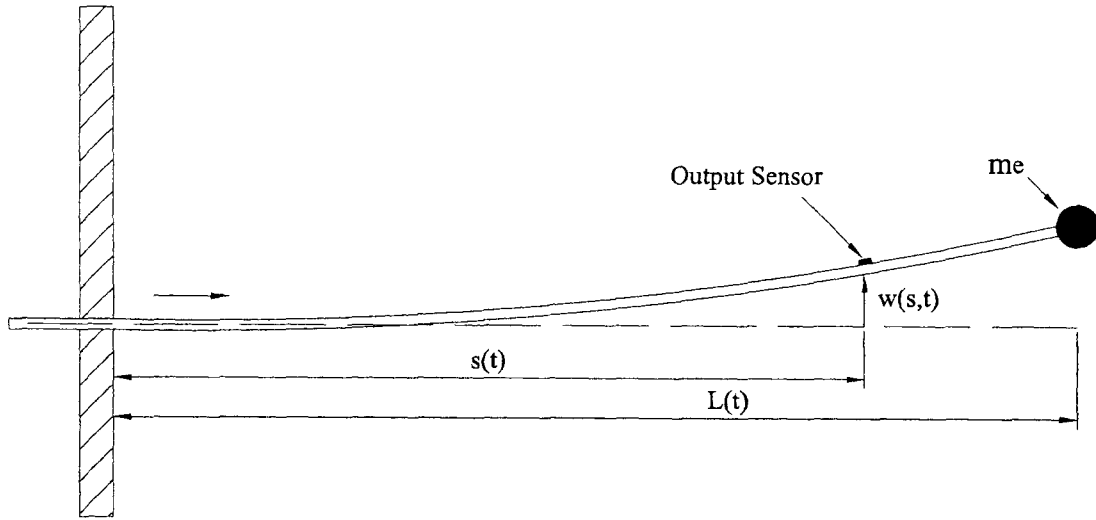


Figure 2.1: Axially moving cantilever beam system

elastic properties.

- Rotary inertia and shear deformation can be neglected.
 - The beam is composed of a linear, homogeneous, isotropic, elastic material without axial load such that cross sections remain plane and the plane of symmetry of the beam is the plane of vibration.
2. The lateral deflection gradients are small.
 3. The axial motion is a function of time only.
 4. Elastic modulus E , moment of inertia I for the cross sectional area A are constants along the beam length.
 5. No physical damping is considered.

Equation of motion of the system is derived by the energy method: Lagrangian function.

The lateral velocity of a particle fixed on the beam and at position s at time t is given as

$$\frac{Dw(s,t)}{Dt} = \frac{\partial w(s,t)}{\partial t} + \dot{L} \frac{\partial w(s,t)}{\partial s} \quad (2.1)$$

where $\frac{D}{Dt}$ is the material time derivative and \dot{L} is the axial velocity of the beam. The lateral deflection of the beam $w(s, t)$ can be expressed as a series of prescribed functions of space with undetermined time dependent terms.

$$w(s, t) = \Phi(s, L)q(t) = \sum_{j=1}^n \phi_j(s, L)q_j(t) \quad (2.2)$$

where $q(t) = \begin{bmatrix} q_1(t) & q_2(t) & \dots & q_n(t) \end{bmatrix}^T$ is a column vector of generalized coordinates, n is the number of the vibratory modes considered, $\Phi(s, L) = \begin{bmatrix} \phi_1(s, L) & \phi_2(s, L) & \dots & \phi_n(s, L) \end{bmatrix}$ is a row vector, $\phi_j(s, L)$ is the j th eigenfunction or mode shape of the "stationary" cantilever beam, which is

$$\phi_j(s, L) = \frac{1}{\sqrt{L(t)}}\psi_j(\alpha) \quad (2.3)$$

$$\Phi(s, L) = \frac{1}{\sqrt{L(t)}}\Psi(\alpha) = \frac{1}{\sqrt{L(t)}} \begin{bmatrix} \psi_1(\alpha) & \psi_2(\alpha) & \dots & \psi_n(\alpha) \end{bmatrix} \quad (2.4)$$

where $\alpha = \frac{s}{L}$ and the mode shape function for the cantilever beam is given by [38],

$$\psi_j(\alpha) = \cosh(\beta_j L \alpha) - \cos(\beta_j L \alpha) - \sigma_j \{ \sinh(\beta_j L \alpha) - \sin(\beta_j L \alpha) \} \quad (2.5)$$

where $\beta_j L$ and σ_j are constants and the values of the first three modes are listed in Table 2.1.

Mode Number	1	2	3
$\beta_j L$	1.8751	4.69409	7.8547
σ_j	0.7341	1.0185	0.9992

Table 2.1: $\beta_j L$ and σ_j of the first three modes of a cantilever beam

To expand the lateral velocity function (2.1) in terms of $q(t)$ and $\Phi(s)$, the following relations are used,

$$\begin{aligned} \frac{\partial w(s, t)}{\partial s} &= w'(s, t) = \frac{1}{L} \frac{1}{\sqrt{L}} \Psi'(\alpha) q(t) \\ \frac{\partial^2 w(s, t)}{\partial s^2} &= w''(s, t) = \frac{1}{L^2} \frac{1}{\sqrt{L}} \Psi''(\alpha) q(t) \\ \frac{\partial w(s, t)}{\partial t} &= \dot{w}(s, t) = \frac{1}{\sqrt{L}} \Psi(\alpha) \dot{q}(t) - \frac{1}{2} \frac{\dot{L}}{L} \frac{1}{\sqrt{L}} \Psi(\alpha) q(t) - \frac{1}{\sqrt{L}} \dot{\Psi}(\alpha) q(t) \end{aligned} \quad (2.6)$$

where

$$\begin{aligned}\psi'_j(\alpha) &= \beta_j L [\sinh(\beta_j L \alpha) + \sin(\beta_j L \alpha) - \sigma_j \{\cosh(\beta_j L \alpha) - \cos(\beta_j L \alpha)\}] \\ \dot{\psi}_j(\alpha) &= -\frac{s\dot{L}}{L^2} \psi'_j(\alpha)\end{aligned}\quad (2.7)$$

By substituting Equations (2.6) and (2.7) in (2.1), the lateral velocity becomes

$$\begin{aligned}\frac{Dw(s,t)}{Dt} &= \frac{1}{\sqrt{L}} \Psi(\alpha) \dot{q}(t) - \frac{1}{2} \frac{\dot{L}}{L} \frac{1}{\sqrt{L}} \Psi(\alpha) q(t) - \frac{s\dot{L}}{L^2} \frac{1}{\sqrt{L}} \Psi'(\alpha) + \frac{\dot{L}}{L} \frac{1}{\sqrt{L}} \Psi'(\alpha) q(t) \\ &= \frac{1}{\sqrt{L}} \Psi(\alpha) \dot{q}(t) - \frac{1}{2} \frac{\dot{L}}{L} \frac{1}{\sqrt{L}} \Psi(\alpha) q(t) + \frac{\dot{L}}{L} (1 - \alpha) \frac{1}{\sqrt{L}} \Psi'(\alpha) q(t) \\ &= \Phi(s, L) \dot{q}(t) + \left[-\frac{1}{2} \frac{\dot{L}}{L} \Phi(s, L) + \frac{\dot{L}}{L} (1 - \frac{s}{L}) \Phi'(s, L) \right] q(t)\end{aligned}\quad (2.8)$$

The kinetic energy of the beam is given by

$$T_b = \int_0^L \frac{\mu}{2} \left(\frac{Dw(s,t)}{Dt} \right)^2 ds \quad (2.9)$$

where μ is the length density of the beam. Substituting Equation (2.8) in (2.9) gives

$$\begin{aligned}T_b &= \int_0^L \frac{\mu}{2} \{ \Phi \dot{q} + \left[-\frac{1}{2} \frac{\dot{L}}{L} \Phi + \frac{\dot{L}}{L} (1 - \frac{s}{L}) \Phi' \right] q \}^T \{ \Phi \dot{q} + \left[-\frac{1}{2} \frac{\dot{L}}{L} \Phi + \frac{\dot{L}}{L} (1 - \frac{s}{L}) \Phi' \right] q \} ds \\ &= \frac{\mu}{2} \dot{q}^T A_1 \dot{q} + \frac{\mu}{2} \frac{2\dot{L}}{L} q^T A_2 \dot{q} + \frac{\mu}{2} \frac{\dot{L}^2}{L^2} q^T A_3 q\end{aligned}\quad (2.10)$$

where

$$\begin{aligned}A_1 &= \int_0^L \Phi^T \Phi ds = \int_0^1 \Psi^T(\alpha) \Psi(\alpha) d\alpha \\ A_2 &= \int_0^L \left[-\frac{1}{2} \Phi^T \Phi + (1 - \frac{s}{L}) \Phi^T \Phi' \right] ds = \int_0^1 \left[-\frac{1}{2} \Psi^T(\alpha) \Psi(\alpha) + (1 - \alpha) \Psi^T(\alpha) \Psi'(\alpha) \right] d\alpha \\ A_3 &= \int_0^L \left[\frac{1}{4} \Phi^T \Phi - (1 - \frac{s}{L}) \Phi^T \Phi' + (1 - \frac{s}{L})^2 \Phi^T \Phi' \right] ds \\ &= \int_0^1 \left[\frac{1}{4} \Psi^T(\alpha) \Psi(\alpha) - (1 - \alpha) \Psi^T(\alpha) \Psi'(\alpha) + (1 - \alpha)^2 \Psi^T(\alpha) \Psi'(\alpha) \right] d\alpha\end{aligned}$$

and note that A_2 is a skew symmetric matrix. The matrix A_1 is an identity matrix according to the orthogonality of the mode shape functions. If three modes are considered, A_2 and A_3 can be numerically found to be

$$A_2 = \begin{bmatrix} 0 & -0.6684 & -0.2243 \\ 0.6684 & 0 & -1.6365 \\ 0.2243 & 1.6365 & 0 \end{bmatrix} \quad A_3 = \begin{bmatrix} 0.4889 & 0.539 & -0.5616 \\ 0.539 & 4.0883 & 3.4414 \\ -0.5616 & 3.4414 & 13.935 \end{bmatrix}$$

The potential energy of the beam due to the flexural deformation is given by

$$U_b = \int_0^L \frac{EI}{2} \left(\frac{\partial^2 w(s,t)}{\partial s^2} \right)^2 ds \quad (2.11)$$

Substituting Equation (2.6) in (2.11) gives

$$U_b = \frac{EI}{2L^4} q^T A_4 q \quad (2.12)$$

where

$$A_4 = \int_0^L \Phi^{T'} \Phi'' ds = \begin{bmatrix} (\beta_1 L)^4 & 0 & 0 \\ 0 & (\beta_2 L)^4 & 0 \\ 0 & 0 & (\beta_3 L)^4 \end{bmatrix}$$

The Lagrangian equation is given by

$$\frac{d}{dt} \frac{\partial T_b}{\partial \dot{q}} - \frac{\partial T_b}{\partial q} + \frac{\partial U_b}{\partial q} = 0 \quad (2.13)$$

from Equations (2.10) and (2.12),

$$\begin{aligned} \frac{\partial T_b}{\partial \dot{q}} &= \mu A_1 \dot{q} + \frac{\mu \dot{L}}{L} A_2 q \\ \frac{d}{dt} \frac{\partial T_b}{\partial \dot{q}} &= \mu A_1 \ddot{q} + \frac{\mu \dot{L}}{L} A_2 \dot{q} + \frac{\mu \ddot{L}}{L} A_2 q - \frac{\mu \dot{L}^2}{L^2} A_2 q \\ \frac{\partial T_b}{\partial q} &= \frac{\mu \dot{L}}{L} A_2^T \dot{q} + \frac{\mu \dot{L}^2}{L^2} A_3 q \\ \frac{\partial U_b}{\partial q} &= \frac{EI}{L^4} q \end{aligned}$$

Substituting the above equations into Equation (2.13) results in

$$\begin{aligned} \mu A_1 \ddot{q} + \frac{\mu \dot{L}}{L} A_2 \dot{q} + \frac{\mu \ddot{L}}{L} A_2 q - \frac{\mu \dot{L}^2}{L^2} A_2 q - \frac{\mu \dot{L}}{L} A_2^T \dot{q} - \frac{\mu \dot{L}^2}{L^2} A_3 q + \frac{EI}{L^4} q &= 0 \\ \mu A_1 \ddot{q} + \frac{2\mu \dot{L}}{L} A_2 \dot{q} + \left[\frac{\mu \ddot{L}}{L} A_2 - \frac{\mu \dot{L}^2}{L^2} (A_2 + A_3) + \frac{EI}{L^4} A_4 \right] q &= 0 \end{aligned} \quad (2.14)$$

Note that $A_2 - A_2^T = 2A_2$, as A_2 is a skew symmetric matrix.

2.2 The Effect of an End Mass on the Model

If a concentrated mass m_e is attached to the end of the axially moving cantilever beam, it is needed to consider the kinetic energy T_e of the end mass and the strain energy U_{F_e} created by

the axial force F_a due to the axial acceleration \ddot{L} . The kinetic energy of the end mass is given by

$$\begin{aligned}
T_e &= \frac{m_e}{2} \left(\frac{Dw(L,t)}{Dt} \right)^2 \\
&= \frac{m_e}{2} \left[\Phi(L)\dot{q} - \frac{1}{2}\frac{\dot{L}}{L}\Phi(L)q \right]^2 \\
&= \frac{m_e}{2} \left[\frac{1}{L}\dot{q}^T \Psi^T(1)\Psi(1)\dot{q} - \frac{\dot{L}}{L^2}\dot{q}^T \Psi^T(1)\Psi(1)q + \frac{1}{4}\frac{\dot{L}^2}{L^3}q^T \Psi^T(1)\Psi(1)q \right] \\
&= \frac{m_e}{2} \frac{1}{L}\dot{q}^T A_5 \dot{q} - \frac{m_e}{2} \frac{\dot{L}}{L^2}\dot{q}^T A_5 q + \frac{m_e}{2} \frac{1}{4} \frac{\dot{L}^2}{L^3} q^T A_5 q
\end{aligned} \tag{2.15}$$

where

$$A_5 = \Psi^T(1)\Psi(1)$$

For the first three modes, A_5 is found to be

$$A_5 = 4 \begin{bmatrix} 1 & -1 & 1 \\ -1 & 1 & -1 \\ 1 & -1 & 1 \end{bmatrix}$$

When the beam is accelerating, the axial force acting at location s is given by the inertial force

$$F_a = -[m_e + \mu(L-s)]\ddot{L} \tag{2.16}$$

The strain energy caused by F_a is given by

$$\begin{aligned}
U_{F_a} &= \frac{1}{2} \int_0^L -[m_e + \mu(L-s)]\ddot{L} \left(\frac{\partial w(s,t)}{\partial s} \right)^2 ds \\
&= -\frac{m_e}{2} \frac{\dot{L}}{L^2} \dot{q}^T A_6 q - \frac{\mu}{2} \frac{\dot{L}}{L} \dot{q}^T A_7 q
\end{aligned} \tag{2.17}$$

where

$$\begin{aligned}
A_6 &= \int_0^L \Phi'^T \Phi' ds = \int_0^1 \Psi'^T(\alpha)\Psi'(\alpha) d\alpha \\
A_7 &= \int_0^L \left(1 - \frac{s}{L}\right) \Phi'^T \Phi' ds = \int_0^1 (1-\alpha)\Psi'^T(\alpha)\Psi'(\alpha) d\alpha
\end{aligned}$$

For the first three modes, A_6 and A_7 are numerically found to be

$$A_6 = \begin{bmatrix} 4.6477 & -7.3846 & 4.0273 \\ -7.3846 & 32.4446 & -22.6413 \\ 4.0273 & -22.6413 & 78.0453 \end{bmatrix} \quad A_7 = \begin{bmatrix} 1.5709 & -0.4223 & -1.0712 \\ -0.4223 & 8.6471 & 1.8901 \\ -1.0712 & 1.8901 & 24.952 \end{bmatrix}$$

To include T_e and U_{F_a} into the Lagrangian equation, the following operations are conducted.

$$\frac{\partial T_e}{\partial \dot{q}} = \frac{m_e}{L} A_5 \dot{q} - \frac{m_e}{2} \frac{\dot{L}}{L^2} A_5 q \quad (2.18)$$

$$\begin{aligned} \frac{d}{dt} \frac{\partial T_e}{\partial \dot{q}} &= -\frac{m_e}{L^2} \dot{L} A_5 \dot{q} + \frac{m_e}{L} A_5 \ddot{q} - \frac{m_e}{2} \frac{\ddot{L}}{L^2} A_5 q + \frac{m_e \dot{L}^2}{L^3} A_5 q - \frac{m_e}{2} \frac{\dot{L}}{L^2} A_5 \dot{q} \\ &= \frac{m_e}{L} A_5 \ddot{q} - \frac{3m_e \dot{L}}{2L^2} A_5 \dot{q} + m_e \left(\frac{\dot{L}^2}{L^3} - \frac{1}{2} \frac{\ddot{L}}{L^2} \right) A_5 q \end{aligned} \quad (2.19)$$

$$\frac{\partial T_e}{\partial q} = -\frac{m_e}{2} \frac{\dot{L}}{L^2} A_5 \dot{q} + \frac{m_e}{4} \frac{\dot{L}^2}{L^3} A_5 q \quad (2.20)$$

$$\frac{\partial U_{F_a}}{\partial q} = -\frac{m_e \ddot{L}}{L^2} A_6 q - \frac{\mu \ddot{L}}{L} A_7 q \quad (2.21)$$

Combining Equations (2.19), (2.20), and (2.21) with Equation (2.14), the equation of motion for the beam with the end mass is given by

$$M(t)\ddot{q} + D(t)\dot{q} + K(t)q = 0 \quad (2.22)$$

where

$$\begin{aligned} M(t) &= \mu A_1 + \frac{m_e}{L} A_5 \\ D(t) &= \frac{2\mu \dot{L}}{L} A_2 - m_e \frac{\dot{L}}{L^2} A_5 \\ K(t) &= \frac{\mu \ddot{L}}{L} A_2 - \frac{\mu \dot{L}^2}{L^2} (A_2 + A_3) + \frac{EI}{L^4} A_4 + \frac{3m_e}{4} \frac{\dot{L}^2}{L^3} A_5 - \frac{m_e}{2} \frac{\dot{L}}{L^2} A_5 - \frac{m_e \ddot{L}}{L^2} A_6 - \frac{\mu \ddot{L}}{L} A_7 \end{aligned} \quad (2.23)$$

2.3 State-Space Representation

By introducing a state vector $x = [q^T(t) \ \dot{q}^T(t)]^T$, the state-space representation is given by

$$\dot{x} = A(t)x(t) \quad (2.24)$$

where the time-varying state matrix $A(t)$ is defined as:

$$A(t) = \begin{bmatrix} 0_{n \times n} & I \\ -M^{-1}(t)K(t) & -M^{-1}(t)D(t) \end{bmatrix}$$

where $0_{i \times j}$ is used to represent an $i \times j$ null matrix.

The response or output of the system is given by

$$y(t) = C(t)x(t) \quad (2.25)$$

where the output matrix $C(t)$ is time-varying and is dependent on the sensor type and location.

For example, if the lateral displacement is observed by a sensor located at $s_1 = L - r_1$ (note that r_1 is constant and measured from the tip of the beam), then the output matrix is defined by

$$C(t) = \begin{bmatrix} \frac{1}{\sqrt{L}}\Psi(\alpha_1) & 0_{1 \times 3} \end{bmatrix} \quad (2.26)$$

where $\alpha_1 = 1 - \frac{r_1}{L}$.

If the lateral velocity is observed by a sensor located at $s_1 = L - r_1$ the output matrix is given by

$$C(t) = \begin{bmatrix} \frac{\dot{L}}{L} \frac{1}{\sqrt{L}} \{-\frac{1}{2}\Psi(\alpha_1) + (1 - \alpha_1)\Psi'(\alpha_1)\} & \frac{1}{\sqrt{L}}\Psi(\alpha_1) \end{bmatrix} \quad (2.27)$$

2.4 Vibration Energy of the System

The total energy of vibration is given by,

$$E_v = T_b + U_b + T_e + U_{F_a} \quad (2.28)$$

Substituting Equations (2.10), (2.12), (2.15) and (2.17) in Equation (2.28) yields

$$\begin{aligned} E_v = & \frac{\mu}{2} \dot{q}^T A_1 \dot{q} + \frac{\mu}{2} \frac{2\dot{L}}{L} q^T A_2 \dot{q} + \frac{\mu}{2} \frac{\dot{L}^2}{L^2} q^T A_3 q + \frac{EI}{2L^4} q^T A_4 q + \frac{m_e}{2} \frac{1}{L} \dot{q}^T A_5 \dot{q} - \frac{m_e}{2} \frac{\dot{L}}{L^2} \dot{q}^T A_5 q \\ & + \frac{m_e}{2} \frac{1}{4} \frac{\dot{L}^2}{L^3} q^T A_5 q - \frac{m_e}{2} \frac{\ddot{L}}{L^2} q^T A_6 q - \frac{\mu}{2} \frac{\dot{L}}{L} q^T A_7 q \end{aligned} \quad (2.29)$$

or

$$E_v = \frac{1}{2} x^T H x \quad (2.30)$$

where

$$\begin{aligned}
H &= \begin{bmatrix} H_{11} & H_{12} \\ H_{21} & H_{22} \end{bmatrix} \\
H_{11} &= \frac{\mu \dot{L}^2}{L^2} A_3 + \frac{EI}{L^4} A_4 + \frac{m_e \dot{L}^2}{4 L^3} A_5 - \frac{m_e \dot{L}}{L^2} A_6 - \frac{\mu \dot{L}}{L} A_7 \\
H_{12} &= \frac{2\mu \dot{L}}{L} A_2 \\
H_{21} &= -\frac{m_e \dot{L}}{L^2} A_5 \\
H_{22} &= \mu A_1 + \frac{m_e}{L} A_5
\end{aligned} \tag{2.31}$$

2.5 Stability of a LTV System

The state-space equation of a LTV system is given by

$$\dot{x}(t) = A(t)x(t) \tag{2.32}$$

Theorem 1: According to Lyapunov stability [39], if the Lyapunov function is chosen as

$$V(t) = x^T(t)x(t) \tag{2.33}$$

therefore,

$$\dot{V}(t) = x^T(t) [A(t) + A^T(t)] x(t) \tag{2.34}$$

the LTV system is asymptotically stable if the eigenvalues of the symmetric matrix $[A(t) + A^T(t)]$ remain strictly in the left-half of the complex plane or the matrix $[A(t) + A^T(t)]$ is negative definite such that

$$[A(t) + A^T(t)] < 0 \tag{2.35}$$

The proof of this Theorem is given in Appendix A.1.

Equation (2.35) is a restrictive sufficient condition, not a necessary condition. That is, some asymptotically stable systems may not satisfy the condition of Equation (2.35). If the negative definiteness of the matrix $[A(t) + A^T(t)]$ does not asymptotically vanish, that is, if there is a constant $\nu > 0$ such that $[A(t) + A^T(t)] \leq -\nu I$ for all t , then the Lyapunov function goes to

zero as t increases [13]. For this reason, more general Lyapunov function can be chosen instead of the Lyapunov function in *Theorem 1*.

Theorem 2: If the Lyapunov function is given by

$$V(t) = x^T(t)Q(t)x(t) \quad (2.36)$$

where $Q(t)$ is a $2n \times 2n$ symmetric matrix and continuously differentiable for all t . The derivative of the function (2.36), is given by

$$\dot{V}(t) = x^T(t) \left[A^T(t)Q(t) + Q(t)A(t) + \dot{Q}(t) \right] x(t) \quad (2.37)$$

According to [13], if the following conditions are satisfied

$$\eta I \leq Q(t) \leq \zeta I \quad (2.38)$$

$$A^T(t)Q(t) + Q(t)A(t) + \dot{Q}(t) \leq -\nu I \quad (2.39)$$

where η , ζ and ν are finite positive constants, and the system of (2.32) is uniformly exponentially stable. If Equations (2.38) and (2.39) are satisfied and $\nu = 0$, system of (2.32) is uniformly stable. The proof of this Theorem is given in Appendix A.2.

Stability Analysis of Multi-Mode Model

When two or more modes are present in the axially moving cantilever beam, the stability of the system can be analyzed according to [17].

a. Extension $\dot{L}(t) > 0$

$$\text{Let } Q(t) = \begin{bmatrix} K_s & 0 \\ 0 & M \end{bmatrix}$$

where $K_s = \frac{K+K^T}{2}$, and the following can be derived as

$$A^T(t)Q(t) + Q(t)A(t) + \dot{Q}(t) = \begin{bmatrix} \dot{K}_s & K_s - K^T \\ K_s - K & \dot{M} - D^T - D \end{bmatrix} \quad (2.40)$$

b. Retraction $\dot{L}(t) < 0$

$$\text{Let } Q(t) = \begin{bmatrix} M^{-1} & 0 \\ 0 & K_s^{-1} \end{bmatrix}$$

where $K_s = \frac{K+K^T}{2}$ and

$$A^T(t)Q(t) + Q(t)A(t) + \dot{Q}(t) = \begin{bmatrix} -M^{-1}\dot{M}M^{-1} & M^{-1} - K^T M^{-1} K_s^{-1} \\ M^{-1} - K_s^{-1} M^{-1} K & -K_s^{-1} \dot{K}_s K_s^{-1} - D^T M^{-1} K_s^{-1} - K_s^{-1} M^{-1} D \end{bmatrix} \quad (2.41)$$

Stability Analysis of One-Mode Model

When only one mode is considered in the axially moving cantilever beam, the stability of the system can be analyzed according to [17].

a. Extension $\dot{L}(t) > 0$

The system is uniformly exponentially stable if the following conditions are satisfied.

$$\begin{aligned} d(t) &\geq \epsilon \\ \dot{L}(t) &\geq 0 \\ k(t) &\leq -\epsilon \end{aligned} \quad (2.42)$$

where ϵ is a positive constant. Let

$$Q(t) = \begin{bmatrix} k(t) & 0 \\ 0 & m(t) \end{bmatrix} \quad (2.43)$$

where d , k and m are the first diagonal elements of D , K , and M matrices respectively. Choose η and ζ such that,

$$\begin{aligned}\eta &= \min\{k_{\min}, \mu A_1 + \frac{m_e}{L_{\max}} A_5\} \\ \zeta &= \max\{k_{\max}, \mu A_1 + \frac{m_e}{L_{\min}} A_5\}\end{aligned}\tag{2.44}$$

Also

$$A^T(t)Q(t) + Q(t)A(t) + \dot{Q}(t) = \begin{bmatrix} \dot{k}(t) & 0 \\ 0 & \dot{m}(t) - 2d(t) \end{bmatrix}\tag{2.45}$$

Rearranging Equations (2.42) and (2.45) results in

$$\begin{bmatrix} \dot{k}(t) & 0 \\ 0 & \dot{m}(t) - 2d(t) \end{bmatrix} \leq \begin{bmatrix} -\epsilon & 0 \\ 0 & -2\epsilon \end{bmatrix}\tag{2.46}$$

Choose $\nu = \max\{-\epsilon, -2\epsilon\}$ to satisfy Equation (2.39).

b. Retraction $\dot{L}(t) < 0$

The system is uniformly exponentially stable if the following conditions are satisfied.

$$\begin{aligned}d(t) &\geq 0 \\ \dot{L}(t) &\leq -\epsilon \\ \dot{k}(t) &\geq \epsilon\end{aligned}\tag{2.47}$$

where ϵ is a positive constant. Let

$$Q(t) = \begin{bmatrix} m^{-1}(t) & 0 \\ 0 & k^{-1}(t) \end{bmatrix}\tag{2.48}$$

Choose η and ζ such that,

$$\begin{aligned}\eta &= \min\{k_{\max}^{-1}, \left[\mu A_1 + \frac{m_e}{L_{\min}} A_5\right]^{-1}\} \\ \zeta &= \max\{k_{\min}^{-1}, \left[\mu A_1 + \frac{m_e}{L_{\max}} A_5\right]^{-1}\}\end{aligned}\tag{2.49}$$

Also

$$A^T(t)Q(t) + Q(t)A(t) + \dot{Q}(t) = \begin{bmatrix} -\dot{m}(t)m^{-2}(t) & 0 \\ 0 & -\dot{k}(t)k^{-2}(t) - 2d(t)m^{-1}(t)k^{-1}(t) \end{bmatrix}\tag{2.50}$$

Rearranging Equations (2.47) and (2.50) results in

$$\begin{bmatrix} -\frac{\dot{m}(t)}{m^2(t)} & 0 \\ 0 & -\frac{\dot{k}(t)}{k^2(t)} - \frac{2d(t)}{m(t)k(t)} \end{bmatrix} \leq \begin{bmatrix} -\frac{m\epsilon A_5}{L_{max}^2 [\mu A_1 + \frac{m\epsilon}{L_{min}} A_5]^2} & 0 \\ 0 & -\frac{\epsilon}{k_{max}^2} \end{bmatrix} \quad (2.51)$$

Choose $\nu = \max\left\{-\frac{m\epsilon A_5}{L_{max}^2 [\mu A_1 + \frac{m\epsilon}{L_{min}} A_5]^2}, -\frac{\epsilon}{k_{max}^2}\right\}$ to satisfy Equation (2.39).

2.6 Computer Simulation

This simulation is performed to study the influence of the axial motion on the lateral vibration of the axially moving cantilever beam and the influence of the end mass on the lateral vibration.

In the simulation, the specifications of the cantilever beam are: the density $\rho = 2800 \text{ kg/m}^3$, modulus of elasticity $E = 70.9 \text{ GPa}$, thickness $b = 3.175 \text{ mm}$, height $h = 50.8 \text{ mm}$.

The trapezoidal velocity profile shown in Figure 2.2, is used and two scenarios are considered.

Scenario A: axial extension in which the beam length varies from $L_{min} = 0.66 \text{ m}$ to $L_{max} =$

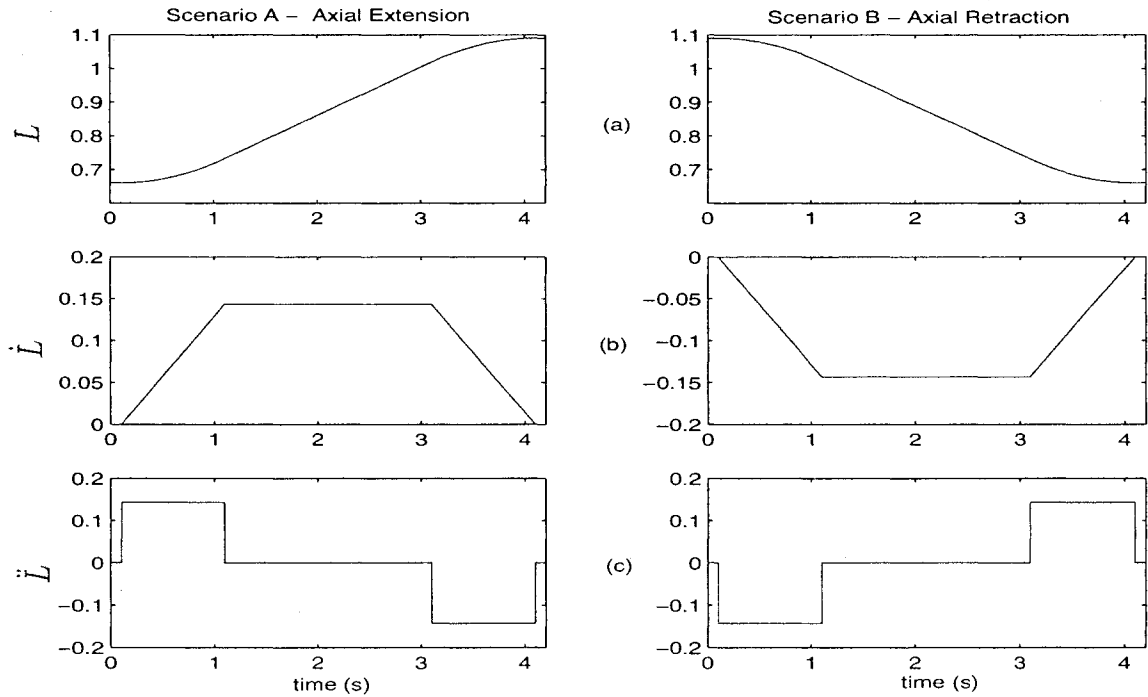


Figure 2.2: Axial motion profiles of Scenario A and Scenario B. (a) Axial displacement. (b) Axial velocity. (c) Axial acceleration.

1.09 m; Scenario B: axial retraction in which the beam length varies from $L_{max} = 1.09$ m to $L_{min} = 0.66$ m.

The first three natural frequencies of the shortest beam and the longest beam are given on Table 2.2. The highest frequency is 103.97 Hz. Therefore the time step Δt for the numerical

	$L=0.66$ m	$L=1.09$ m
f_1 (Hz)	5.92	2.17
f_2 (Hz)	37.13	13.61
f_3 (Hz)	103.97	38.12

Table 2.2: Natural frequencies of the beam with the shortest length and longest length

integration is chosen to be 0.0005 sec. The fourth order Runge-Kutta method is used to solve the equation numerically. In this simulation, the first three vibratory modes are considered. Thus the system order $n_x = 6$.

Simulations are performed with the end mass ($m_e = 0.4$ Kg) and without the end mass ($m_e = 0$ Kg). The axial force is also considered in the simulation. Initial conditions $[q_1(0) \ q_2(0) \ q_3(0)]$ are determined according to a prescribed deflection curve with $w(L, 0) = 0.01$ m to be, $[-394.29e^{-5} \ 10.26e^{-5} \ -3.95e^{-5}]$ for extension and $[-506.71e^{-5} \ 13.19e^{-5} \ -5.08e^{-5}]$ for retraction. This procedure is explained in Appendix A.3. Initial velocities are considered to be, $\dot{q}_1(0) = \dot{q}_2(0) = \dot{q}_3(0) = 0$ for extension and retraction.

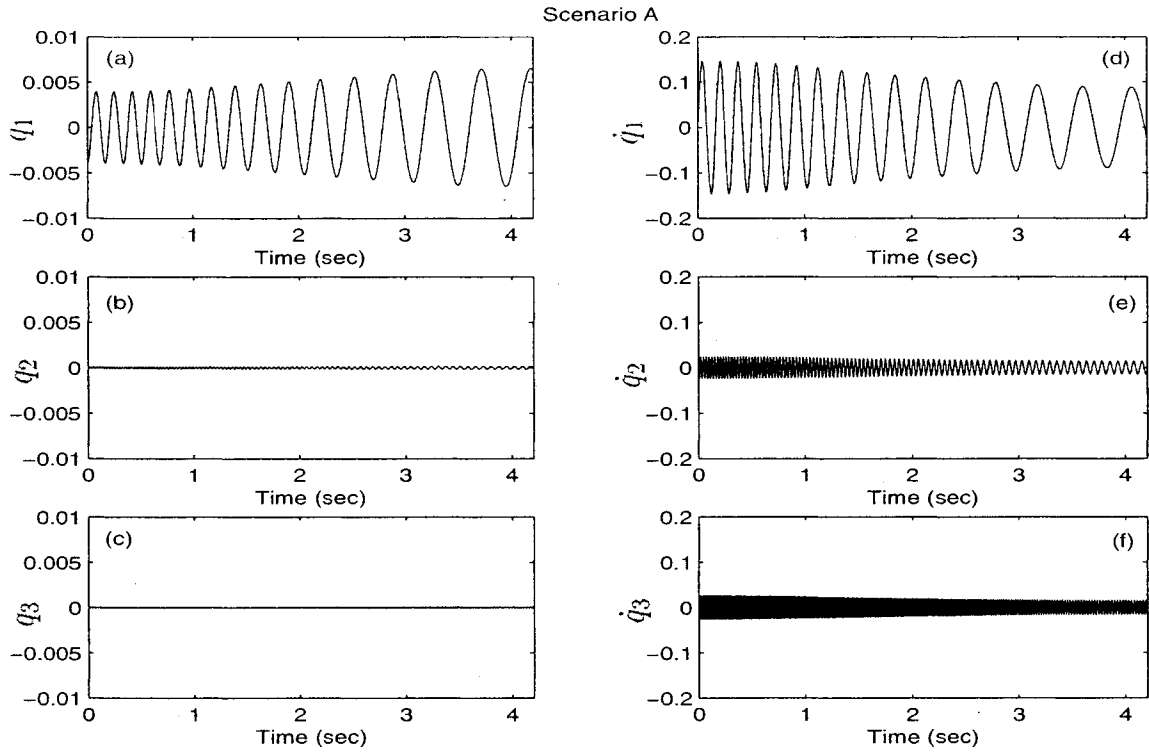


Figure 2.3: State response for axial extension without the end mass ($m_e = 0$). (a),(b),(c) generalized coordinates. (d),(e),(f) generalized velocities.

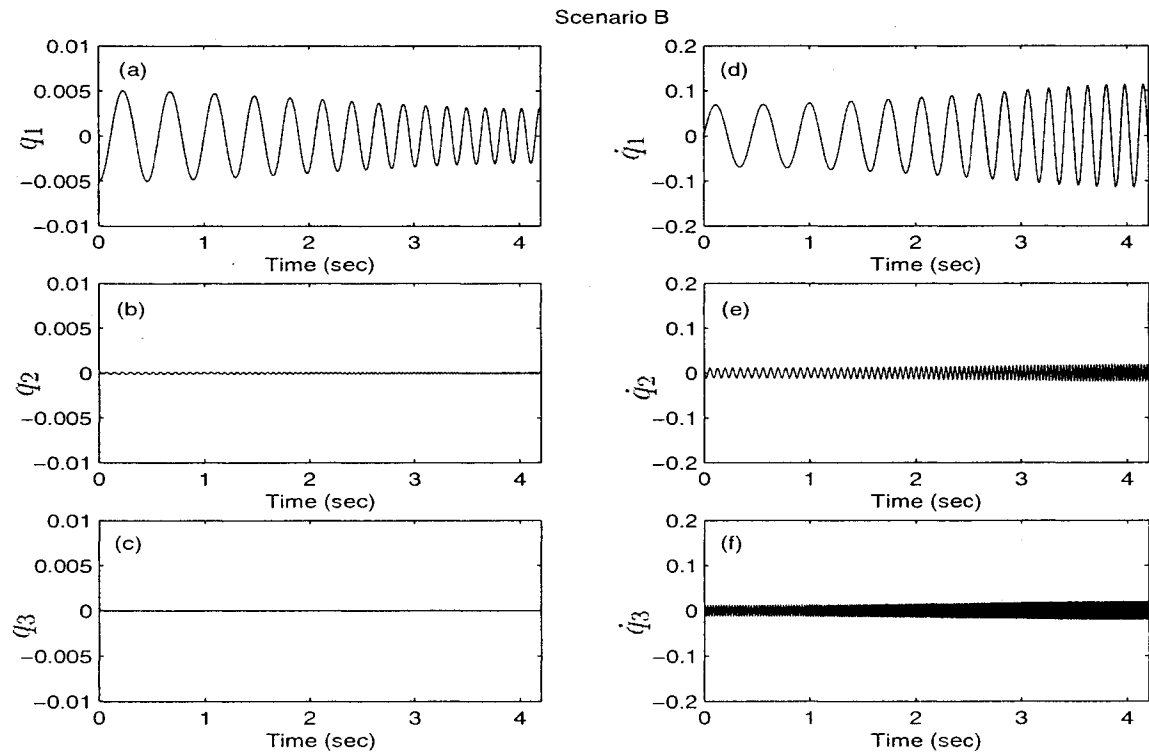


Figure 2.4: State response for axial retraction without the end mass ($m_e = 0$). (a),(b),(c) generalized coordinates. (d),(e),(f) generalized velocities.

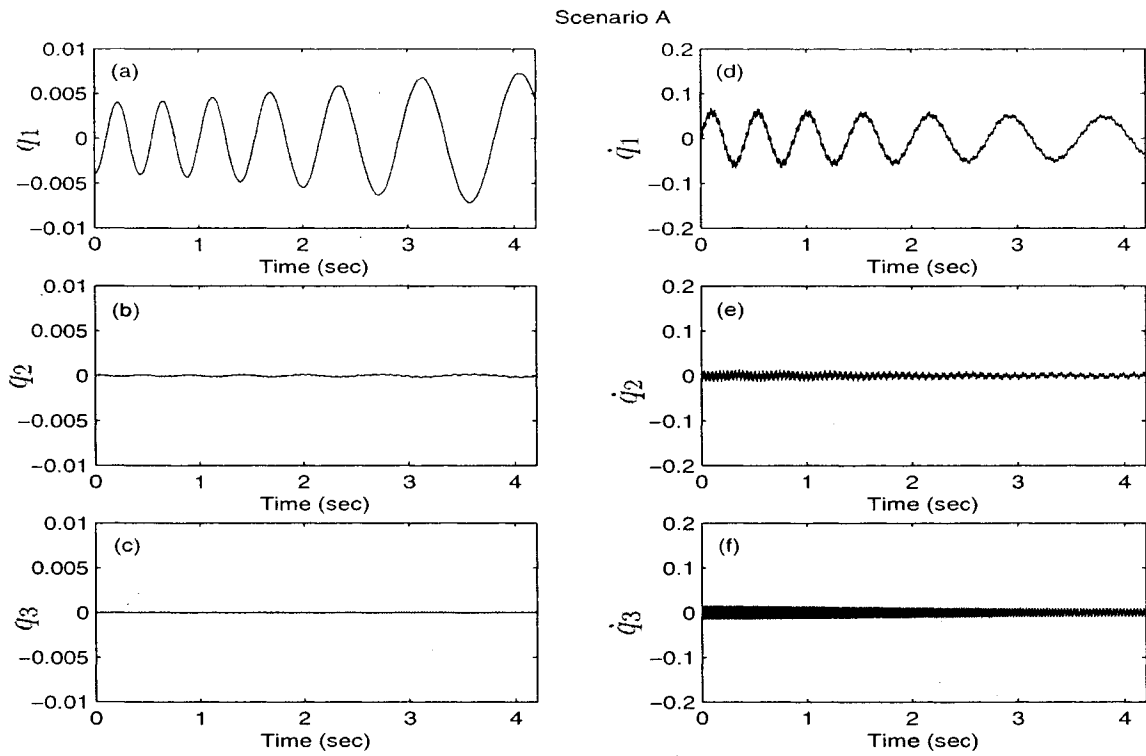


Figure 2.5: State response for axial extension with the end mass ($m_e = 0.4$ Kg). (a),(b),(c) generalized coordinates. (d),(e),(f) generalized velocities.

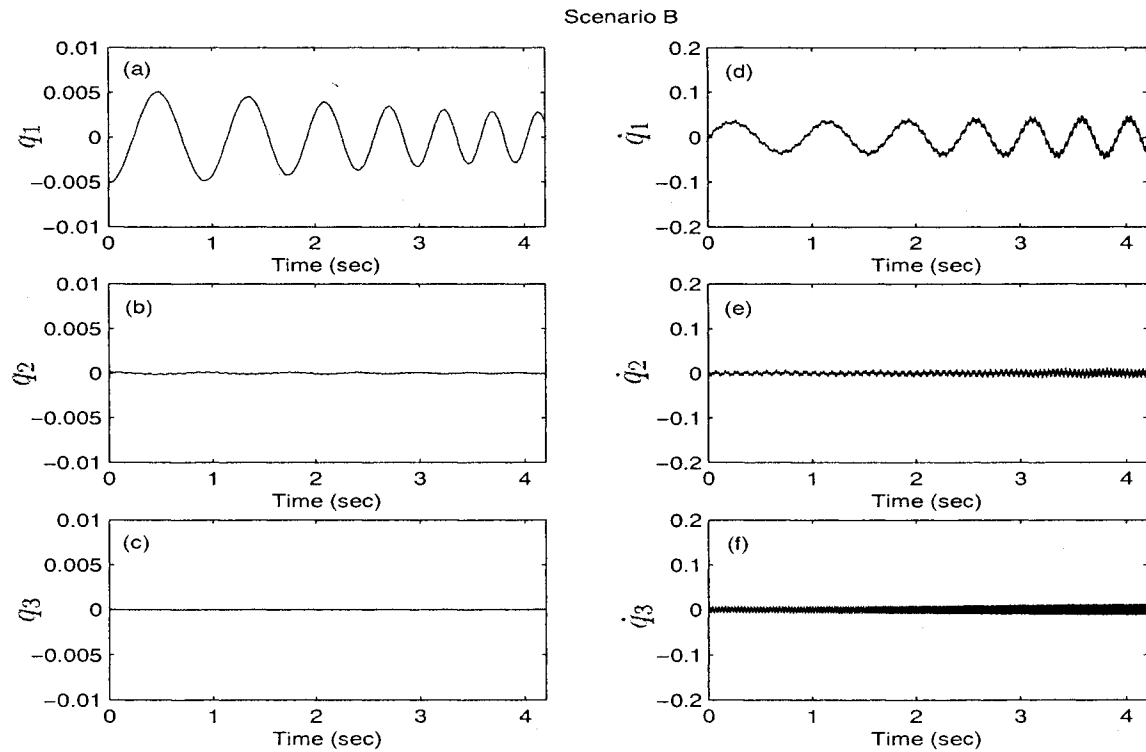


Figure 2.6: State response for axial retraction with the end mass ($m_e = 0.4$ Kg). (a),(b),(c) generalized coordinates. (d),(e),(f) generalized velocities.

From the state response in Figures 2.3 to 2.6, the following observations are drawn:

- The generalized coordinates and velocities in axial retraction is larger than those in axial extension. This is because, the initial stiffness of the beam in retraction is smaller than it is for extension.
- The magnitude of the generalized coordinates in axial extension shows increasing results, and the magnitude of the generalized velocities show decreasing results. For the retraction, the magnitude of the generalized coordinates is decreasing and the magnitude of the generalized velocities is increasing. This is because of the variation of the beam stiffness. The axial extension reduces the stiffness of the beam, which makes the beam more flexible. The axial retraction increases the stiffness of the beam, which makes the beam's flexing more difficult.
- The magnitude of the first mode is much greater than the magnitude of the second and third modes in the generalized coordinates. The magnitude of the third mode is smaller than the magnitude of the first and the second modes in the generalized velocities.
- The presence of the end mass reduces the frequency of oscillation.

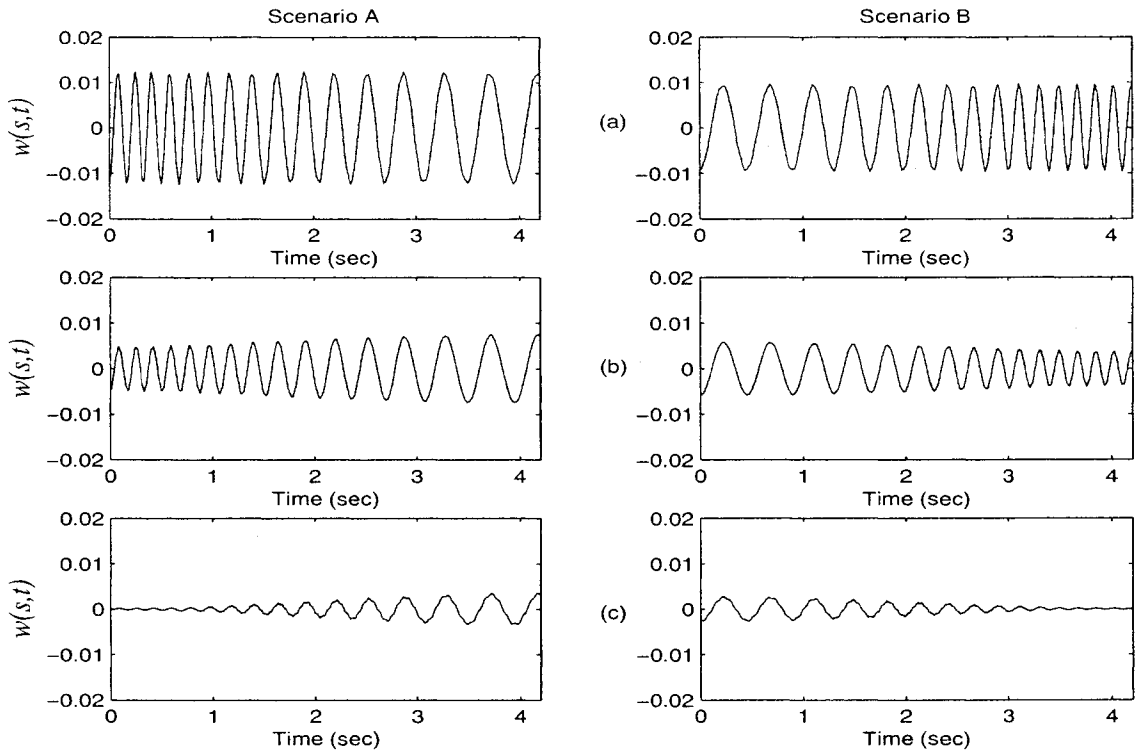


Figure 2.7: Displacement responses without the end mass. (a) Output at $r_1 = 0$ m, (b) Output at $r_1 = 0.3$ m, (c) Output at $r_1 = 0.6$ m.

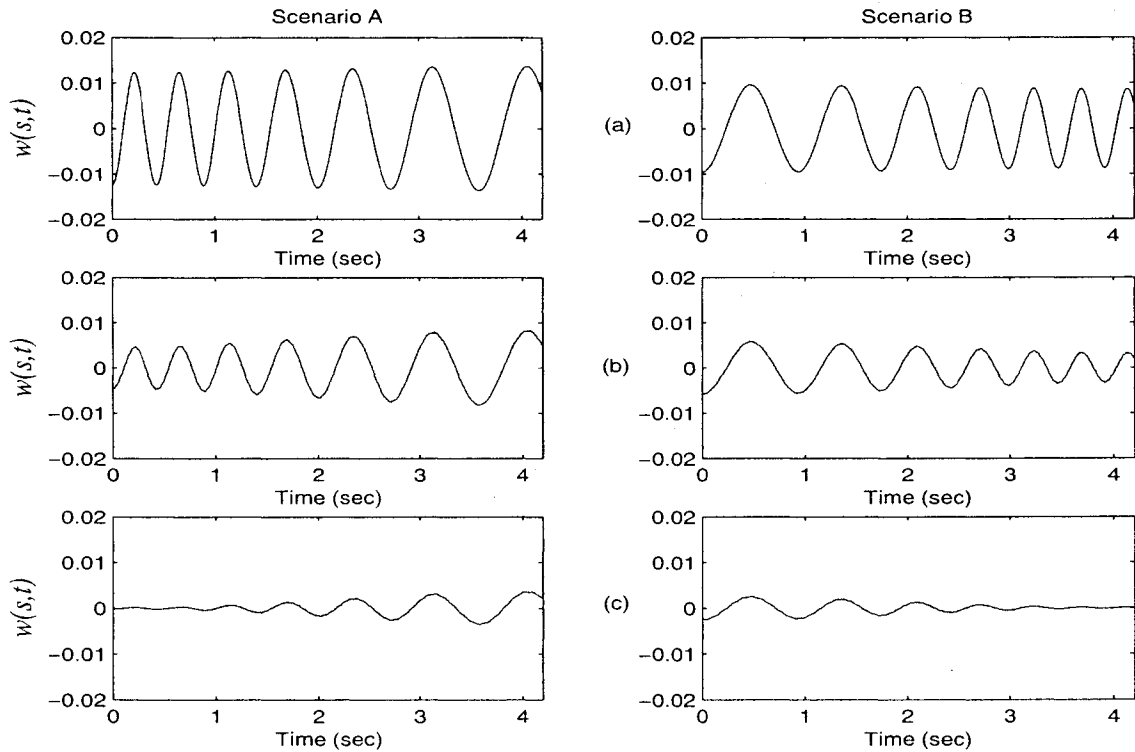


Figure 2.8: Displacement output responses with the end mass ($m_e = 0.4$ Kg). (a) Output at $r_1 = 0$ m, (b) Output at $r_1 = 0.3$ m, (c) Output at $r_1 = 0.6$ m.

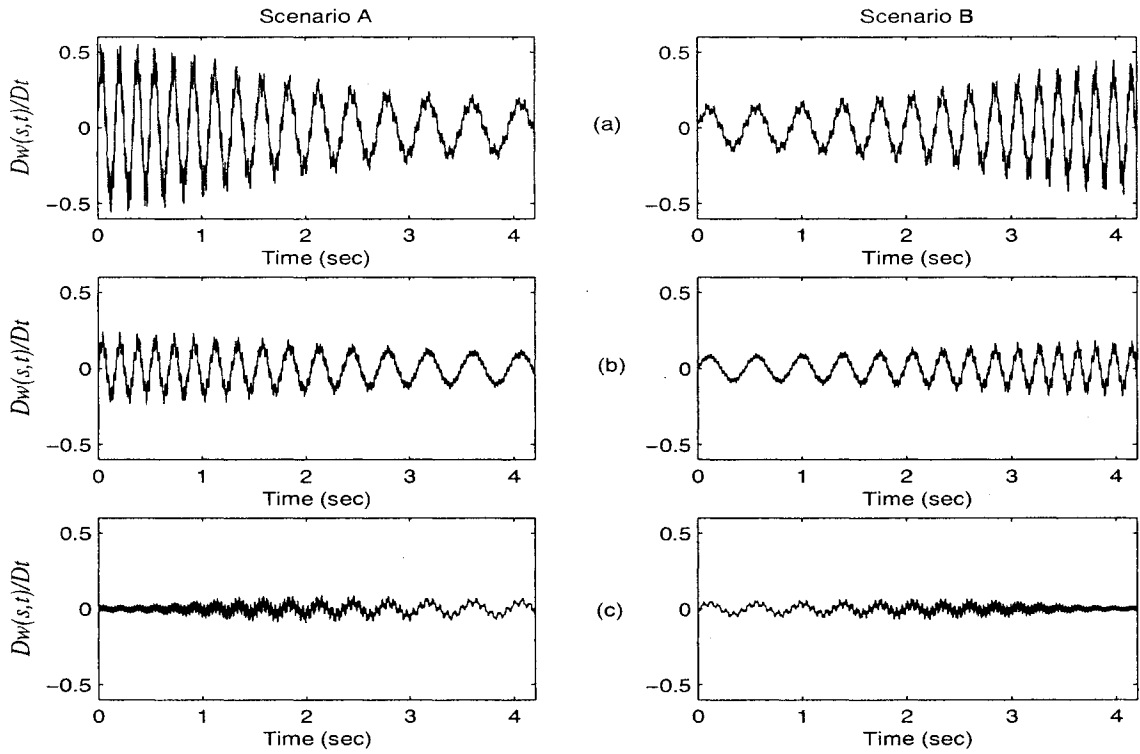


Figure 2.9: Velocity responses without the end mass. (a) Output at $r_1 = 0$ m, (b) Output at $r_1 = 0.3$ m, (c) Output at $r_1 = 0.6$ m.

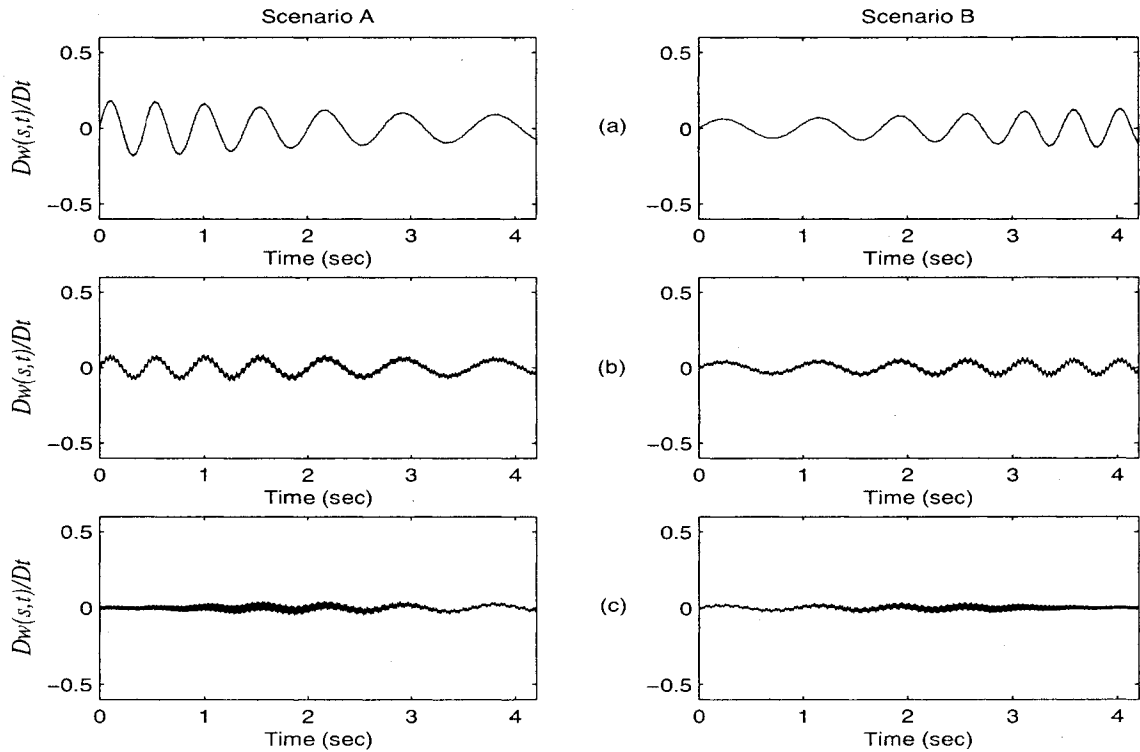


Figure 2.10: Velocity responses with the end mass ($m_e = 0.4$ Kg). (a) Output at $r_1 = 0$ m, (b) Output at $r_1 = 0.3$ m, (c) Output at $r_1 = 0.6$ m.

The beam displacement and velocity responses are observed at different locations. Three different location responses at $r_1 = 0$ m, $r_1 = 0.3$ m and $r_1 = 0.6$ m are presented in Figures 2.7 to 2.10. From them, the following observations are drawn:

- The magnitude of the first mode is much greater than the magnitude of the second and third modes in the deflection and velocity responses.
- The deflection and the velocity responses are larger in magnitude, as well as the rates of change in the magnitudes are smaller when they are observed at the tip of the beam.
- The deflection response shows that the end mass introduces destabilizing effect during extension and stabilizing effect during retraction. During extension the end mass introduces negative stiffness and negative damping effect, therefore the deflection is larger in magnitude. For retraction, the end mass introduces positive stiffness and positive damping effect, therefore the deflection is smaller.
- The presence of the end mass reduces the frequency of oscillation.

The vibration energy for axial extension and axial retraction are given on Figure 2.11 for $m_e = 0$ and $m_e = 0.4$. The individual energies T_b , U_b and T_e are given on Figure 2.12. In Figure 2.12 (a), the kinetic energy T_e caused by the end mass is zero and the strain energy U_{F_a} caused by the F_a is very small compared to all the other energies. Similarly, in Figure 2.12 (b), U_{F_a} is very small compared to all the other energies.

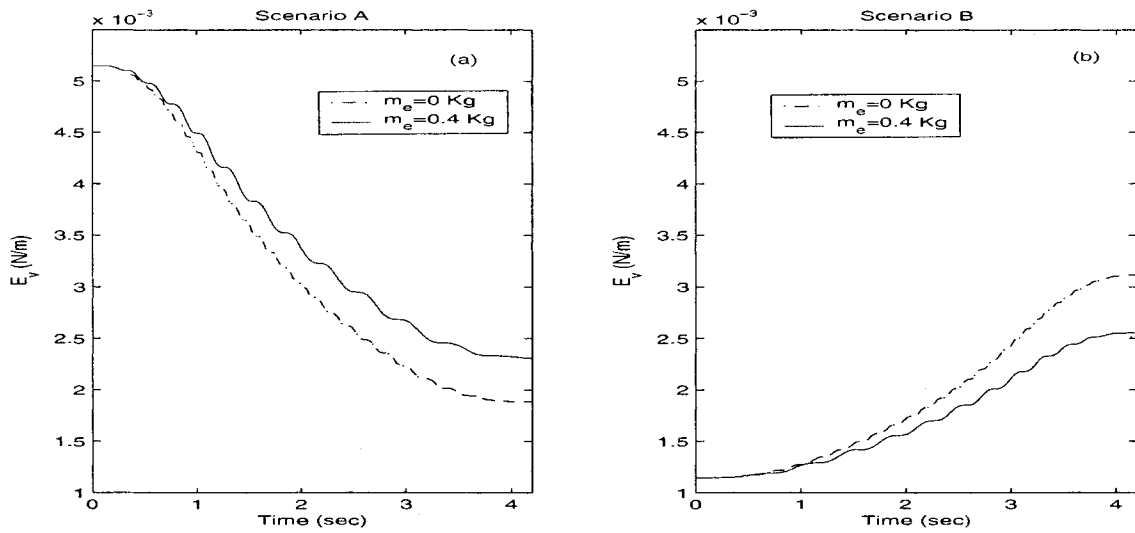


Figure 2.11: The vibration energies. (a) Axial extension, (b) Axial retraction. broken line represents the energy without end mass. Solid line represents the energy with end mass.

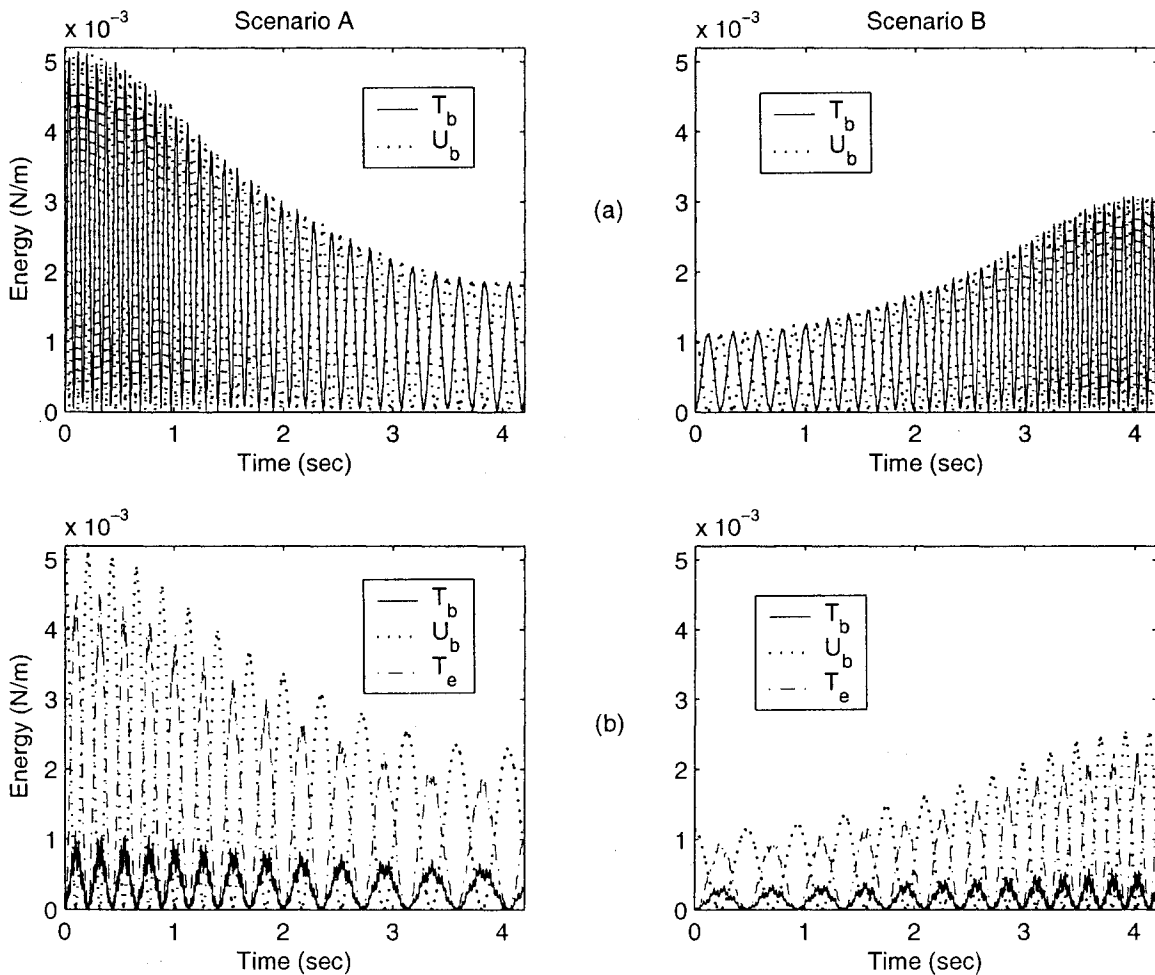


Figure 2.12: The energies. T -kinetic energy of the beam. U -potential energy of the beam T_e -kinetic energy of the end mass. (a) Energies when $m_e = 0$, (b) Energies when $m_e = 0.4$

From Figures 2.11 and 2.12 the following observations are drawn:

- The vibration energy of the beam decreases and increases monotonically during extension and retraction respectively.
- As the end mass increases, the vibration energy of the system increases for axial extension and decreases for axial retraction.
- The strain energy U_{F_a} caused by F_a is very small compared to all the other energies.

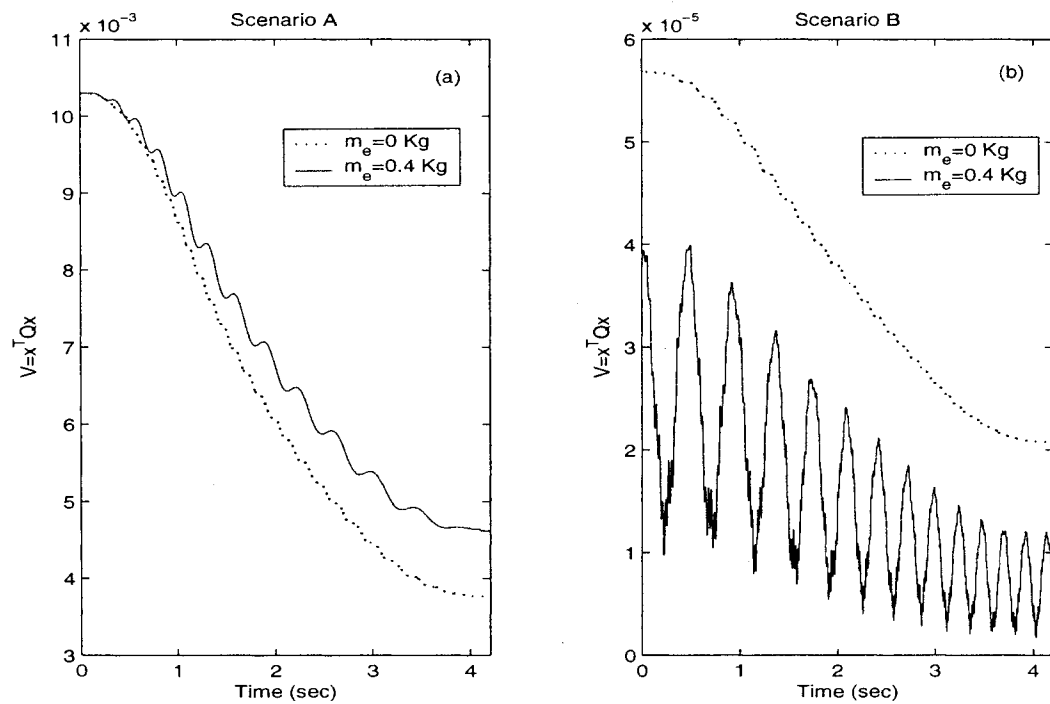


Figure 2.13: Lyapunov function $V = x^T Q x$. (a) Axial extension, (b) Axial retraction. Dotted line represents the energy without the end mass. Solid line represents the energy with the end mass.

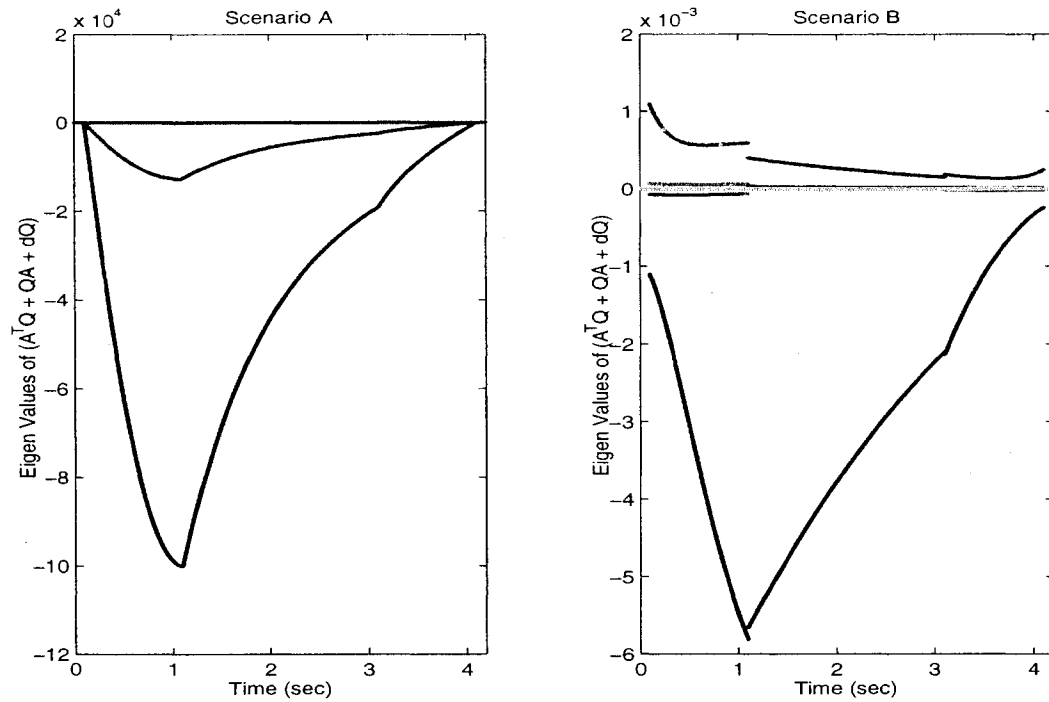


Figure 2.14: Eigenvalues of the Lyapunov stability condition $A^T(t)Q(t) + Q(t)A(t) + \dot{Q}(t)$. (a) Axial extension, (b) Axial retraction.

From Figures 2.13 and 2.14 the following observations are drawn:

- Lyapunov function in Figure 2.13 shows decaying results in both extension and retraction.
- The eigenvalues of the matrix $A^T(t)Q(t) + Q(t)A(t) + \dot{Q}(t)$ from Equation (2.39) show that, for extension, the eigenvalues are either negative or zero, thus the system is stable. For retraction, some of the eigenvalues are positive, therefore the Lyapunov stability condition of (2.39) is not satisfied. The system is not uniformly exponentially stable.

2.7 Summary

- The mathematical model of the lateral vibration of the axially moving cantilever beam is presented. The model is a linear time-varying system.
- The model further includes the effect of an end mass attached to the tip of the beam.
- A computer simulation is conducted. The beam axial motion is assumed to have a trapezoidal velocity profile.
- The deflection and the velocity output responses are sensed at the tip, middle and base locations.
- The difference between the system's vibration energy with and without an end mass is discussed.
- The stability of the system is analyzed using the Lyapunov function.

Chapter 3

Direct Velocity Feedback Control of Lateral Vibration of an Axially Moving Cantilever Beam

This chapter is organized as follows: Section 3.1 describes the use of piezoelectric actuators and their control actions through velocity feedback on the axially moving cantilever beam. Section 3.2 describes the systems with constant gain feedback control. Section 3.3 explains the main challenge in this research, which is the spillover instability problem. Section 3.4 shows the stability analysis of a slowly-varying linear system. Section 3.5 explains the frozen system and its eigenvalues. Section 3.6 gives the proposed control strategies to control the vibration with two-output and three-output feedback system. Section 3.7 shows the computer simulations of the closed-loop responses and the observations. Section 3.8 is a brief summary of the chapter.

3.1 Velocity Feedback Control

Figure 3.1 shows the model of the axially moving cantilever beam, attached with two piezoelectric (PZT) actuators. The PZT actuators are located over the region of $s_{in1}(t)$ and $s_{in2}(t)$. The polarity of the voltage applied to the PZT plates is chosen in such a way that the PZT plate on one side expands while the PZT plate on the other side contracts and vice versa. Such an action results in a pair of concentrated bending moments exerted at locations $s_{in1}(t)$ and $s_{in2}(t)$ respectively [29]. The output sensor is located at $s_1(t)$.

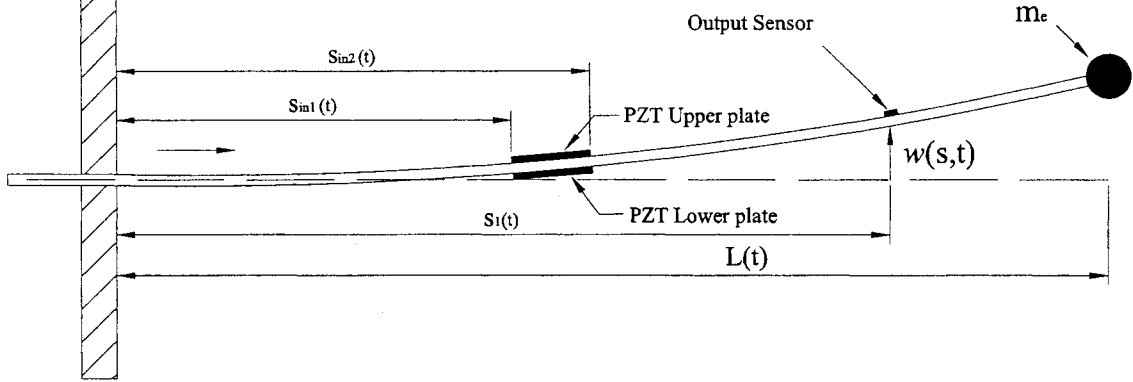


Figure 3.1: Axially moving cantilever beam system with PZT actuators

The Lagrangian equation for the beam is given as

$$\frac{d}{dt} \frac{\partial T}{\partial \dot{q}} - \frac{\partial T}{\partial q} + \frac{\partial U}{\partial q} = Q_F \quad (3.1)$$

where the terms on the left-hand side of the equation have been obtained in the previous chapter and Q_F is the generalized force vector caused by the PZT actuating moments. To find Q_F , the virtual work produced by the PZT actuating moments is given by [6].

$$\delta W = \int_0^L M_p'' \delta w ds \quad (3.2)$$

and the moment M_p is given by

$$M_p = g_p V(t) [H(s - s_{in1}) - H(s - s_{in2})] \quad (3.3)$$

where g_p is a constant related to the properties of the PZT material, $V(t)$ is the voltage applied to the PZT layers and $H(\cdot)$ is the Heaviside step function.

Substituting Equation (3.3) in Equation (3.2) gives

$$\begin{aligned} \delta W &= g_p V(t) \int_0^L \frac{\partial^2}{\partial s^2} [H(s - s_{in1}) - H(s - s_{in2})] \delta w ds \\ &= g_p V(t) \int_0^L \frac{\partial}{\partial s} [\delta(s - s_{in1}) - \delta(s - s_{in2})] \delta w ds \end{aligned} \quad (3.4)$$

where $\delta(s - s_{in1})$ and $\delta(s - s_{in2})$ are *Dirac Delta* functions. Solving Equation (3.4) using integration by parts, results in

$$\begin{aligned}\delta W &= g_p V(t) \left[\delta w [\delta(s - s_{in1}) - \delta(s - s_{in2})] - \int_0^L [\delta(s - s_{in1}) - \delta(s - s_{in2})] \delta w' ds \right] \\ &= g_p V(t) [\delta w'(s_{in2}, t) - \delta w'(s_{in1}, t)]\end{aligned}\quad (3.5)$$

Note that according to the properties of *Dirac Delta* function, $\delta(s - s_{in1}) = 0$ and $\delta(s - s_{in2}) = 0$. Also $\int_0^L [\delta(s - s_{in1})] \delta w' ds = \delta w'(s_{in1}, t)$ and $\int_0^L [\delta(s - s_{in2})] \delta w' ds = \delta w'(s_{in2}, t)$.

The derivative of the deflection with respect to the axial position is given by

$$\delta w'(s_{in}, t) = \frac{1}{L} \frac{1}{\sqrt{L}} \Psi'(\alpha_{in}) \delta q(t) \quad (3.6)$$

therefore, Equation (3.5) becomes

$$\delta W = \sum_{j=1}^n Q_{F_j} \delta q_j(t) \quad (3.7)$$

where

$$Q_{F_j} = g_p V(t) \frac{1}{L} \frac{1}{\sqrt{L}} [\psi'_j(\alpha_{in2}) - \psi'_j(\alpha_{in1})] \quad (3.8)$$

and

$$Q_F = g_p A_8 V(t) \quad (3.9)$$

where

$$A_8 = \frac{1}{L} \frac{1}{\sqrt{L}} [\Psi'(\alpha_{in2}) - \Psi'(\alpha_{in1})]^T \quad (3.10)$$

The equation of motion (3.1) becomes

$$M(t)\ddot{q} + D(t)\dot{q} + K(t)q = B_1(t)V(t) \quad (3.11)$$

where $M(t)$, $D(t)$ and $K(t)$ are given in Equation (2.23) and

$$B_1(t) = g_p A_8 \quad (3.12)$$

The state-space representation is given by

$$\dot{x} = A(t)x(t) + B(t)V(t) \quad (3.13)$$

For a direct velocity feedback, the voltage $V(t)$ applied to the PZT actuators is taken to be proportional to the velocity output,

$$V(t) = -g_{v1}y(t) \quad (3.14)$$

where g_{v1} is the feedback gain. If the velocity of lateral motion at $s_1 = L - r_1$ is measured, the output is given by

$$y(t) = C(t)x(t) \quad (3.15)$$

where

$$C(t) = \left[\frac{\dot{L}}{L} \frac{1}{\sqrt{L}} \left\{ -\frac{1}{2}\Psi(\alpha_1) + (1 - \alpha_1)\Psi'(\alpha_1) \right\} \quad \frac{1}{\sqrt{L}}\Psi(\alpha_1) \right] \quad (3.16)$$

with $\alpha_1 = \frac{s_1}{L}$. With such a feedback scheme, the state equation becomes

$$\dot{x}(t) = A(t)x(t) - B(t)g_{v1}C(t)x(t) = \bar{A}(t)x(t) \quad (3.17)$$

where $\bar{A}(t)$ is the closed-loop system matrix given as

$$\bar{A}(t) = \begin{bmatrix} 0_{n \times n} & I \\ -\bar{K}(t) & -\bar{D}(t) \end{bmatrix} \quad (3.18)$$

where

$$\begin{aligned} \bar{K}(t) &= M^{-1}(t)K(t) + M^{-1}(t)B_1(t)g_{v1} \left[\frac{\dot{L}}{L} \frac{1}{\sqrt{L}} \left\{ -\frac{1}{2}\Psi(\alpha_1) + (1 - \alpha_1)\Psi'(\alpha_1) \right\} \right] \\ \bar{D}(t) &= M^{-1}(t)D(t) + M^{-1}(t)B_1(t)g_{v1} \frac{1}{\sqrt{L}}\Psi(\alpha_1) \\ B(t) &= \begin{bmatrix} 0_{n \times 1} \\ B_1(t) \end{bmatrix} \end{aligned} \quad (3.19)$$

If $V(t)$ is taken to be proportional to two velocity outputs,

$$V(t) = - \begin{bmatrix} g_{v1} & g_{v2} \end{bmatrix} \begin{bmatrix} y_1(t) \\ y_2(t) \end{bmatrix} \quad (3.20)$$

where g_{v1} and g_{v2} are two feedback gains corresponding to the outputs at locations $s_1 = L - r_1$ and $s_2 = L - r_2$. The velocity outputs are given by

$$\begin{bmatrix} y_1(t) \\ y_2(t) \end{bmatrix} = C(t)x(t) \quad (3.21)$$

where

$$C(t) = \begin{bmatrix} \frac{\dot{L}}{L} \frac{1}{\sqrt{L}} \left\{ -\frac{1}{2} \Psi(\alpha_1) + (1 - \alpha_1) \Psi'(\alpha_1) \right\} & \frac{1}{\sqrt{L}} \Psi(\alpha_1) \\ \frac{\dot{L}}{L} \frac{1}{\sqrt{L}} \left\{ -\frac{1}{2} \Psi(\alpha_2) + (1 - \alpha_2) \Psi'(\alpha_2) \right\} & \frac{1}{\sqrt{L}} \Psi(\alpha_2) \end{bmatrix} \quad (3.22)$$

With such feedback scheme, the state equation becomes

$$\dot{x}(t) = A(t)x(t) - B(t) \begin{bmatrix} g_{v1} & g_{v2} \end{bmatrix} C(t)x(t) = \bar{A}(t)x(t) \quad (3.23)$$

where

$$\bar{A}(t) = \begin{bmatrix} 0_{n \times n} & I \\ -\bar{K}(t) & -\bar{D}(t) \end{bmatrix}$$

and

$$\begin{aligned} \bar{K}(t) &= M^{-1}(t)K(t) + M^{-1}(t)B_1(t) \begin{bmatrix} g_{v1} & g_{v2} \end{bmatrix} \begin{bmatrix} \frac{\dot{L}}{L} \frac{1}{\sqrt{L}} \left\{ -\frac{1}{2} \Psi(\alpha_1) + (1 - \alpha_1) \Psi'(\alpha_1) \right\} \\ \frac{\dot{L}}{L} \frac{1}{\sqrt{L}} \left\{ -\frac{1}{2} \Psi(\alpha_2) + (1 - \alpha_2) \Psi'(\alpha_2) \right\} \end{bmatrix} \\ \bar{D}(t) &= M^{-1}(t)D(t) + M^{-1}(t)B_1(t) \begin{bmatrix} g_{v1} & g_{v2} \end{bmatrix} \begin{bmatrix} \frac{1}{\sqrt{L}} \Psi(\alpha_1) \\ \frac{1}{\sqrt{L}} \Psi(\alpha_2) \end{bmatrix} \end{aligned} \quad (3.24)$$

3.2 Constant Gain Feedback

To study the response of the feedback system with constant gains, the following cases are considered.

- One output: collocated
- One output: noncollocated
- Two outputs: one collocated and one noncollocated
- Two outputs: both noncollocated

If the system parameters are considered to be frozen at the moment t , then the stability of the frozen system can be determined by the eigenvalues of \bar{A} . Following this idea, the constant

gains can be chosen such that the eigenvalues of \bar{A} are complex and expressed as

$$\lambda_i = -\zeta_i \omega_i + j \omega_i \sqrt{1 - \zeta_i^2} \quad (3.25)$$

where ω_i and ζ_i are referred to as i th natural frequency and damping ratio respectively, and $j = \sqrt{-1}$. To ensure the stability, all the damping ratios must be greater than or equal to zero.

An index can be defined to measure the system stability such that

$$J = \begin{cases} \sum_{i=1}^3 \zeta_i & \text{if all } \zeta_i > 0; \\ \text{sum of those } \zeta_i \text{'s that are less than zero} \end{cases} \quad (3.26)$$

Greater the index J , the more stable the feedback system or the faster the vibration diminishing. The gain is chosen such that the damping index J to be within 5% - 20% design range.

In the following computer simulation, the PZT actuators are located from $r_{in1} = 0.655$ m to $r_{in2} = 0.619$ m measured from the tip of the beam. The beam is released from a deflection caused by a concentrated force applied at the tip. The two motion scenarios used in the previous chapter are considered here again. The end mass is taken as zero.

Figures 3.2 to 3.6 show deflections, damping indexes J and state responses of feedback system with one output. Three different sensor locations $r_1 = 0$ m, $r_1 = 0.3$ m and collocated sensor $r_1 = 0.66$ m are used. The constant gain is $g_{v1} = 1$.

Figures 3.7 to 3.11 show deflections, damping indexes J and state responses of feedback system with two outputs. Responses with two noncollocated sensors ($r_1 = 0$ m and $r_2 = 0.3$ m) and with one noncollocated and one collocated sensors ($r_1 = 0.3$ m and $r_2 = 0.66$ m) are shown. The constant gains are $g_{v1} = 1$ and $g_{v2} = 1$.

From Figures 3.2 to 3.11, the following observations can be drawn:

- Most of the deflection responses are either diverging or temporarily diverging. It should be noted that the diverging responses are dominated by higher modes.
- The damping ratio and the damping index indicate that it is not possible to maintain the damping index always positive.
- The damping ratio of the first mode is always positive while the damping ratio of the second mode or third mode may become negative when the beam assumes a certain length.
- The damping ratio and the damping index of Scenario A show a mirror image of the damping ratio and the damping index of Scenario B.
- The responses of the generalized coordinates further confirm that the instability is caused by the higher modes. This phenomenon is referred to as spillover instability.

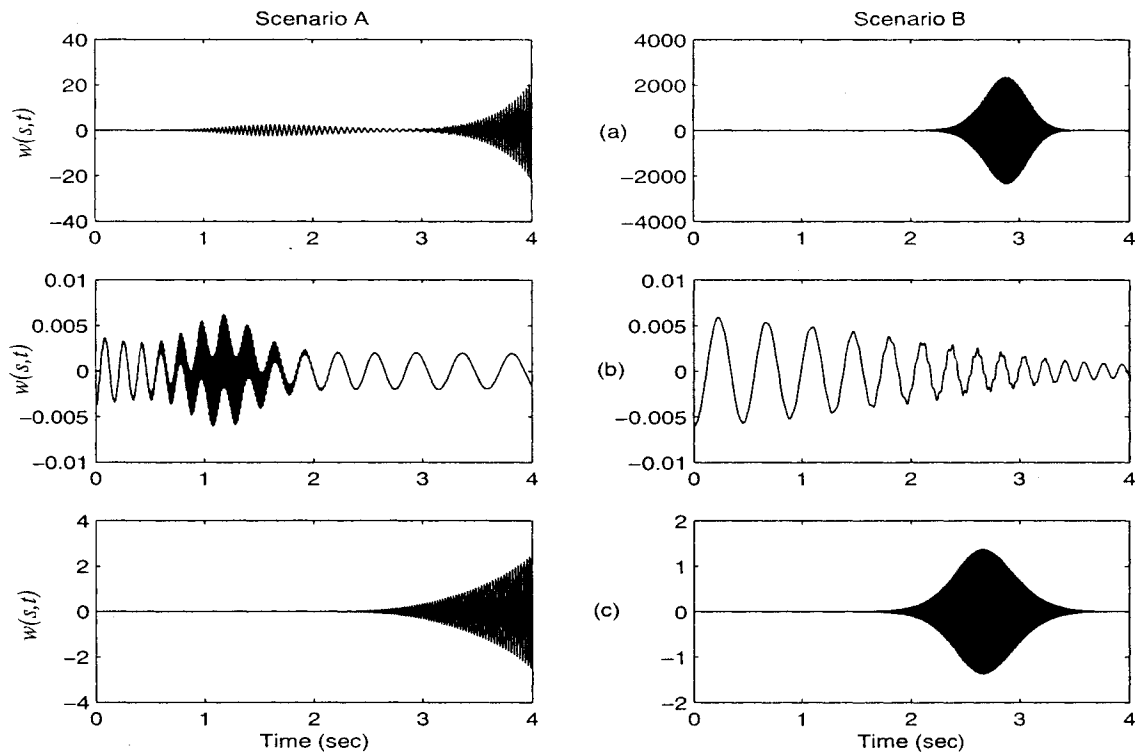


Figure 3.2: Deflection responses for Scenario A and Scenario B with one output feedback. (a) noncollocated $r_1 = 0$ m, (b) noncollocated $r_1 = 0.3$ m, (c) collocated $r_1 = 0.66$ m.

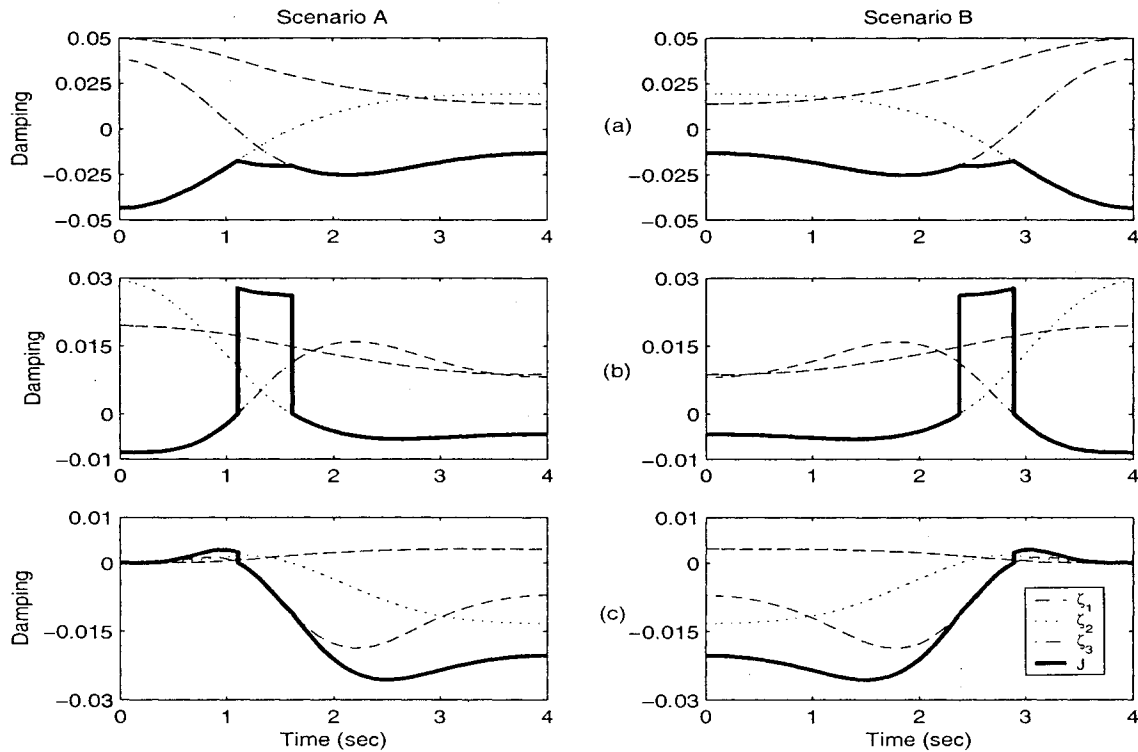


Figure 3.3: Damping ratios ζ_i and damping index J of one output feedback system for Scenario A and Scenario B. (a) noncollocated $r_1 = 0$ m, (b) noncollocated $r_1 = 0.3$ m, (c) collocated $r_1 = 0.66$ m.

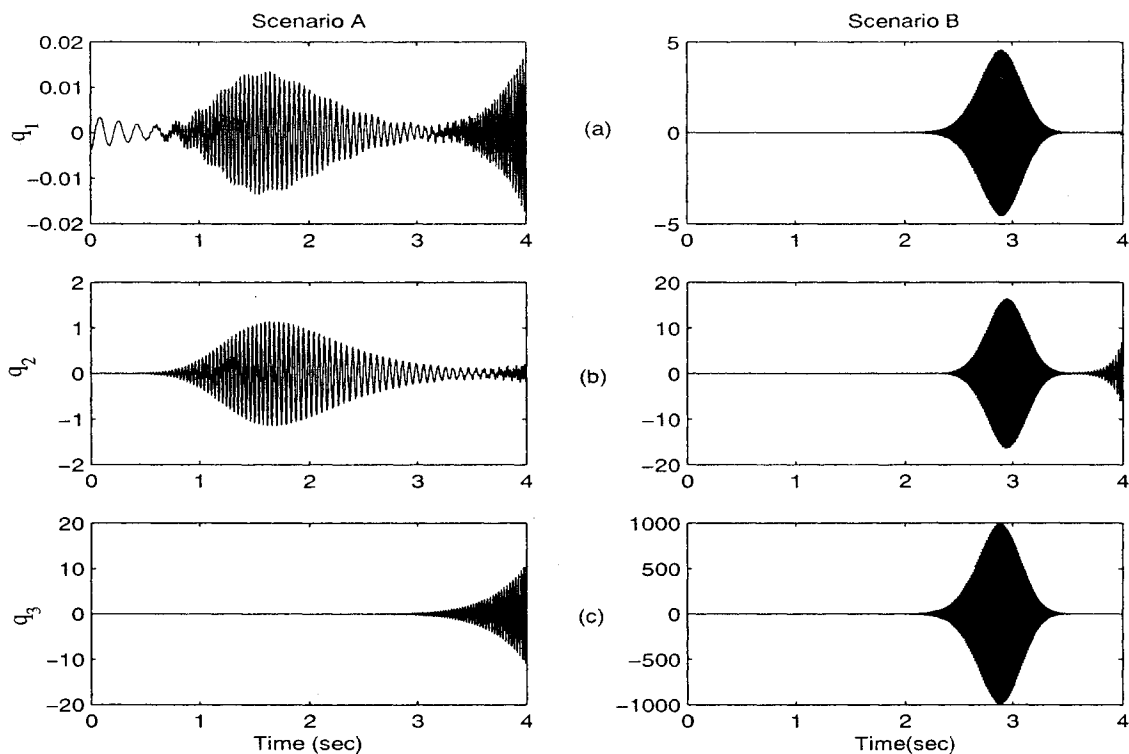


Figure 3.4: State responses of one output feedback system for Scenario A and Scenario B when $r_1 = 0$ m. (a) q_1 , (b) q_2 , (c) q_3 .

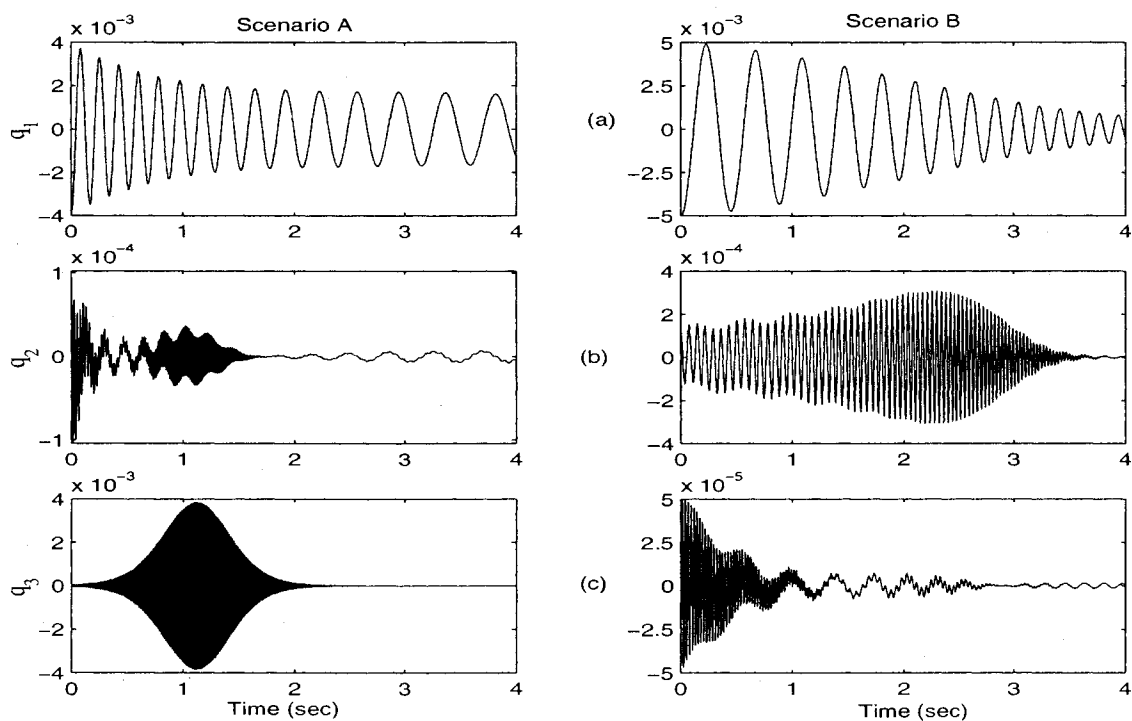


Figure 3.5: State responses of one output feedback system for Scenario A and Scenario B when $r_1 = 0.3$ m. (a) q_1 , (b) q_2 , (c) q_3 .

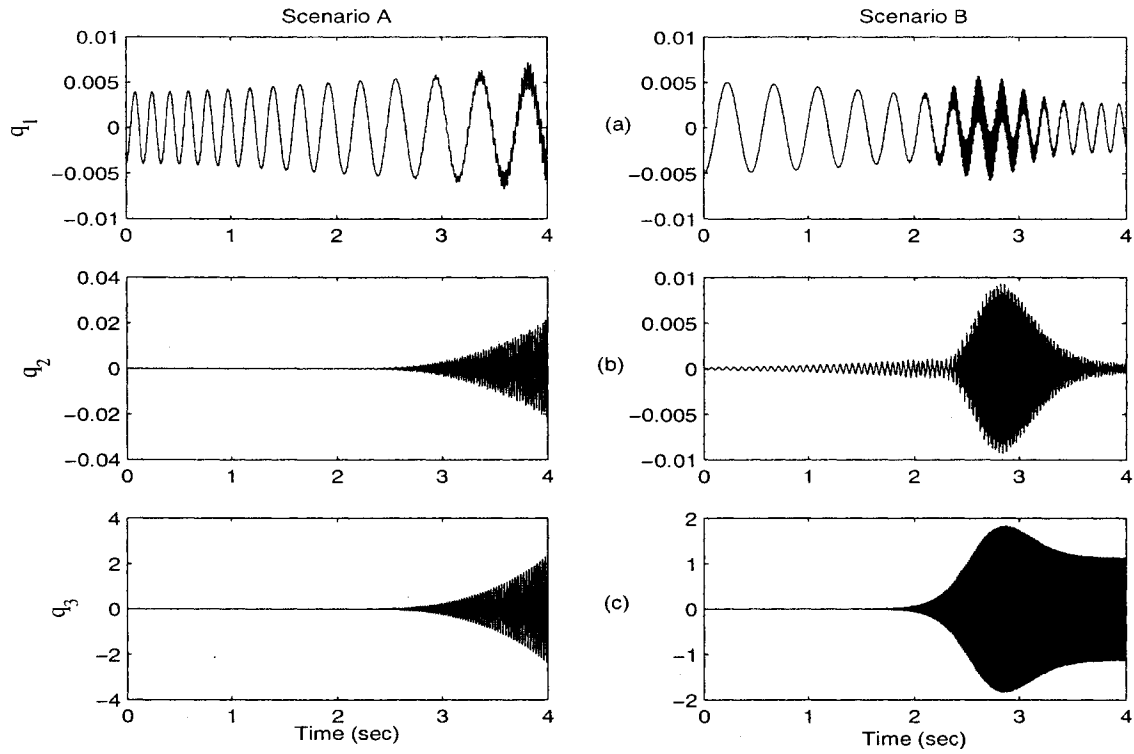


Figure 3.6: State responses of one output feedback system for Scenario A and Scenario B when $r_1 = 0.66$ m. (a) q_1 , (b) q_2 , (c) q_3 .

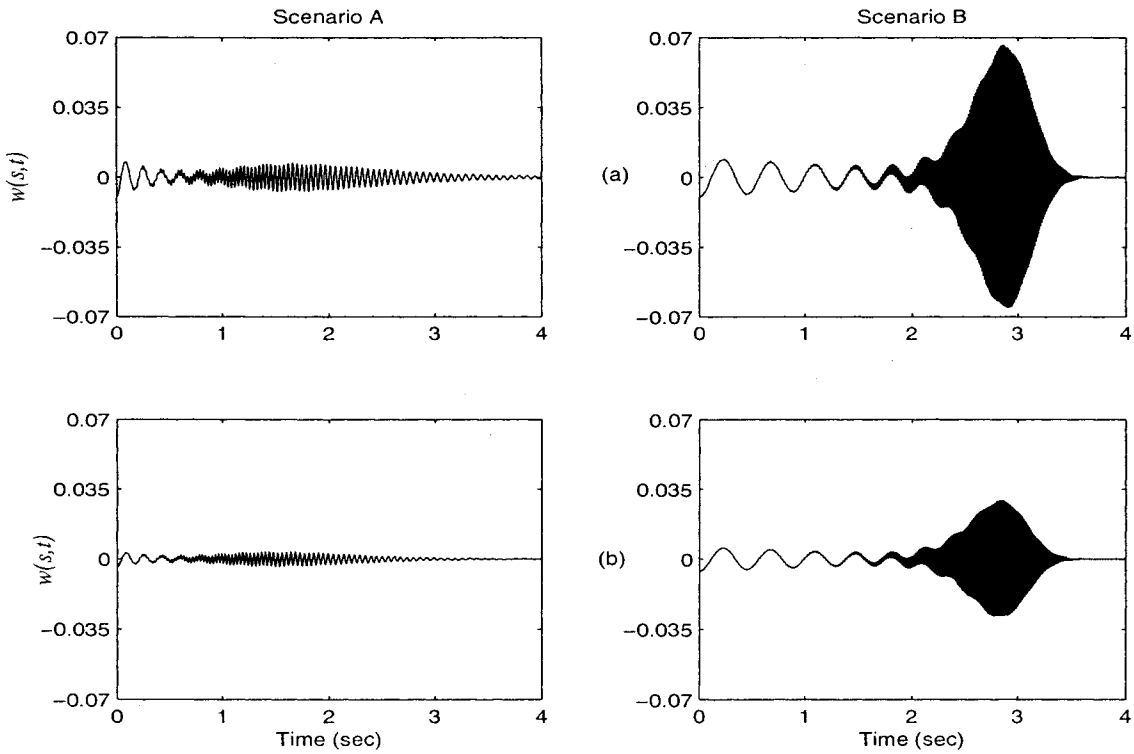


Figure 3.7: Deflection responses for Scenario A and Scenario B with two noncollocated outputs feedback. (a) $r_1 = 0$ m, (b) $r_2 = 0.3$ m.

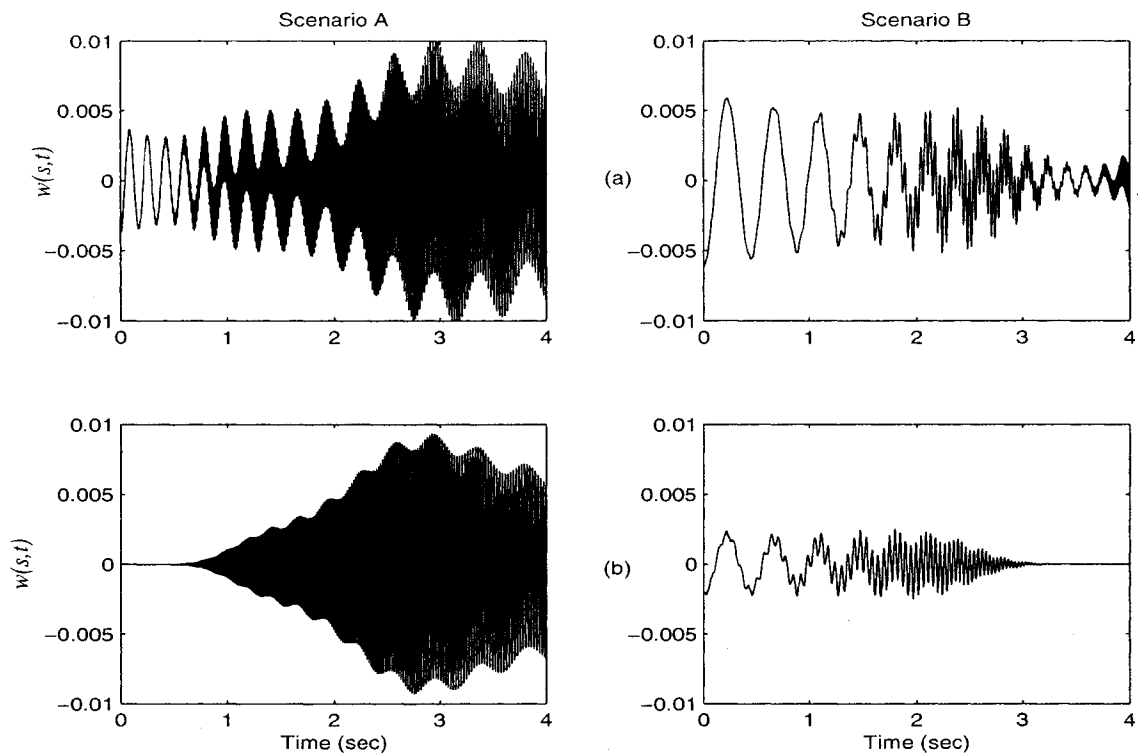


Figure 3.8: Deflection responses for Scenario A and Scenario B with one collocated and the other noncollocated outputs feedback. (a) $r_1 = 0.3$ m. (b) collocated $r_2 = 0.66$ m.

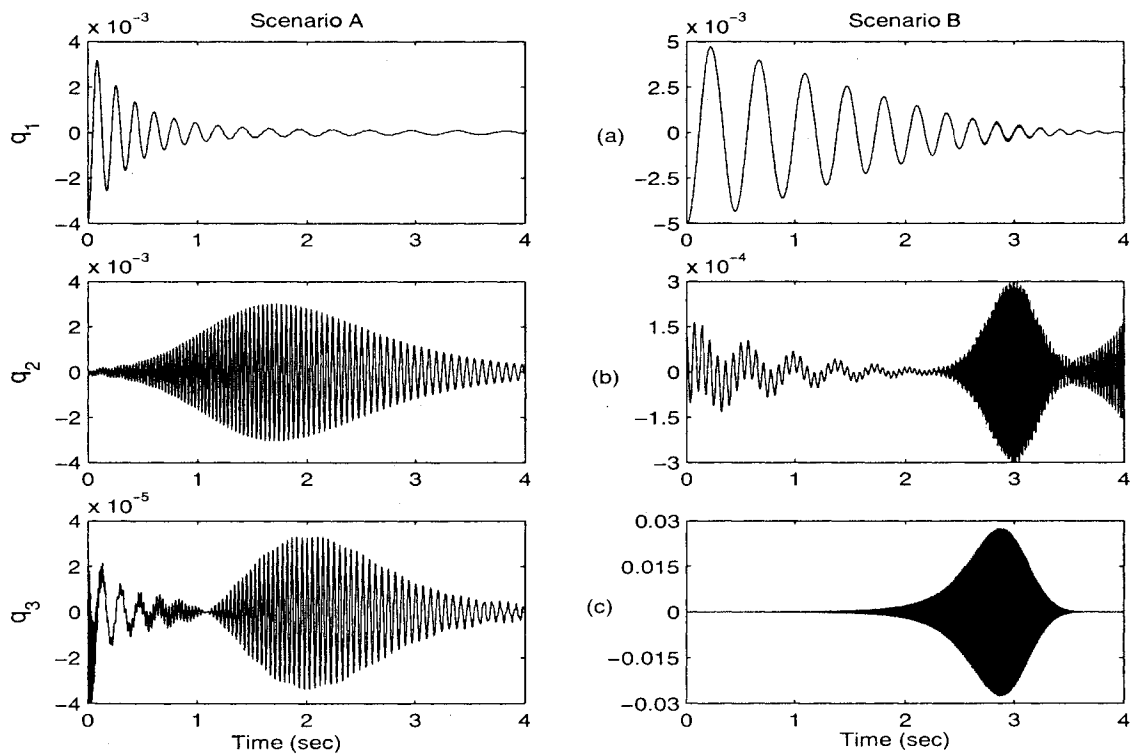


Figure 3.9: State responses of the two output feedback system for Scenario A and Scenario B when $r_1 = 0$ m and $r_2 = 0.3$ m. (a) q_1 , (b) q_2 , (c) q_3 .

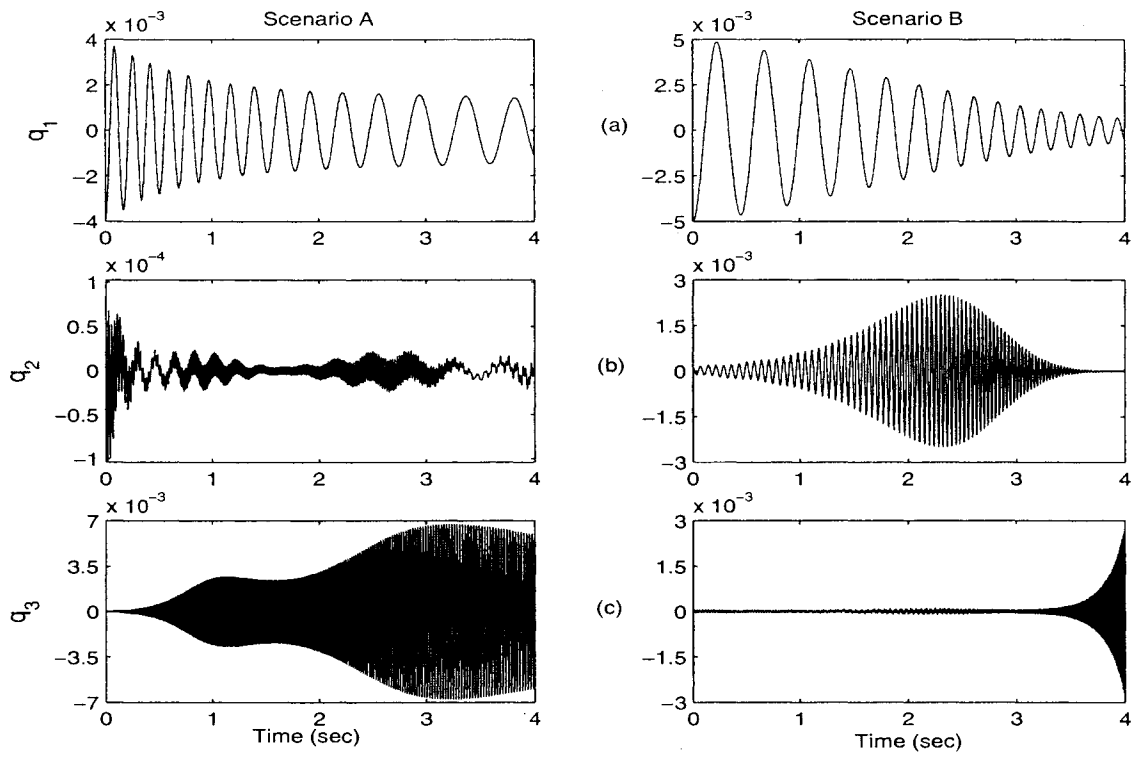


Figure 3.10: State responses of the two output feedback system for Scenario A and Scenario B when $r_1 = 0.3$ m and $r_2 = 0.66$ m. (a) q_1 , (b) q_2 , (c) q_3 .

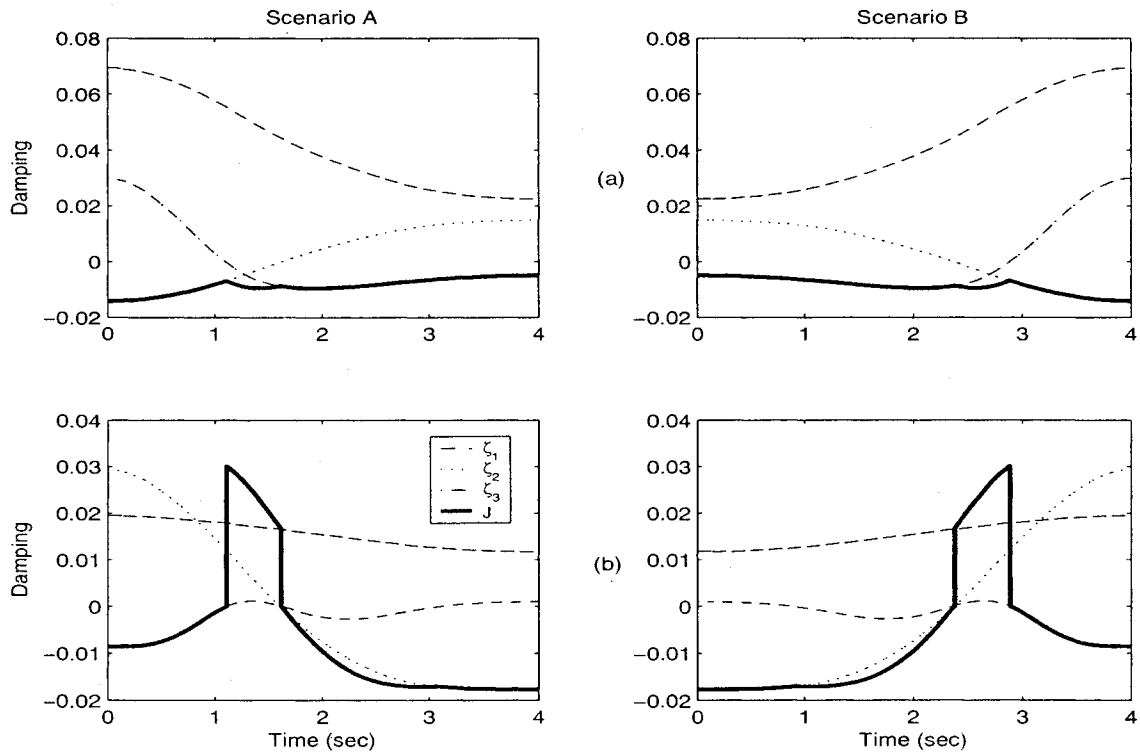


Figure 3.11: Damping ratios ζ_i and damping index J of two output feedback system for Scenario A and Scenario B. (a) $r_1 = 0$ m and $r_2 = 0.3$ m. (b) $r_1 = 0.3$ m $r_2 = 0.66$ m.

3.3 Spillover Instability

The challenge in this research is to use a single actuator to control the vibration of the time-varying system in the presence of higher modes. In essence, a velocity feedback is used to enhance the damping of the closed-loop system. The measurement of the sensor contains all the modes. When such a signal is feedback to an actuator, it may not be possible to ensure a positive damping effect for all the modes. When the feedback introduces a negative damping effect to a mode, the response of the mode will diverge instead of decaying. It is well known that a collocated control guarantees the stability of the first mode, not necessarily higher modes. Instability of higher modes due to a feedback is referred to as output spillover instability. The spillover poses an even greater challenge for the present system because the output matrix is time-varying.

3.4 Stability of a Slowly-Varying System

For multi-mode models, the following method can be used to determine the stability of the system if the system is slowly-varying. According to [13] *Theorem 8.7* says, for the open-loop linear state Equation (2.32) with continuously differentiable $A(t)$ there exist finite positive constants κ and ε such that, for all t ,

$$\|A(t)\| \leq \kappa \quad (3.27)$$

and every eigenvalue of $A(t)$ satisfies,

$$\operatorname{Re}[\lambda(t)] \leq -\varepsilon \quad (3.28)$$

then there exists a positive constant β such that if the time-derivative of $A(t)$ satisfies

$$\|\dot{A}(t)\| \leq \beta \quad \forall t \quad (3.29)$$

and the open-loop linear state Equation (2.32) is uniformly exponentially stable. The proof is summarized in Appendix A.4.

Similarly, for the closed-loop linear state Equation (3.17), Equation (3.27) becomes

$$\|\bar{A}(t)\| \leq \kappa \quad (3.30)$$

and every eigenvalue of $\bar{A}(t)$ satisfies,

$$\text{Re}[\lambda(t)] \leq -\varepsilon \quad (3.31)$$

then there exists a positive constant β such that if the time-derivative of $\bar{A}(t)$ satisfies

$$\|\dot{\bar{A}}(t)\| \leq \beta \quad \forall t \quad (3.32)$$

and the closed-loop linear state Equation (3.17) is uniformly exponentially stable. The proof is same as for the open-loop system given in Appendix A.4. The condition of (3.31) indicates that for a slowly-varying system, the stability can be determined by the eigenvalues of the matrix $\bar{A}(t)$.

3.5 Eigenvalues of the Frozen System

A “frozen” system is a stationary cantilever beam corresponding to any axial position at which the beam may stop. At the stopped moment, the system is a time invariant system. The equation of motion of the frozen system is given by

$$M\ddot{q} + \tilde{D}\dot{q} + \tilde{K}q = 0 \quad (3.33)$$

where

$$M = \mu A_1 \quad (3.34)$$

$$\tilde{K} = \frac{EI}{L^4} A_4 \quad (3.35)$$

$$\tilde{D} = B_1 g_v \frac{1}{\sqrt{L}} \Psi(\alpha_1) \quad (3.36)$$

The state-space representation is given by

$$\dot{x} = \bar{A}x(t) \quad (3.37)$$

where

$$\tilde{A} = \begin{bmatrix} 0_{n \times n} & I \\ -M^{-1}\tilde{K} & -M^{-1}\tilde{D} \end{bmatrix} \quad (3.38)$$

The stability of the frozen system can be defined by the eigenvalues of \tilde{A} defined as

$$\tilde{\lambda}_i = -\tilde{\zeta}_i\tilde{\omega}_i \pm j\tilde{\omega}_i\sqrt{1 - \tilde{\zeta}_i^2} \quad (3.39)$$

where $\tilde{\omega}_i$ and $\tilde{\zeta}_i$ are the i^{th} natural frequency and damping ratio of the frozen system, and $j = \sqrt{-1}$.

The stability of the frozen system can also be determined by the properties of the matrix \tilde{D} . According to [30] to find a stability condition, a Lyapunov function can be defined as

$$V = \frac{1}{2}\dot{q}^T\dot{q} + \frac{1}{2}q^T\tilde{K}q \quad (3.40)$$

Note that \tilde{K} is positive definite, and the derivative of V is given by

$$\begin{aligned} \dot{V} &= \dot{q}^T\ddot{q} + q^T\tilde{K}\dot{q} \\ &= \dot{q}^T(-\tilde{D}\dot{q} - \tilde{K}q) + q^T\tilde{K}\dot{q} \\ &= -\dot{q}^T\tilde{D}\dot{q} \end{aligned} \quad (3.41)$$

It shows that, if \tilde{D} is positive definite, the frozen system is stable. A asymmetric \tilde{D} matrix can be separated into two matrices

$$\tilde{D} = \frac{1}{2}(\tilde{D} + \tilde{D}^T) + \frac{1}{2}(\tilde{D} - \tilde{D}^T) \quad (3.42)$$

where, $(\tilde{D} + \tilde{D}^T)$ is a symmetric matrix and $(\tilde{D} - \tilde{D}^T)$ is a skew symmetric matrix with zero diagonal elements, which gives

$$\dot{q}^T \frac{\tilde{D} - \tilde{D}^T}{2} \dot{q} = 0 \quad (3.43)$$

and

$$\dot{V} = -\dot{q}^T \frac{\tilde{D} + \tilde{D}^T}{2} \dot{q} \quad (3.44)$$

Therefore, as long as $\frac{\tilde{D} + \tilde{D}^T}{2}$ is positive definite, the frozen system is stable. One of the necessary conditions for the positive definiteness of a symmetric matrix is that all its diagonal elements

must be positive, or \tilde{D}_{ii} must be positive. With the mode shape functions, \tilde{D}_{11} is always positive as $\psi_1(\alpha)$ increases monotonically. For the higher modes, \tilde{D}_{ii} may become negative when the beam takes certain lengths.

Figures 3.12 and 3.13 show the diagonal elements \tilde{D}_{ii} and the damping ratios ζ_i of the "frozen" system with collocated ($r_1 = 0.66$ m) and noncollocated ($r_1 = 0.17$ m) output sensors. Figures 3.14 and 3.15 show possible locations of sensors which would control the "frozen" feedback system.

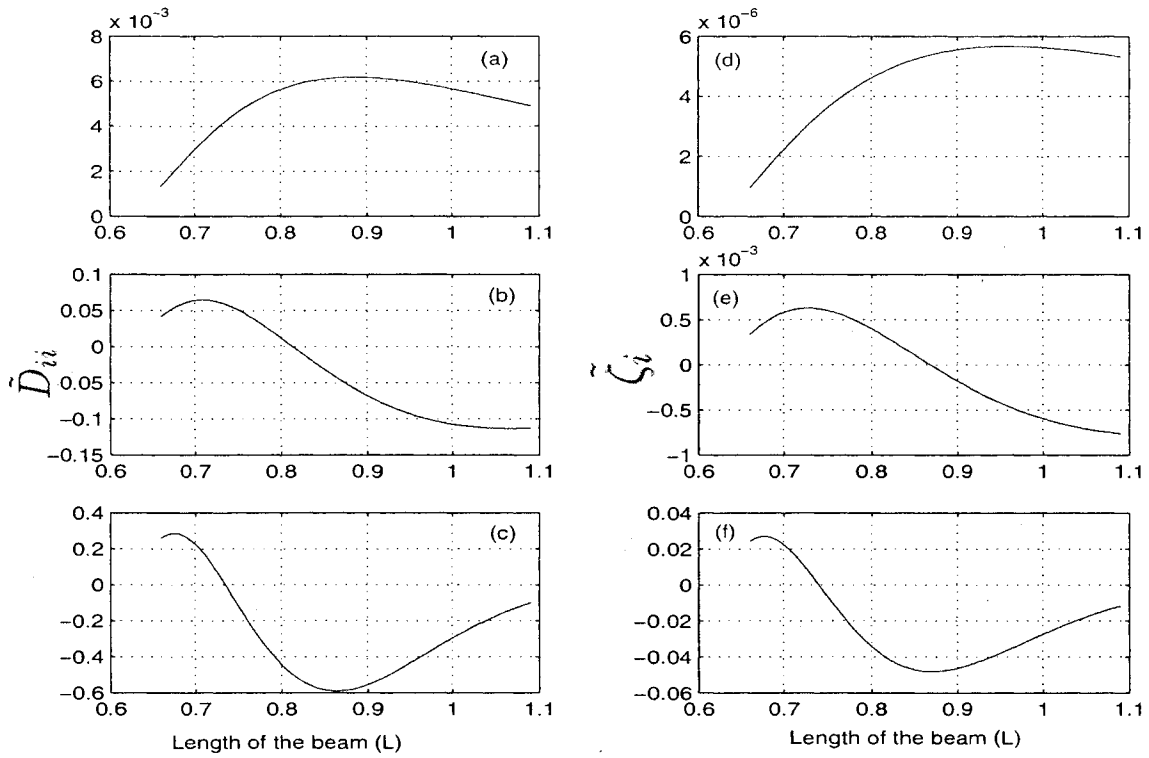


Figure 3.12: \tilde{D}_{ii} and $\tilde{\zeta}_i$ of the frozen system with $r_1 = 0.66$ m a collocated output feedback. (a),(d) $i = 1$. (b),(e) $i = 2$. (c),(f) $i = 3$.

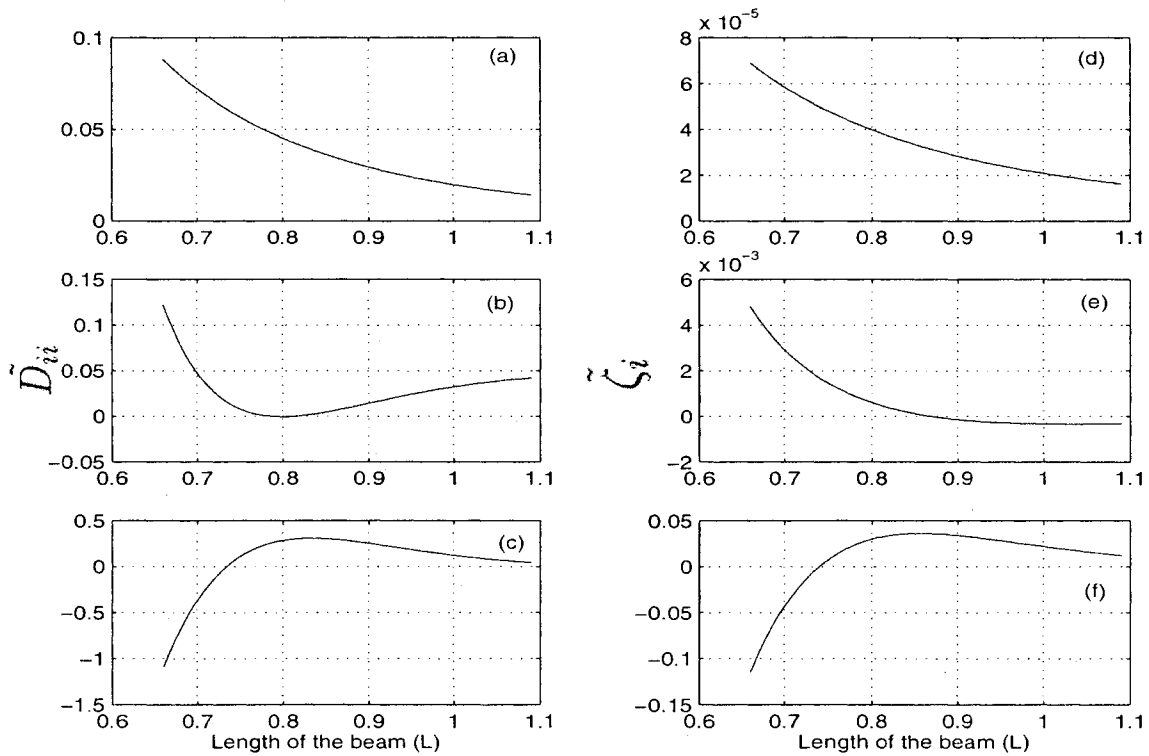


Figure 3.13: \tilde{D}_{ii} and $\tilde{\zeta}_i$ of the frozen system with a non-collocated output feedback $r_1 = 0.17$ m. (a),(d) $i = 1$. (b),(e) $i = 2$. (c),(f) $i = 3$.

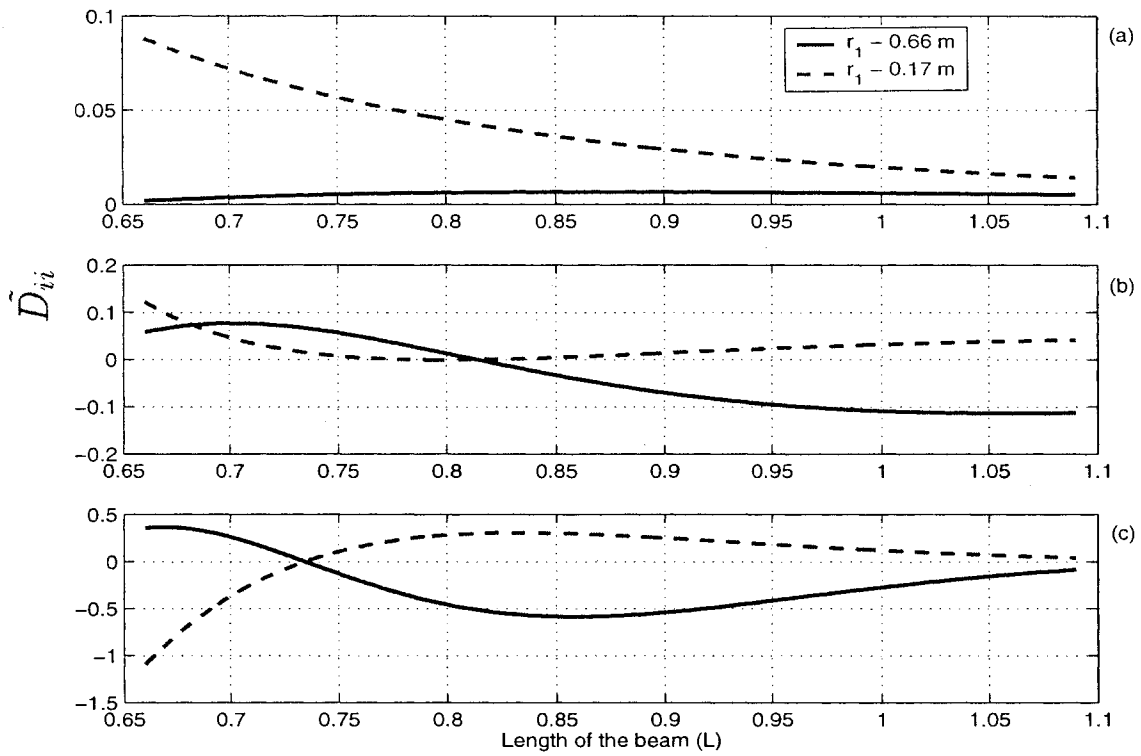


Figure 3.14: \tilde{D}_{ii} of the frozen system. Two sensors, Collocated $r_1 = 0.66$ m and non-collocated $r_1 = 0.17$ m. (a) $i = 1$. (b) $i = 2$. (c) $i = 3$.

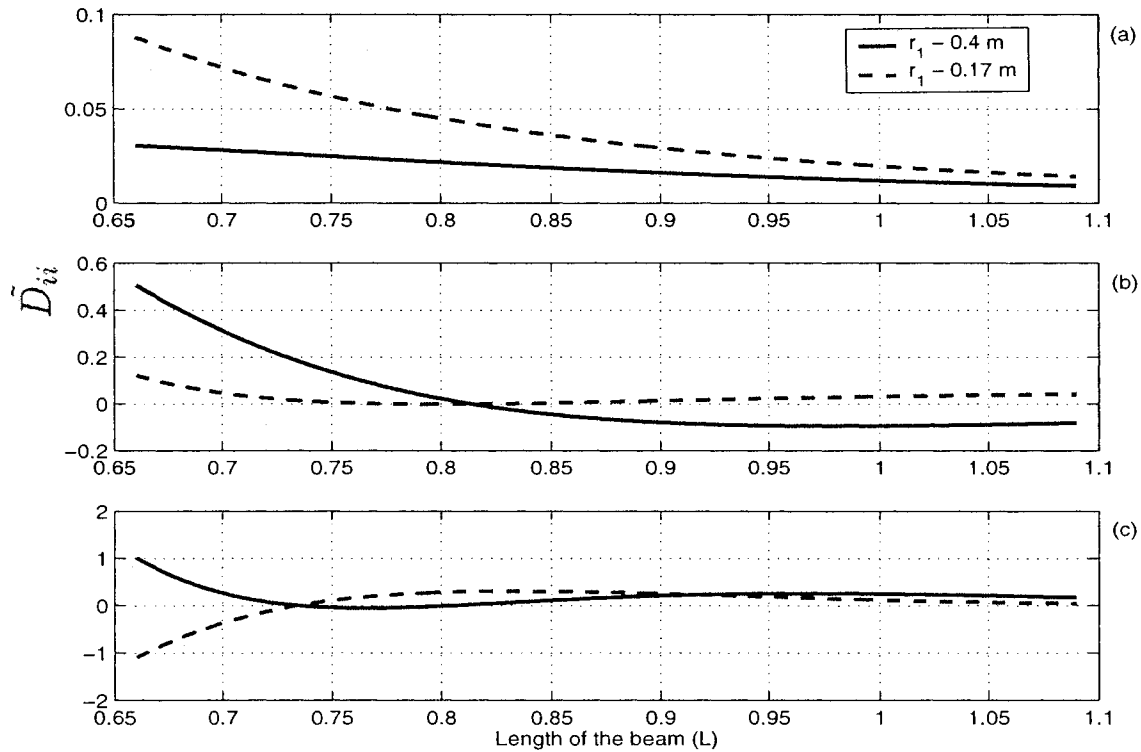


Figure 3.15: \tilde{D}_{ii} of the frozen system. Two non-collocated outputs at $r_1 = 0.4$ m and $r_1 = 0.17$ m. (a) $i = 1$. (b) $i = 2$. (c) $i = 3$.

From Figures 3.12 and 3.15, the following observations can be drawn:

- The sign of \tilde{D}_{ii} and the sign of $\tilde{\zeta}_i$ has a correlation.
- Negative $\tilde{\zeta}_i$ indicates an unstable system.
- \tilde{D}_{ii} and $\tilde{\zeta}_i$ are always positive for the first mode. While for the second mode and the third mode they may become negative when the beam assumes a certain length. \tilde{D}_{22} and $\tilde{\zeta}_2$ are positive for $0.66 \leq L < 0.82$ m, and negative for $0.82 < L \leq 1.09$ m. \tilde{D}_{33} and $\tilde{\zeta}_3$ are positive for $0.66 \leq L < 0.73$ m, and negative for $0.73 < L \leq 1.09$ m.
- With a non-collocated control, where $r_1 = 0.17$ m, \tilde{D}_{11} and $\tilde{\zeta}_1$ are always positive, \tilde{D}_{22} and $\tilde{\zeta}_2$ are positive or very close to zero. While \tilde{D}_{33} and $\tilde{\zeta}_3$ are negative, for $0.66 \leq L < 0.73$ m and positive for $0.73 < L \leq 1.09$.
- If two sensors are used, the frozen system can be stabilized by using one collocated sensor r_1 for $0.66 \leq L \leq 0.73$ m and one non-collocated sensor $r_2 = 0.17$ m for $0.73 < L \leq 1.09$. Another way to stabilize the frozen system is to place one sensor at $r_1 = 0.4$ m for $0.66 \leq L \leq 0.73$ and another sensor at $r_2 = 0.17$ m for $0.73 < L \leq 1.09$.

3.6 Control Strategies

To control the vibration and to overcome the spillover instability, three control strategies have been proposed.

(1) On-off gain scheduling scheme: Gain-scheduling with two outputs. One sensor is collocated and the other non-collocated. An on-off gain scheduling scheme is designed for each of the outputs such that the damping ratios of the frozen system are kept positive for all the beam lengths.

(2) Two-output feedback with time-varying gains: The previous study has shown that the sign of \tilde{D}_{ii} is correlated with the sign of ζ_i . This method intends to determine the

feedback gains by prescribing \tilde{D}_{ii} to be some positive values. A relationship between two feedback gains and \tilde{D}_{ii} can be found. By prescribing a proper positive value to each of \tilde{D}_{ii} , the variable gains can be found using a pseudo-inverse algorithm.

From Equation (3.24), it can be written as

$$\bar{D} = M^{-1}D + M^{-1}\tilde{D} \quad (3.45)$$

where

$$\tilde{D} = \begin{bmatrix} B_{11} \\ B_{12} \\ B_{13} \end{bmatrix} \begin{bmatrix} g_{v1} & g_{v2} \end{bmatrix} \begin{bmatrix} \frac{1}{\sqrt{L}}\psi_1(\alpha_1) & \frac{1}{\sqrt{L}}\psi_2(\alpha_1) & \frac{1}{\sqrt{L}}\psi_3(\alpha_1) \\ \frac{1}{\sqrt{L}}\psi_1(\alpha_2) & \frac{1}{\sqrt{L}}\psi_2(\alpha_2) & \frac{1}{\sqrt{L}}\psi_3(\alpha_2) \end{bmatrix} \quad (3.46)$$

The diagonals of the \tilde{D} matrix are given as

$$\begin{aligned} \begin{bmatrix} \tilde{D}_{11} \\ \tilde{D}_{22} \\ \tilde{D}_{33} \end{bmatrix} &= \begin{bmatrix} B_{11}g_{v1}\frac{1}{\sqrt{L}}\psi_1(\alpha_1) + B_{11}g_{v2}\frac{1}{\sqrt{L}}\psi_1(\alpha_2) \\ B_{12}g_{v1}\frac{1}{\sqrt{L}}\psi_2(\alpha_1) + B_{12}g_{v2}\frac{1}{\sqrt{L}}\psi_2(\alpha_2) \\ B_{13}g_{v1}\frac{1}{\sqrt{L}}\psi_3(\alpha_1) + B_{13}g_{v2}\frac{1}{\sqrt{L}}\psi_3(\alpha_2) \end{bmatrix} \\ &= \begin{bmatrix} B_{11}\frac{1}{\sqrt{L}}\psi_1(\alpha_1) & B_{11}\frac{1}{\sqrt{L}}\psi_1(\alpha_2) \\ B_{12}\frac{1}{\sqrt{L}}\psi_2(\alpha_1) & B_{12}\frac{1}{\sqrt{L}}\psi_2(\alpha_2) \\ B_{13}\frac{1}{\sqrt{L}}\psi_3(\alpha_1) & B_{13}\frac{1}{\sqrt{L}}\psi_3(\alpha_2) \end{bmatrix} \begin{bmatrix} g_{v1} \\ g_{v2} \end{bmatrix} \end{aligned} \quad (3.47)$$

Equation (3.47) is an over-determined system, i.e, the number of equations is greater than the number of unknowns. It can be solved by using a pseudo-inverse method.

The gains g_{v1} and g_{v2} are estimated such that

$$\begin{bmatrix} g_{v1} \\ g_{v2} \end{bmatrix} = \begin{bmatrix} B_{11}\frac{1}{\sqrt{L}}\psi_1(\alpha_1) & B_{11}\frac{1}{\sqrt{L}}\psi_1(\alpha_2) \\ B_{12}\frac{1}{\sqrt{L}}\psi_2(\alpha_1) & B_{12}\frac{1}{\sqrt{L}}\psi_2(\alpha_2) \\ B_{13}\frac{1}{\sqrt{L}}\psi_3(\alpha_1) & B_{13}\frac{1}{\sqrt{L}}\psi_3(\alpha_2) \end{bmatrix}^+ \begin{bmatrix} \tilde{D}_{11} \\ \tilde{D}_{22} \\ \tilde{D}_{33} \end{bmatrix} \quad (3.48)$$

where “+” denotes the pseudo-inverse and \tilde{D}_{11} , \tilde{D}_{22} and \tilde{D}_{33} are prescribed positive numbers.

(3) **Three-output feedback with time-varying gains:** A relationship between the three feedback gains and \tilde{D}_{ii} is found and by prescribing a positive value for each \tilde{D}_{ii} , the variable gains can be found using a direct matrix inverse method. The gains g_{v1} , g_{v2} and g_{v3} can be found by

$$\begin{bmatrix} g_{v1} \\ g_{v2} \\ g_{v3} \end{bmatrix} = \begin{bmatrix} B_{11} \frac{1}{\sqrt{L}} \psi_1(\alpha_1) & B_{11} \frac{1}{\sqrt{L}} \psi_1(\alpha_2) & B_{11} \frac{1}{\sqrt{L}} \psi_1(\alpha_3) \\ B_{12} \frac{1}{\sqrt{L}} \psi_2(\alpha_1) & B_{12} \frac{1}{\sqrt{L}} \psi_2(\alpha_2) & B_{12} \frac{1}{\sqrt{L}} \psi_2(\alpha_3) \\ B_{13} \frac{1}{\sqrt{L}} \psi_3(\alpha_1) & B_{13} \frac{1}{\sqrt{L}} \psi_3(\alpha_2) & B_{13} \frac{1}{\sqrt{L}} \psi_3(\alpha_3) \end{bmatrix}^{-1} \begin{bmatrix} \tilde{D}_{11} \\ \tilde{D}_{22} \\ \tilde{D}_{33} \end{bmatrix} \quad (3.49)$$

3.7 Computer Simulation

Figure 3.16 shows the displacement responses and the damping index of the on-off gain scheduling method. With one collocated output and one non-collocated output. The feedback gains g_{v1} for the output at $r_1 = 0.66$ m and g_{v2} for the output at $r_2 = 0.17$ m are chosen such that $g_{v1} = 1, g_{v2} = 0$ for $0.66 \leq L \leq 0.73$ m and $g_{v1} = 0, g_{v2} = 1$ for $0.73 < L \leq 1.09$ m.

Figure 3.17 shows the results when two non-collocated outputs are used. The feedback gains g_{v1} for the output at $r_1 = 0.4$ m and g_{v2} for the output at $r_2 = 0.17$ m are chosen such that $g_{v1} = 1, g_{v2} = 0$ for $0.66 \leq L \leq 0.73$ m and $g_{v1} = 0, g_{v2} = 1$ for $0.73 < L \leq 1.09$ m.

The following observations are drawn from the figures:

- Most of the deflection responses are decaying, while some deflection responses for extension show temporary diverging and then overall decay.
- Both the simulation cases indicate that the damping index J is always greater than zero.

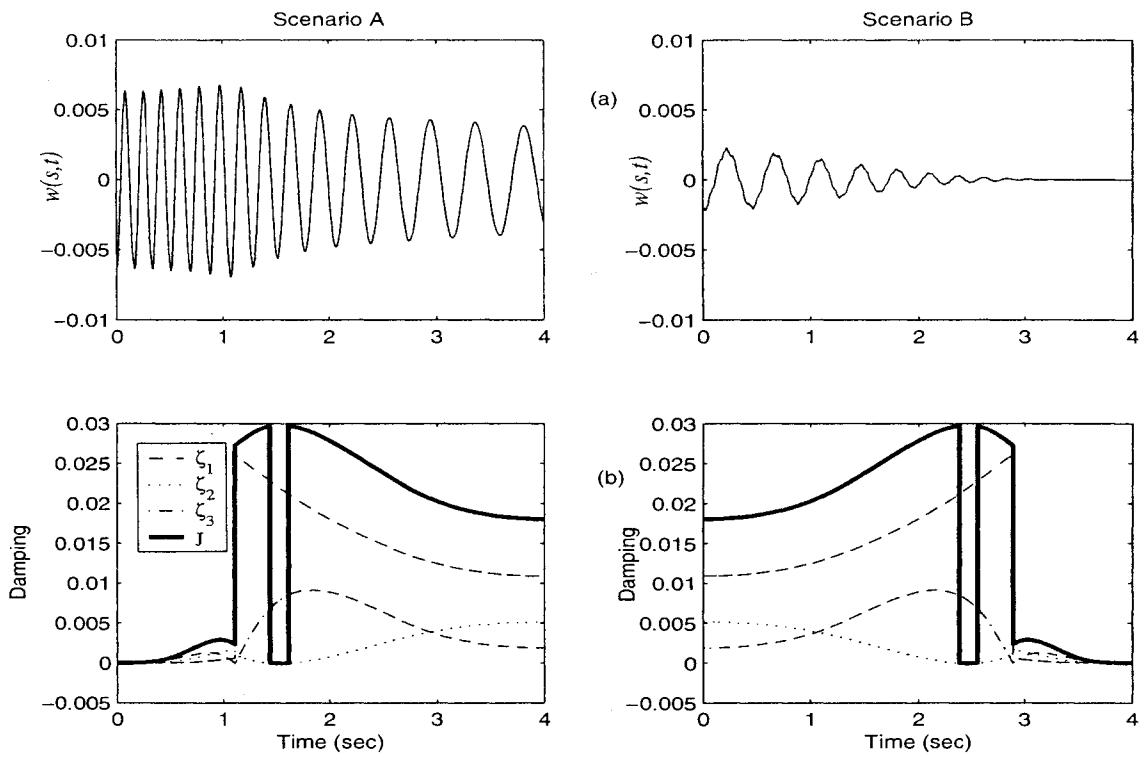


Figure 3.16: On-off gain scheduling scheme for the axially moving beam. Collocated $r_1 = 0.66$ m and $r_2 = 0.17$ m. (a) Displacement response. (b) Damping index J .

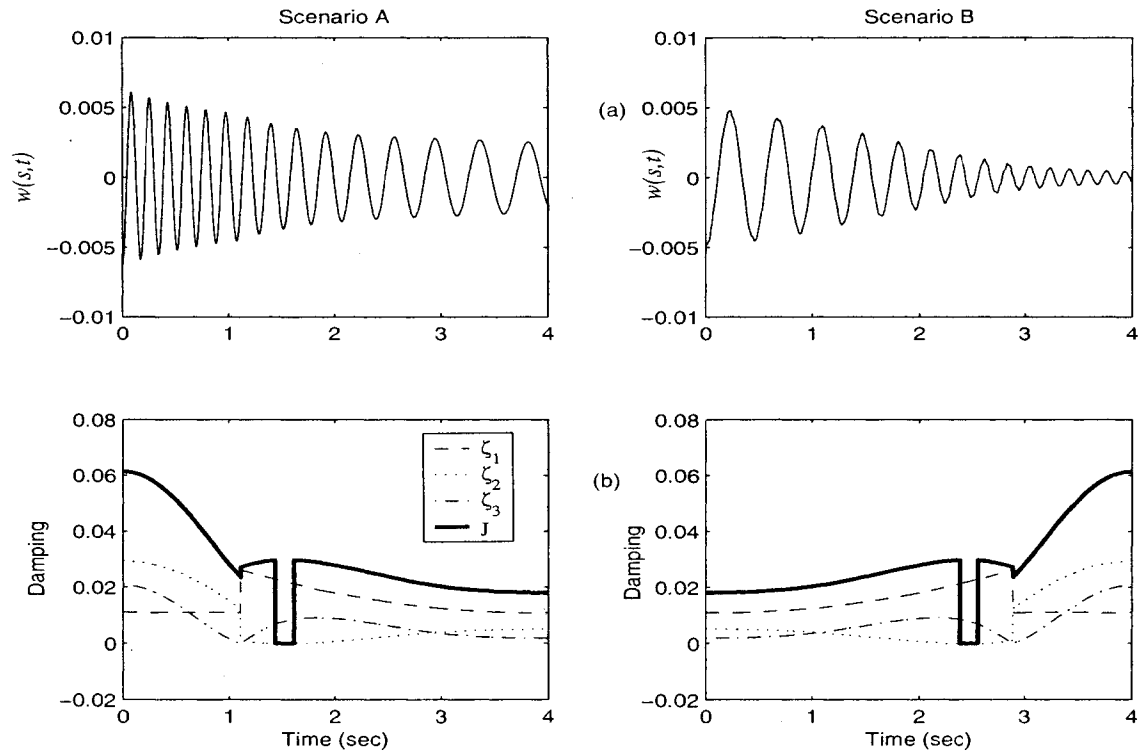


Figure 3.17: On-off gain scheduling scheme for the axially moving beam. $r_1 = 0.4$ m and $r_2 = 0.17$ m. (a) Displacement response. (b) Damping index J .

Figures 3.18 to 3.21 show the results of using the second control method. The values of \tilde{D}_{11} , \tilde{D}_{22} , \tilde{D}_{33} are specified to be $\tilde{D}_{11} = 1$, $\tilde{D}_{22} = 2$ and $\tilde{D}_{33} = 3$. Two cases are considered, the first is a collocated output ($r_2 = 0.65$ m) and a non-collocated output ($r_1 = 0.3$ m) feedback system, the second is a two non-collocated ($r_1 = 0.2$ m, $r_2 = 0.4$ m) outputs feedback system. The computed gains and the corresponding damping indices are also shown. The following observations are drawn from the figures:

- For one collocated and one non-collocated feed back system, the deflection responses are diverging for extension and decaying for retraction.
- For two non-collocated feedback system, for extension the deflection responses start to diverge at the beginning and decay at the end. For retraction, the responses are decaying.
- For $r_1 = 0.3$ m and $r_2 = 0.65$, the damping index J indicates that for extension it becomes negative after 1.7 seconds that makes the responses diverge and for retraction J becomes positive after 3 seconds and that makes the responses decay.
- For $r_1 = 0.2$ m and $r_2 = 0.4$, the damping index J indicates that for extension it becomes positive after 2 seconds that makes the responses decay slowly and for retraction J becomes positive after 3.1 seconds and that makes the responses decay slowly.
- The damping index J and the deflection responses show that the system will start to decay as long as the damping index is greater than zero.

Figures 3.22 to 3.25 show the responses using the third control method. Deflection responses are given for three output feedback system. Two cases are considered, first with one collocated ($r_3 = 0.65$ m) and two non-collocated ($r_1 = 0.2$ m, $r_2 = 0.4$ m) output feedback system, second with all three non-collocated ($r_1 = 0.1$ m, $r_2 = 0.3$ m, $r_3 = 0.5$ m) output feedback system. The varying gains and the corresponding damping indices are also shown. The following observations are drawn from the figures:

- All the deflection responses are decaying or decaying after a temporary diverging.
- During extension, the gains take a sudden change at 1.12 sec and 1.67 sec. During retraction, the sudden change is at 2.52 sec and 3.07 sec. This change can be observed in the damping index J as well. These sudden spikes takes place when the sign of the mode shapes $\Psi(\alpha)$ changes.
- Any three output sensors can be located arbitrarily. This method has the freedom of choosing the sensor location. It is clearly seen that for n number of modes, n number of output sensors will give a stable system through this inverse method regardless of the sensor locations. This is because, with three outputs it can be guaranteed that the diagonal elements \tilde{D}_{ii} are always positive, which makes the system stable.

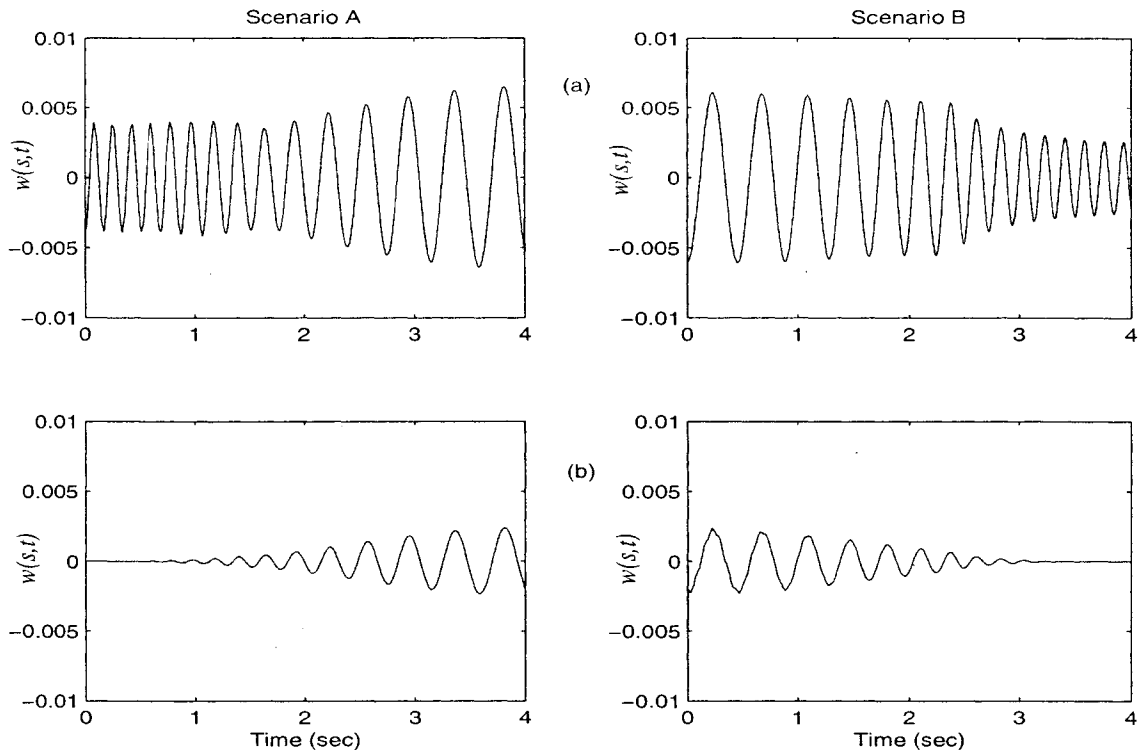


Figure 3.18: Deflection responses using the second control method. One collocated and one non-collocated feedback system. (a) Displacement response at $r_1 = 0.3$ m. (b) Displacement response at collocated sensor $r_2 = 0.65$ m.

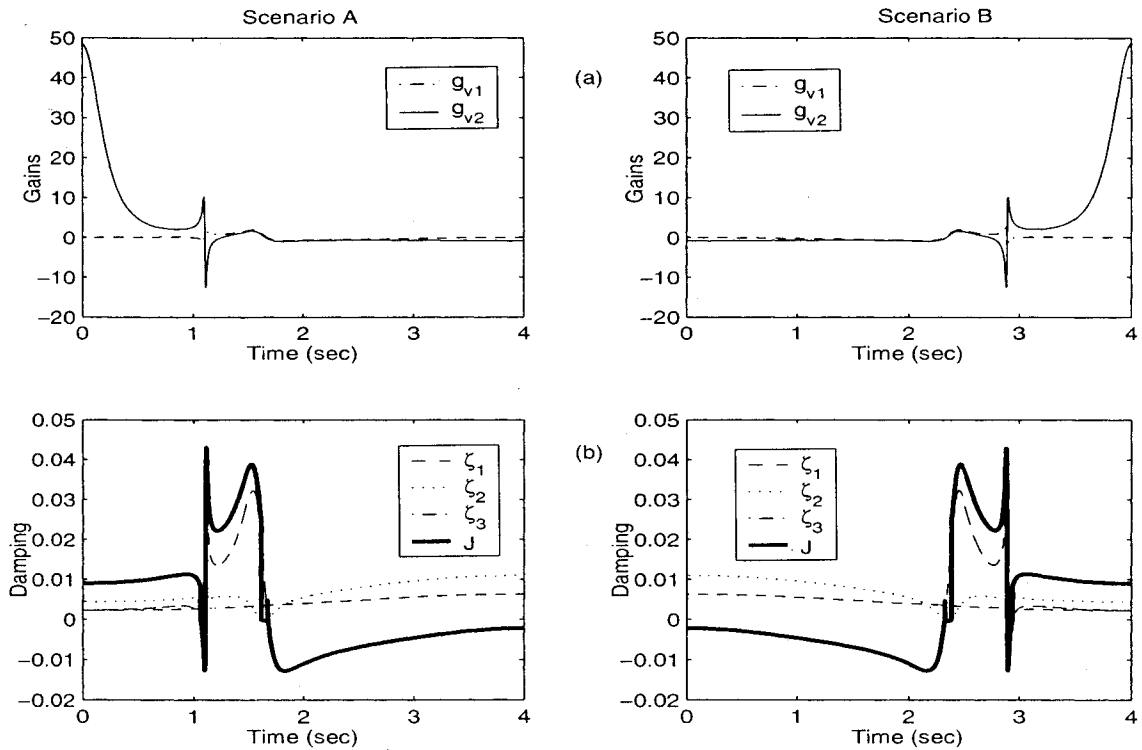


Figure 3.19: Gains and damping using the second control method. One collocated and one non-collocated feedback system. (a) Gains g_{v1} and g_{v2} for $r_1 = 0.3$ m and $r_2 = 0.65$ m. (b) Damping ratios ζ_i and damping index J

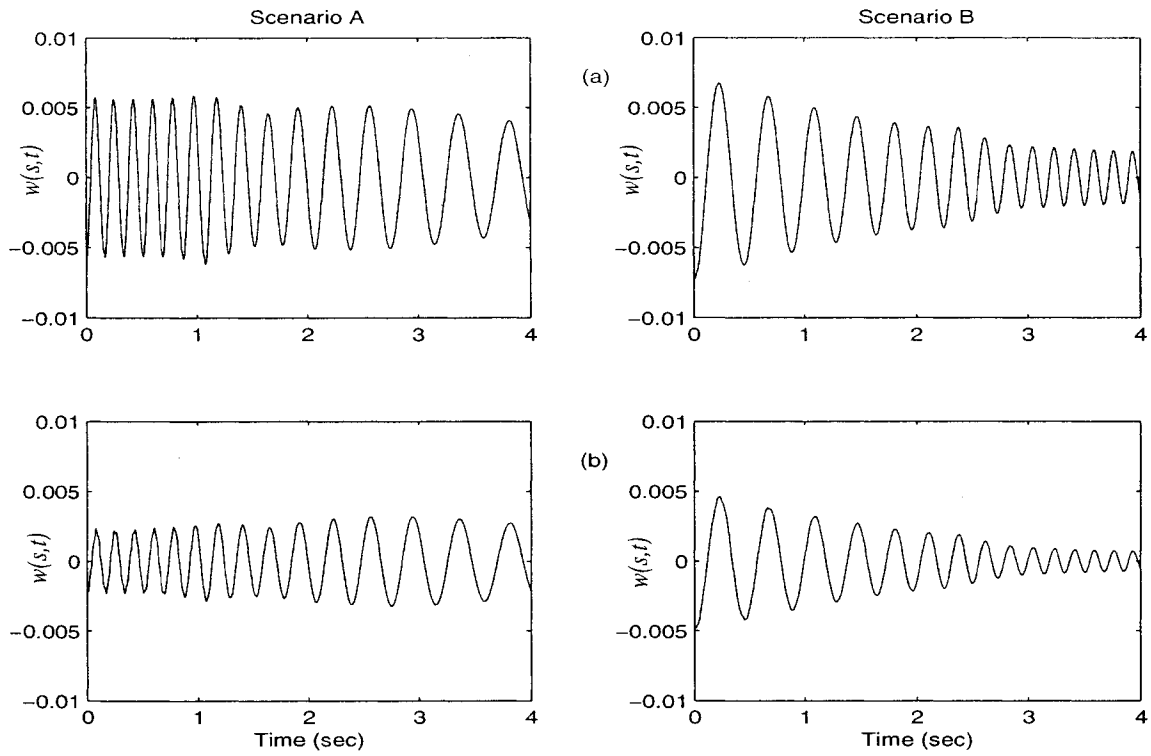


Figure 3.20: As Figure 3.18. Two non-collocated outputs feedback system. (a) Displacement response at $r_1 = 0.2$ m. (b) Displacement response at collocated sensor $r_2 = 0.4$ m.

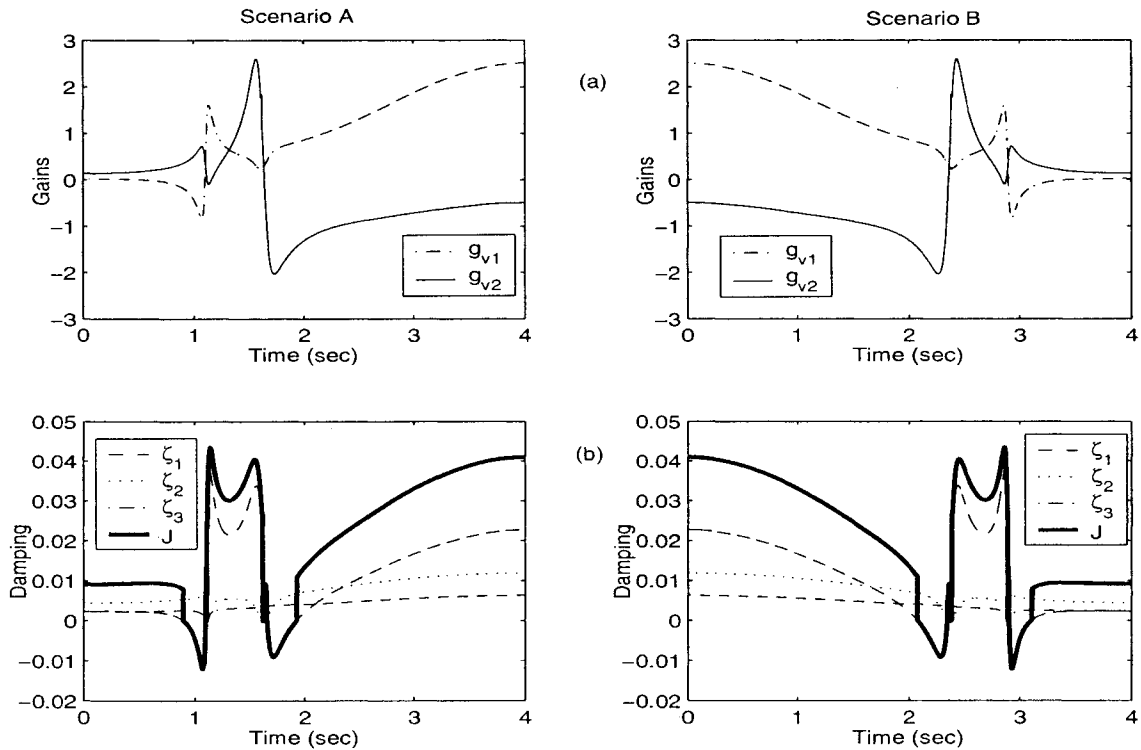


Figure 3.21: As Figure 3.19. Two non-collocated outputs feedback system. (a) Gains g_{v1} and g_{v2} for $r_1 = 0.2$ m and $r_2 = 0.4$ m. (b) Damping ratios ζ_i and damping index J

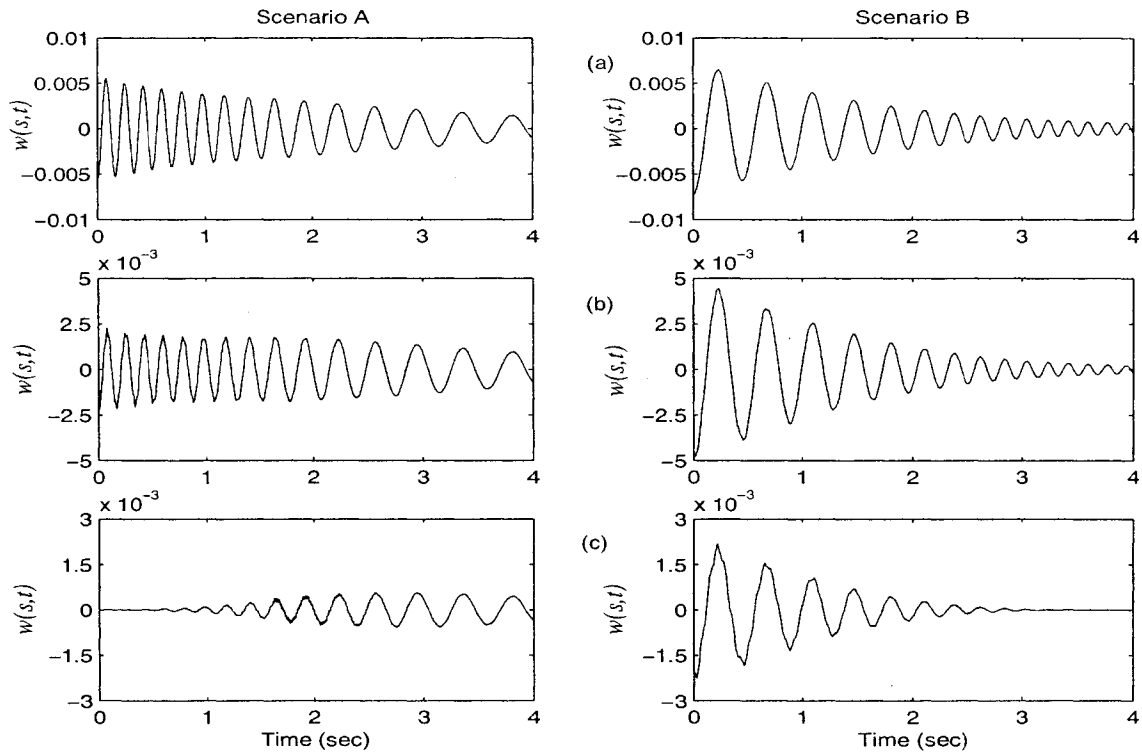


Figure 3.22: Deflection responses using the third control method. Two non-collocated and one collocated outputs feedback system. (a) $r_1 = 0.2$ m, (b) $r_2 = 0.4$ m, (c) $r_3 = 0.65$ m.

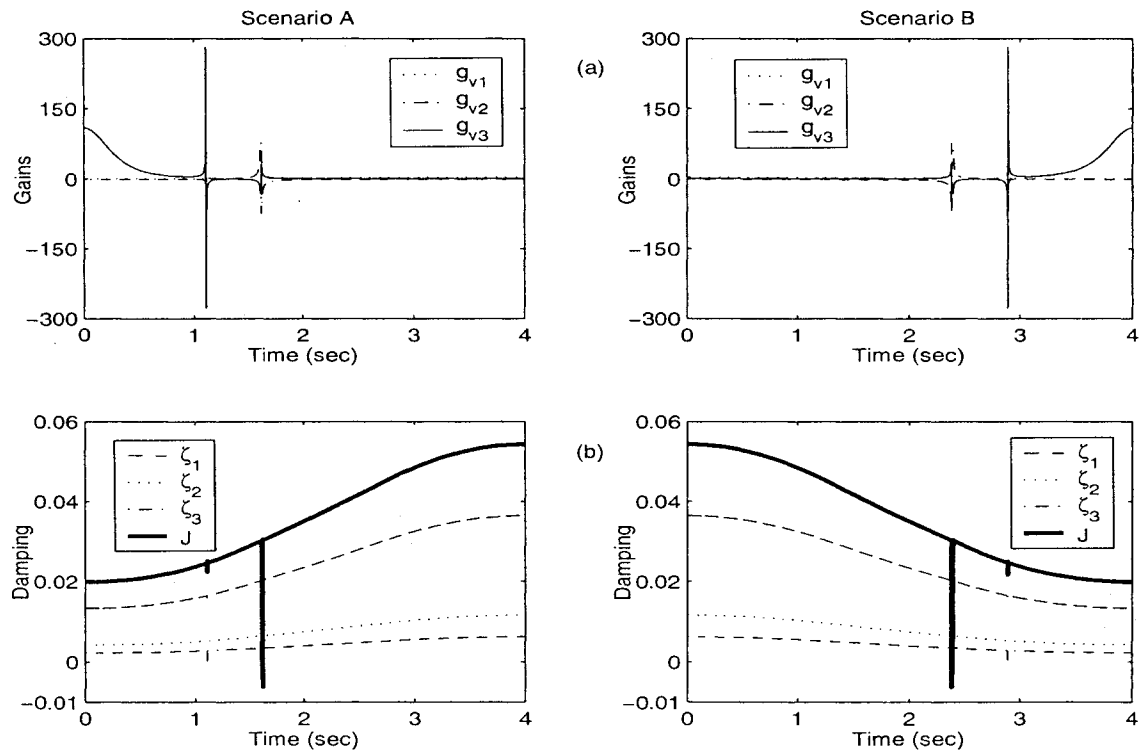


Figure 3.23: Gains and damping using the third control method. Two non-collocated and one collocated outputs feedback system. (a) Gains g_{v1} , g_{v2} and g_{v3} for $r_1 = 0.2$ m, $r_2 = 0.4$ m and $r_3 = 0.65$ m respectively. (b) Damping ratios ζ_i and damping index J .

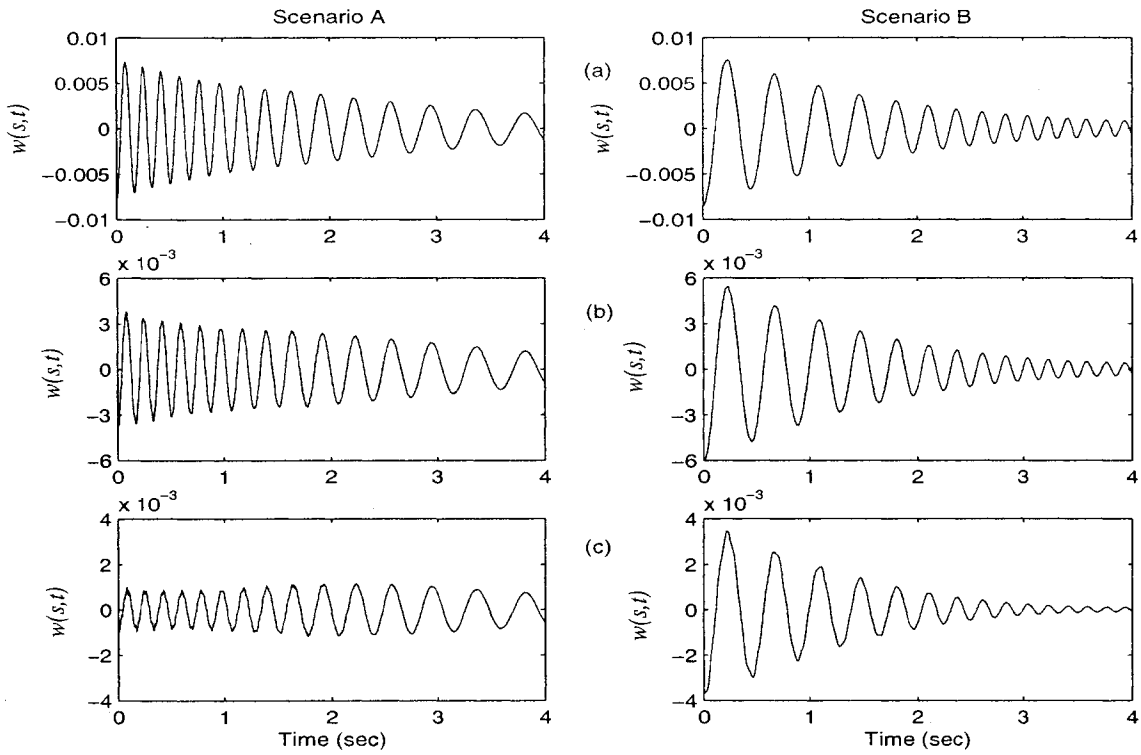


Figure 3.24: As Figure 3.22. Three non-collocated outputs feedback system. (a) $r_1 = 0.1$ m, (b) $r_2 = 0.3$ m, (c) $r_3 = 0.5$ m.

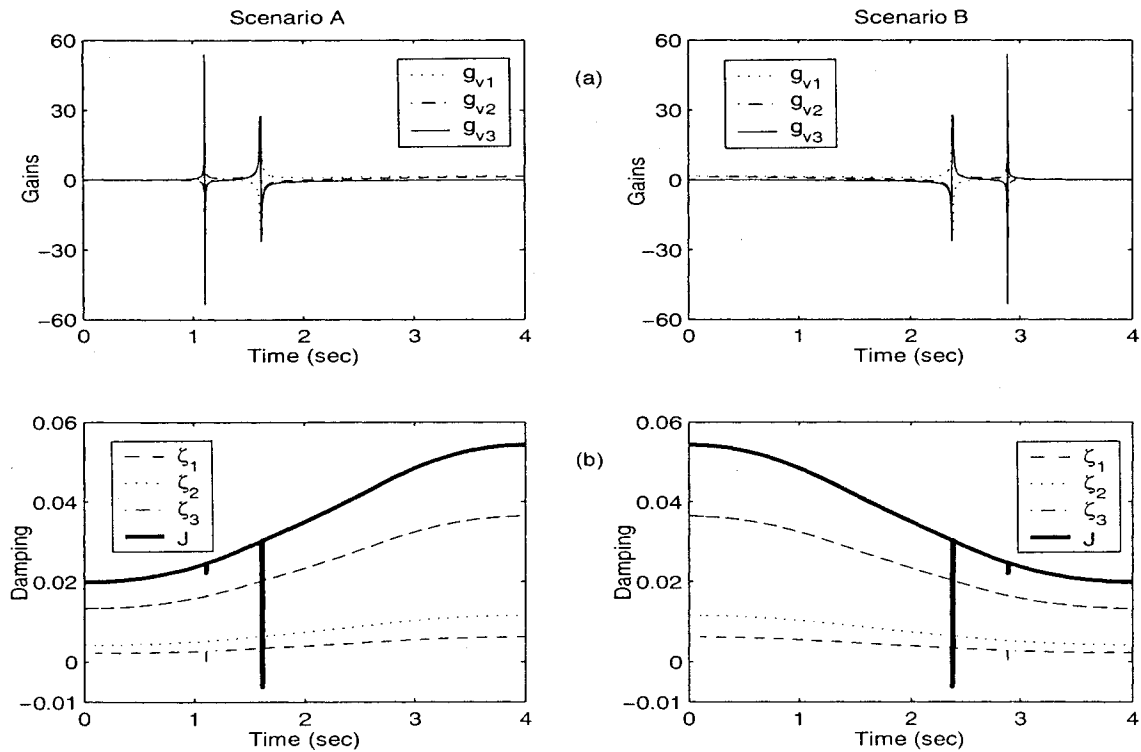


Figure 3.25: As Figure 3.23. Three non-collocated outputs feedback system. (a) Gains g_{v1} , g_{v2} and g_{v3} for $r_1 = 0.1$ m, $r_2 = 0.3$ m and $r_3 = 0.5$ m respectively. (b) Damping ratios ζ_i and damping index J .

3.8 Conclusion

In this chapter, a model of an axially moving cantilever beam with a pair of piezoelectric plates bonded on the beam is given. The control action is a pair of concentrated bending moments that counteract the beam's flexing. Velocity feedback controllers to introduce damping using one output, two outputs and three outputs are considered. The computer simulation indicates that the feedback system is always stable for a lower mode, and not necessarily for higher modes. This is referred to as spillover instability.

It is shown that the one output feedback system with constant gain gives unstable system due to spillover instability. To overcome the spillover instability problem, three control strategies are proposed. 1. Gain scheduling with two outputs. An on-off gain scheduling is designed for each of the outputs such that the damping ratios of the "frozen" system are kept positive for all the beam lengths. 2. Varying gains with two outputs. The variable gains can be found using a pseudo-inverse algorithm. 3. Varying gains with three outputs. With three outputs, the variable gains can be determined using a matrix inverse method.

The two output feedback system using the on-off gain scheduling method does not have the freedom to choose an arbitrary output location. For the two-output feedback with time-varying gains, it has the freedom of choosing the sensor locations but it cannot guarantee positive \bar{D}_{ii} . The three-output feedback system with time-varying gains allows to locate the three sensors arbitrarily.

Chapter 4

Active Control Design for the Axially Moving Cantilever Beam Based on the Gradient Algorithm

This chapter is organized as follows: Section 4.1 gives a brief introduction to the purpose of this chapter. Section 4.2 describes the transition matrix and the stability analysis of the open-loop system. Section 4.3 gives the controllability grammian and the uniform controllability condition of the time-varying system. Section 4.4 gives the observability grammian and the uniform observability condition of the time-varying system. Section 4.5 describes the gradient algorithm method. Section 4.6 explains the state feedback controller design. Section 4.7 explains the observer based state feedback controller design. Section 4.8 is a brief summary of the chapter.

4.1 Introduction

The purpose of this chapter is to design a controller for a parametrically excited system using the gradient algorithm. A linear time-varying state space model can be transformed into a structure that matches the gradient algorithm for a time interval. From the design, a stabilizing state feedback control can be obtained.

Parametrically excited system is a time-varying system and it may become unstable due to internal excitations. A typical example in mechanical system is, pendulum with vertically

vibrating support. Parametric excitation can be stationary or non-stationary. For stationary excitation, the amplitudes and the frequencies of the internal excitations are constant. For non-stationary excitation, the amplitudes and the frequencies of the internal excitations are time-varying. The analysis of a parametrically excited system conventionally relies on the system's stability and the amplitude of the internal excitations. The stability analysis is available only if the system is linear and the excitation is periodical. Previous studies of linear time-varying systems require to know how the non-stationary excitations vary in the future in order to calculate the desired control input. In [12], an approach based on the gradient algorithm is developed to design the controller for a dynamic system subject to stationary or non-stationary parametric excitation. With the gradient method, there is no need to predict how the parametric excitations vary in the future as long as past and present information of the system is available. In this chapter, this design approach is applied to design the controllers for suppression of lateral vibration of the axially moving beam.

4.2 Transition Matrix and Stability of Closed-loop System

A zero-input linear time-varying system is given as

$$\dot{x} = A(t)x, \quad x(kT) = x_k, \quad k = 0, 1, 2, \dots \quad (4.1)$$

and its solution can be expressed by

$$x(t) = \Phi(t, kT)x_k \quad (4.2)$$

where $\Phi(t, kT)$ is referred to as the transition matrix. The transition matrix satisfies the following equation,

$$\dot{\Phi}(t, kT) = A(t)\Phi(t, kT), \quad \Phi(kT, kT) = I \quad (4.3)$$

According to Rugh [13],

Theorem: The linear state Equation (4.1) is uniformly stable if and only if there exists a finite positive constant μ such that

$$\|\Phi(t, \tau)\| \leq \mu \quad (4.4)$$

for all t, τ such that $t \geq \tau$.

To examine the stability of the axially moving cantilever beam, the transition matrix is numerically found by a method given in Appendix A.5. Then the singular values of the transition matrices are evaluated. Figure 4.1 shows the maximum and minimum singular values of the transition matrices when the beam is engaged in the extension and in the retraction. In this simulation, the time interval $T = 1$ second and the step time $\Delta t = 0.0005$ second were used.

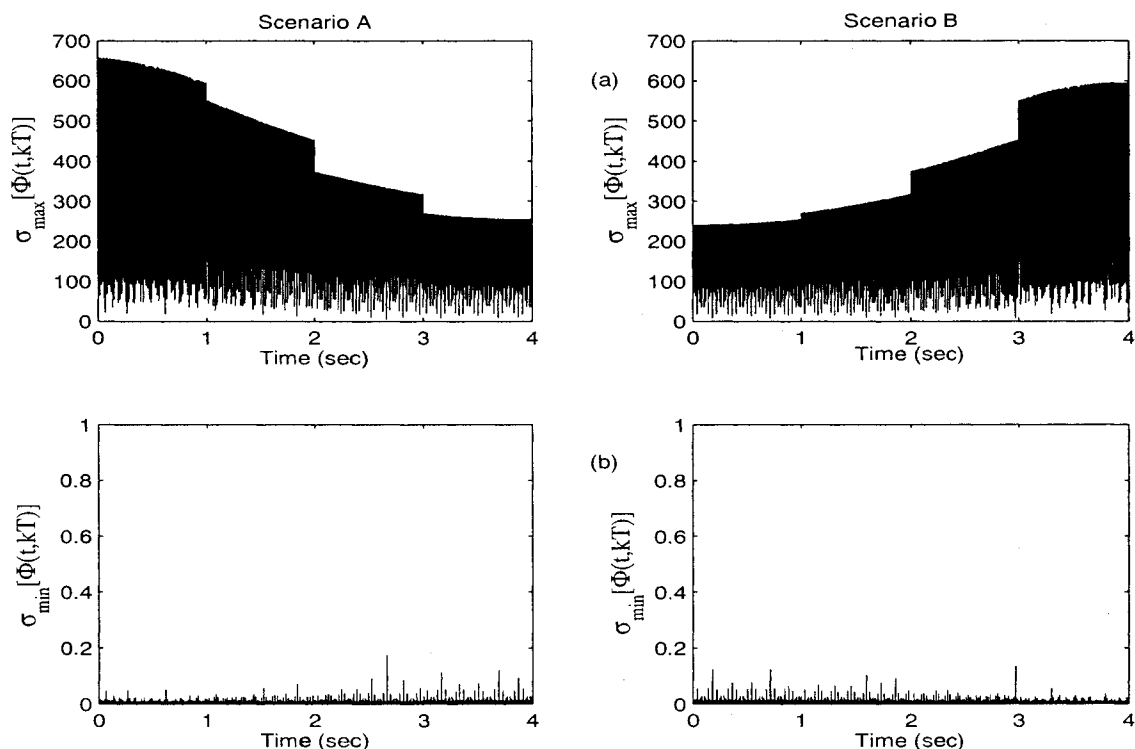


Figure 4.1: (a) Maximum singular values, (b) minimum singular values of the transition matrices for Scenario A and Scenario B.

From Figures 4.1 and 4.2, the following observations can be drawn:

- The maximum singular values of the transition matrices fluctuate. The overall trend

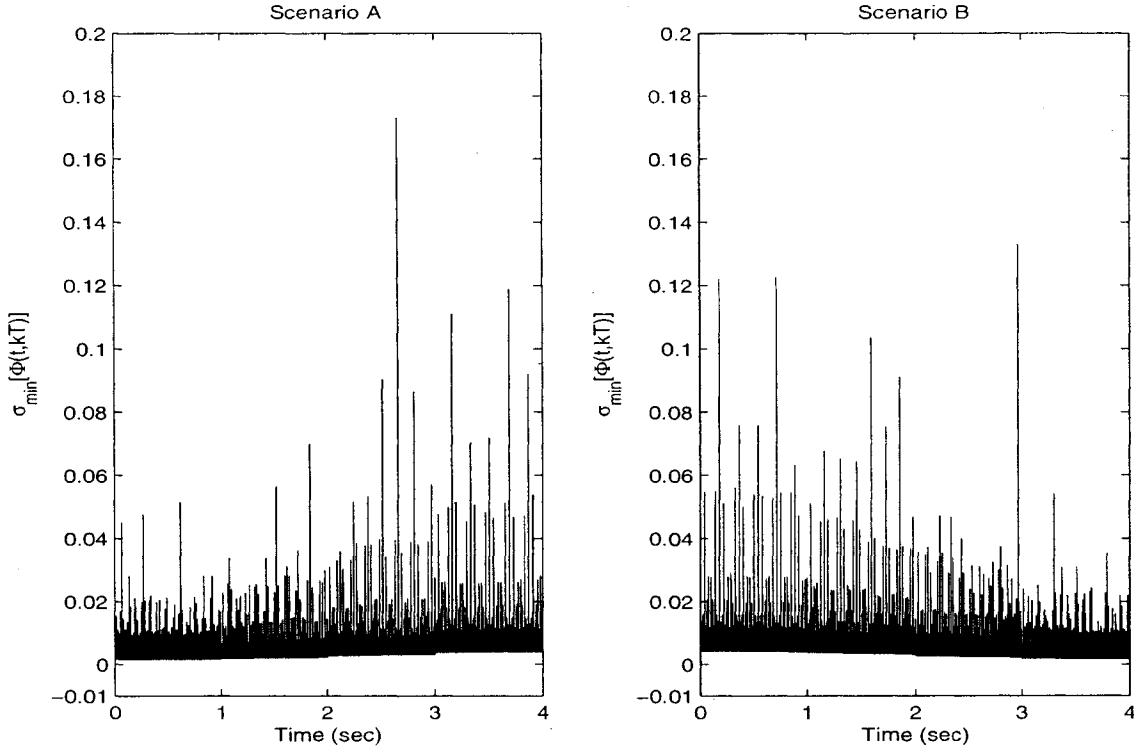


Figure 4.2: Same as Figure 4.1 (b). $\sigma_{min}[\Phi(t, kT)]$ axis is magnified.

of $\sigma_{max}[\Phi(t, kT)]$ for extension is reducing while the overall trend of $\sigma_{max}[\Phi(t, kT)]$ for retraction is increasing. Thus the system under extension is stable as σ_{max} is bounded while the system under retraction is unstable as σ_{max} is not bounded.

- In every 1 second interval, σ_{max} has a sudden drop for Scenario A and a sudden rise for Scenario B. This is due to the resetting of $\Phi(kT, kT) = I$ at each time interval $T = 1$ second.
- All $\sigma_{min}[\Phi(t, kT)]$ values lie between $0 < \sigma_{min} \leq 1$. For Scenario A, the lowest is 0.0015 and for Scenario B, the lowest is 0.0016.
- When $\sigma_{min}[\Phi(t, kT)]$ gets close to zero, $[\Phi(t, kT)]$ is near singular. It should be noted that when the transition matrix becomes singular or uninvertible, the condition of Equation (4.4) is not satisfied and the system is unstable.

4.3 Controllability

A linear system

$$\dot{x} = A(t)x + B(t)u \quad (4.5)$$

is controllable if, for all initial times and all initial states $x(t_0)$, there exist some input functions, that drive the state vector to any final state $x(t_1)$ at some finite time $t_1 > t_0$. Controllability of the system is determined by matrices $A(t)$ and $B(t)$. The controllability grammian performs the test.

$A(t)$ and $B(t)$ are uniformly controllable if there exists Δ and constants β_1 and β_2 such that,

$$\beta_1 I \leq P_c(t) \leq \beta_2 I \quad \forall t > 0 \quad (4.6)$$

where, $P_c(t)$ is the controllability grammian defined by,

$$P_c(t) = \int_{t-\Delta}^t \Phi(t-\Delta, \tau) B(\tau) B^T(\tau) \Phi^T(t-\Delta, \tau) d\tau \quad (4.7)$$

For the system under study, $P_c(t)$ can be found numerically. Figure 4.3 shows the maximum and minimum singular values of $P_c(t)$. From the figure, the following observations are drawn:

- The maximum and minimum singular values of $P_c(t)$ takes zero at the beginning of each second. The system is not uniformly controllable if β_1 and β_2 are not positive constants. The rank of $P_c(t)$ should be full rank for the system to be controllable. Here the rank of $P_c(t)$ takes less than full rank at the beginning of each interval.
- It is noted that the minimum singular values of $P_c(t)$ are very small.

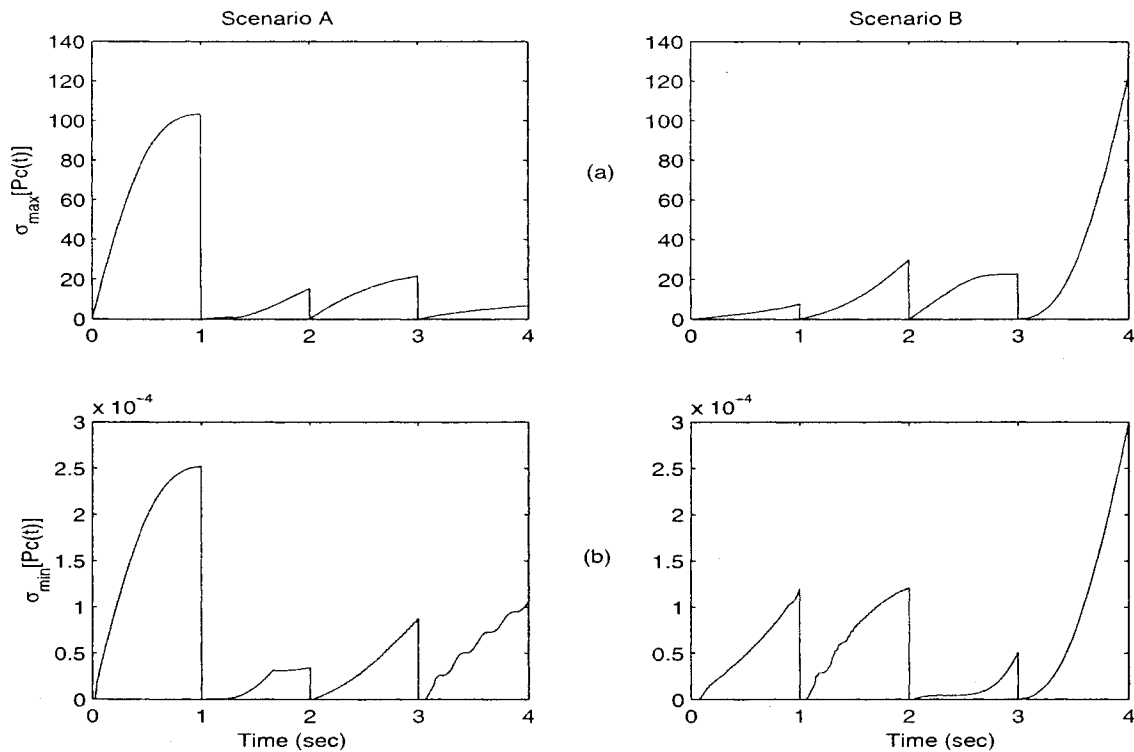


Figure 4.3: Controllability testing using the gramian for extension and retraction. (a) maximum singular values of $P_c(t)$, (b) minimum singular values of $P_c(t)$.

4.4 Observability

A linear system

$$\begin{aligned} \dot{x} &= A(t)x + B(t)u \\ y &= C(t)x \end{aligned} \quad (4.8)$$

is completely observable if, for all initial times, the state vector $x(t_0)$ can be determined from the output function $y(t_1)$, defined over a finite time $t_1 > t_0$. Observability involves the matrices $A(t)$ and $C(t)$. The Observability gramian performs the test.

$A(t)$ and $C(t)$ are uniformly observable if there exists Δ and constants γ_1 and γ_2 such that

$$\gamma_1 I \leq P_o(t) \leq \gamma_2 I \quad \forall t > 0 \quad (4.9)$$

where, $P_o(t)$ is the observability gramian defined by,

$$P_o(t) = \int_{t-\Delta}^t \Phi^T(\tau, t-\Delta) C^T(\tau) C(\tau) \Phi(\tau, t-\Delta) d\tau \quad (4.10)$$

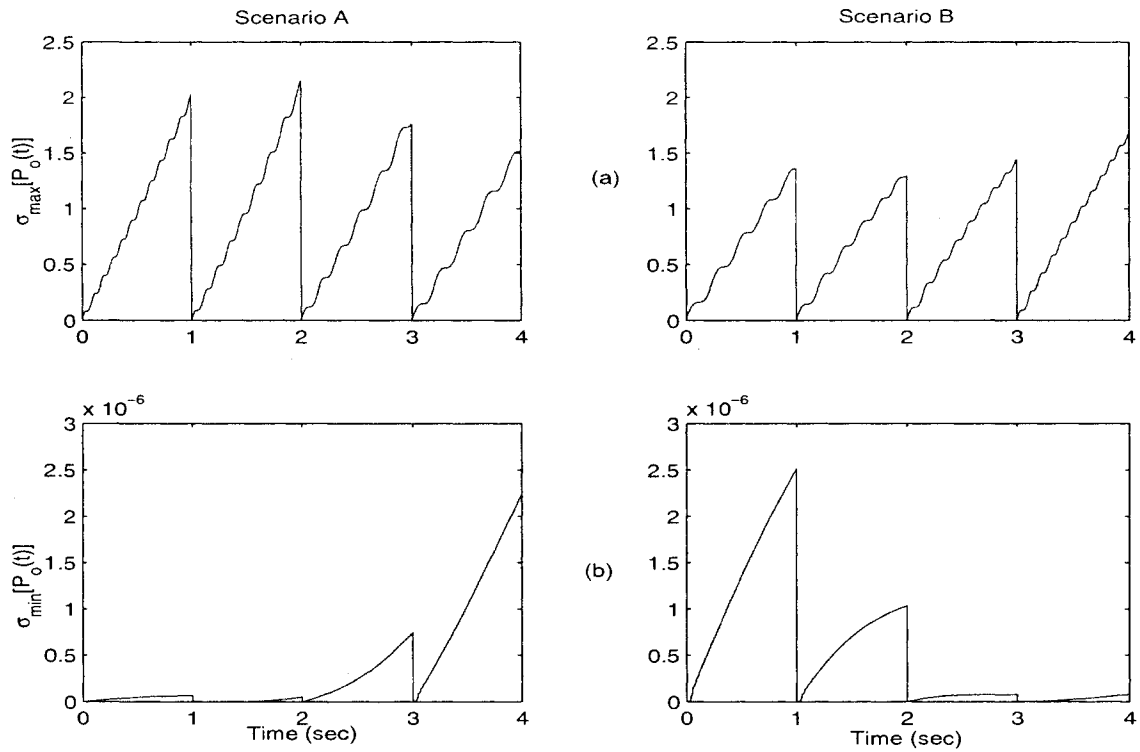


Figure 4.4: Observability testing using grammian for extension and retraction. The deflection output is observed at $r_1 = 0.1$ m. (a) maximum singular values of $P_o(t)$, (b) minimum singular values of $P_o(t)$.

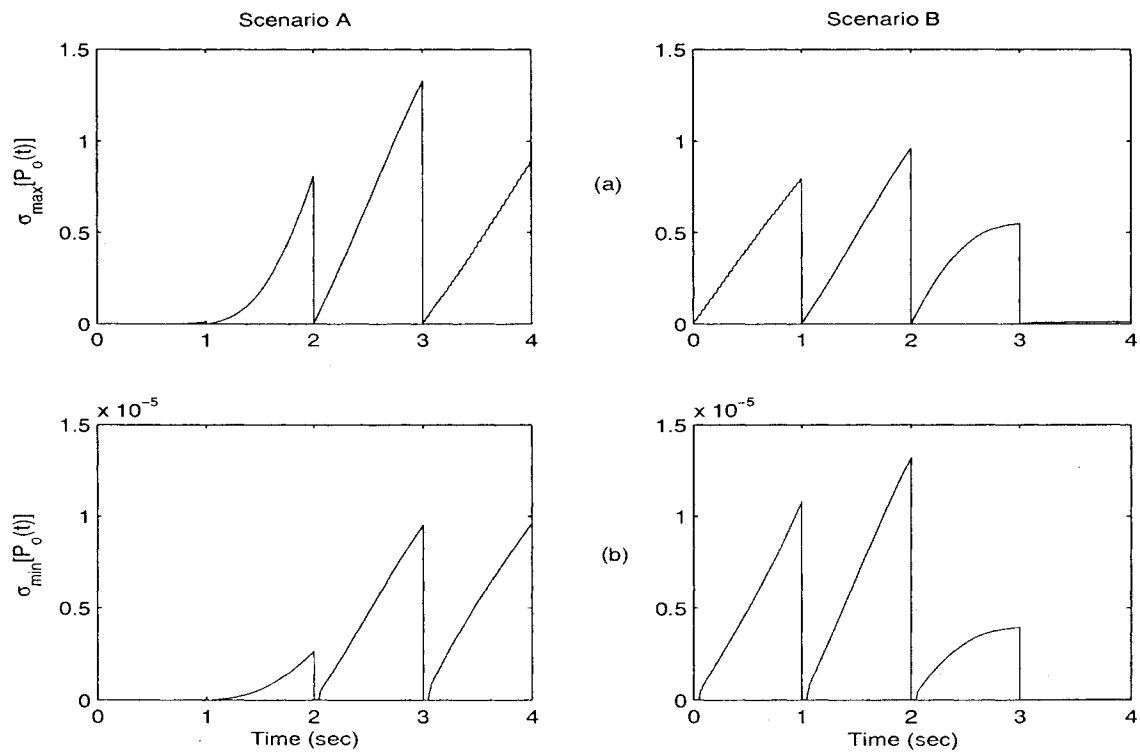


Figure 4.5: Observability testing using the grammian for extension and retraction. The deflection output is observed at the collocated sensor location $r_1 = 0.66$ m. (a) maximum singular values of $P_o(t)$, (b) minimum singular values of $P_o(t)$.

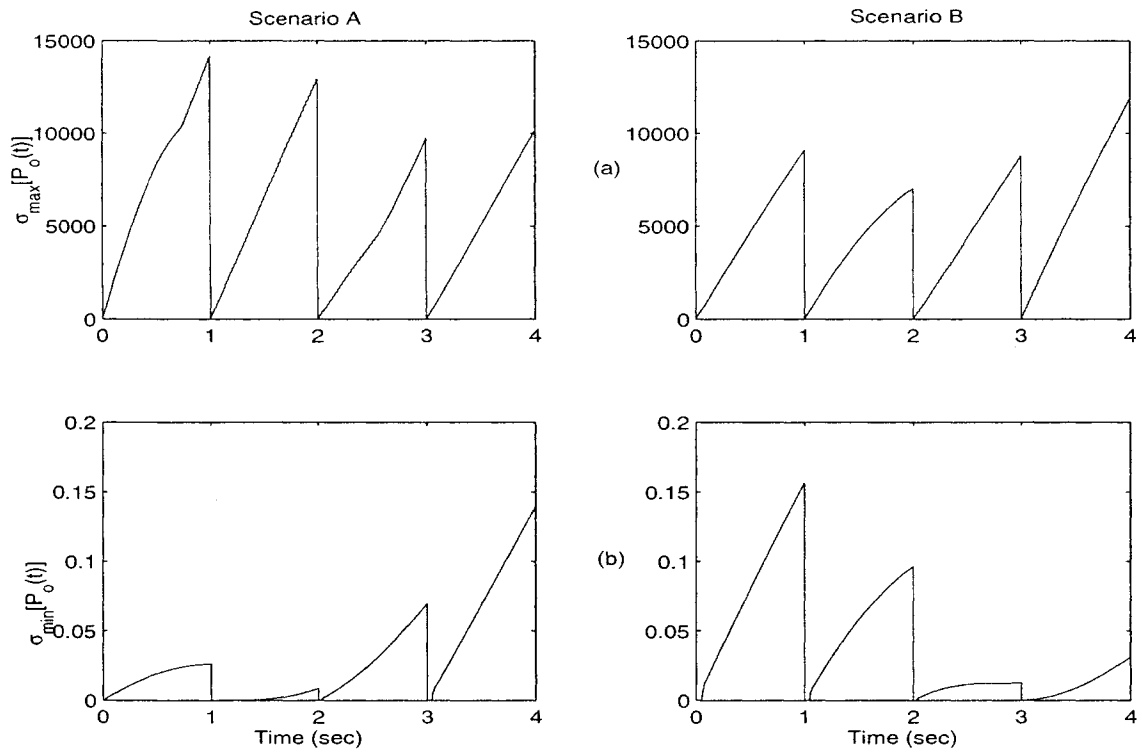


Figure 4.6: Observability testing using the gramman for extension and retraction. The velocity output is observed at $r_1 = 0.1$ m. (a) maximum singular values of $P_o(t)$, (b) minimum singular values of $P_o(t)$.

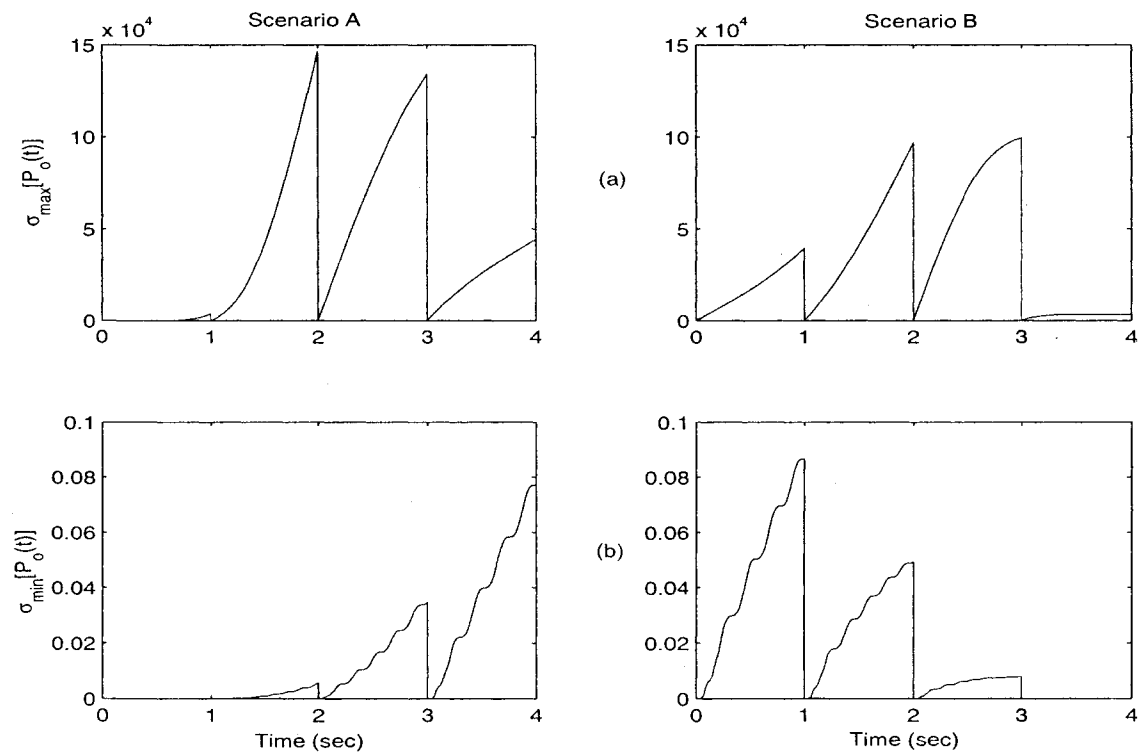


Figure 4.7: Observability testing using the gramman for extension and retraction. The velocity output is observed at the collocated sensor location $r_1 = 0.66$ m. (a) maximum singular values of $P_o(t)$, (b) minimum singular values of $P_o(t)$.

For the system under study, $P_o(t)$ can be found numerically. Figures 4.6 and 4.7 show the maximum and minimum singular values of $P_o(t)$, observed at $r_1 = 0.1$ m and $r_1 = 0.66$ m. From the figures the following observations are drawn:

- The maximum and minimum singular values of $P_o(t)$ takes zero at the beginning of each second. The system is not uniformly observable if γ_1 and γ_2 are not positive constants. The rank of $P_o(t)$ should be full rank for the system to be observable. Here the rank of $P_o(t)$ takes less than full rank at the beginning of each second.
- The minimum singular values of $P_o(t)$ are very small.

4.5 Gradient Algorithm

The gradient algorithm was developed for the parameter identification purpose. In [12], the gradient algorithm was utilized for the controller and the observer designs for parametrically excited systems. A brief review of the gradient algorithm is given below.

Let $Z(t)$ represents the parameter error between the true parameter vector θ and the estimated parameter vector $\hat{\theta}$. If $\hat{\theta}$ is updated based on the gradient algorithm, the governing equation of $Z(t)$ is given by

$$\dot{Z}(t) = -\gamma w(t)w^T(t)Z(t) \quad (4.11)$$

where γ is any positive constant, and $w(t)$ is called the “regressor vector”. A well-known sufficient condition on the exponential stability of the system is that the regressor vector be “persistently exciting” as defined below.

The regressor vector $w(t)$ is persistently exciting if there exists positive constants Δ , α_1 and α_2 such that [12]

$$\alpha_1 I \leq \int_{t-\Delta}^t w(\tau)w^T(\tau)d\tau \leq \alpha_2 I, \quad \forall t > 0. \quad (4.12)$$

Under this persistent exciting condition, the parameter error $Z(t)$ converges to zero exponentially such that [41]

$$\| Z(k\Delta) \| \leq \rho^k \| Z(0) \| \quad (4.13)$$

where $k = 1, 2, \dots$ and

$$0 < \left[\rho = \sqrt{1 - \frac{2\gamma\alpha_1}{(1 + \gamma\alpha_2\sqrt{n})^2}} \right] < 1, \quad \forall \gamma > 0. \quad (4.14)$$

When $Z(t)$ converges to zero, the estimated parameters converge to the true parameters.

4.6 State Feedback Control

If the state variables $x(t)$ are accessible for measurement, the state feedback control is given by,

$$u(t) = -K(t)x(t) \quad (4.15)$$

where $K(t)$ is the feedback gain vector which is derived by transforming the system to match the gradient algorithm in Equation (4.11). For this purpose, the coordinate transformation is given by,

$$x(t) = \Phi(t, kT)Z_k(t) \quad t \in [kT, (k+1)T) \quad (4.16)$$

therefore, the derivative of $x(t)$ will become

$$\dot{x}(t) = \frac{\partial \Phi(t, kT)}{\partial t} Z_k(t) + \Phi(t, kT) \dot{Z}_k(t). \quad (4.17)$$

Substituting Equation (4.3) in Equation (4.17) gives

$$\dot{x}(t) = A(t)\Phi(t, kT)Z_k(t) + \Phi(t, kT)\dot{Z}_k(t). \quad (4.18)$$

Substituting Equation (4.16) in Equation (4.5) gives

$$\dot{x}(t) = A(t)\Phi(t, kT)Z_k(t) + B(t)u(t). \quad (4.19)$$

Equating Equations (4.18) and (4.19) gives

$$\dot{Z}_k(t) = \Phi^{-1}(t, kT)B(t)u(t) = w_c(t)u(t) \quad (4.20)$$

where $w_c(t) = \Phi^{-1}(t, kT)B(t)$. If the control $u(t)$ is chosen to be

$$u(t) = -\gamma_c w_c^T(t) Z_k(t) \quad (4.21)$$

where γ_c is a positive constant controller gain, so that the transformed closed-loop dynamics

$$\dot{Z}_k(t) = -\gamma_c w_c(t) w_c^T Z_k(t), \quad t \in [kT, (k+1)T) \quad (4.22)$$

has exactly the same structure as the gradient algorithm in Equation (4.11) on the time interval $[kT, (k+1)T)$.

From Equation (4.16) $Z_k(t)$ can be written as

$$Z_k(t) = \Phi^{-1}(t, kT)x(t) \quad (4.23)$$

Substituting Equation (4.23) in (4.21) gives

$$u(t) = -\gamma_c B^T(t) \Phi^{-T}(t, kT) \Phi^{-1}(t, kT)x(t). \quad (4.24)$$

The controller gain $K(t)$ can be expressed as

$$K(t) = -\gamma_c B^T(t) \Phi^{-T}(t, kT) \Phi^{-1}(t, kT). \quad (4.25)$$

If the system is uniformly controllable, the regressor vector $w_c(t)$ is persistently exciting over the time interval $[kT, (k+1)T)$ in the sense that

$$\alpha_1 I \leq P_c^z(t) = \int_{t-\Delta}^t w_c(\tau) w_c^T(\tau) d\tau \leq \alpha_2 I, \quad t \in [kT, (k+1)T). \quad (4.26)$$

where $\alpha_1 = \frac{\beta_1}{m_2^2}$ and $\alpha_2 = \frac{\beta_2}{m_1^2}$, in which β_1 and β_2 are as in Equation (4.6), m_1 and m_2 are two positive constants satisfying

$$m_1 \leq \sigma_i[\Phi(t, kT)] \leq m_2, \quad t \in [kT, (k+1)T), \quad \forall k. \quad (4.27)$$

Figures 4.8 to 4.10 show the state feedback displacement responses at $r_1 = 0.1$ m without controller and with control inputs $u(t)$ when $\gamma_c = 2$, $\gamma_c = 12$ and $\gamma_c = 16$, respectively. Figure 4.11 shows how to choose a suitable γ_c using u_{max} for $t < 1$ sec and u_{max} for $t \geq 1$ sec for

various γ_c 's. Since the control input before the first 1 sec period does not affect the output response, and the control input after $t \geq 1$ sec does affect the output response, it is efficient if a γ_c is chosen such that the control input is smaller when $t < 1$ sec and larger when $t \geq 1$ sec. When the control input is large, it is important to consider weather it is feasible and economic in practise. Figure 4.12 gives a measure of the output response $y(t)$ to show the effect of each γ_c on the output. The measure is defined by finding the Euclidian norm of the output response with control and by normalizing it using the Euclidian norm of the output without control. It can be written as

$$R = \frac{\|y(t)_{control}\|_2}{\|y(t)_{no_control}\|_2}. \quad (4.28)$$

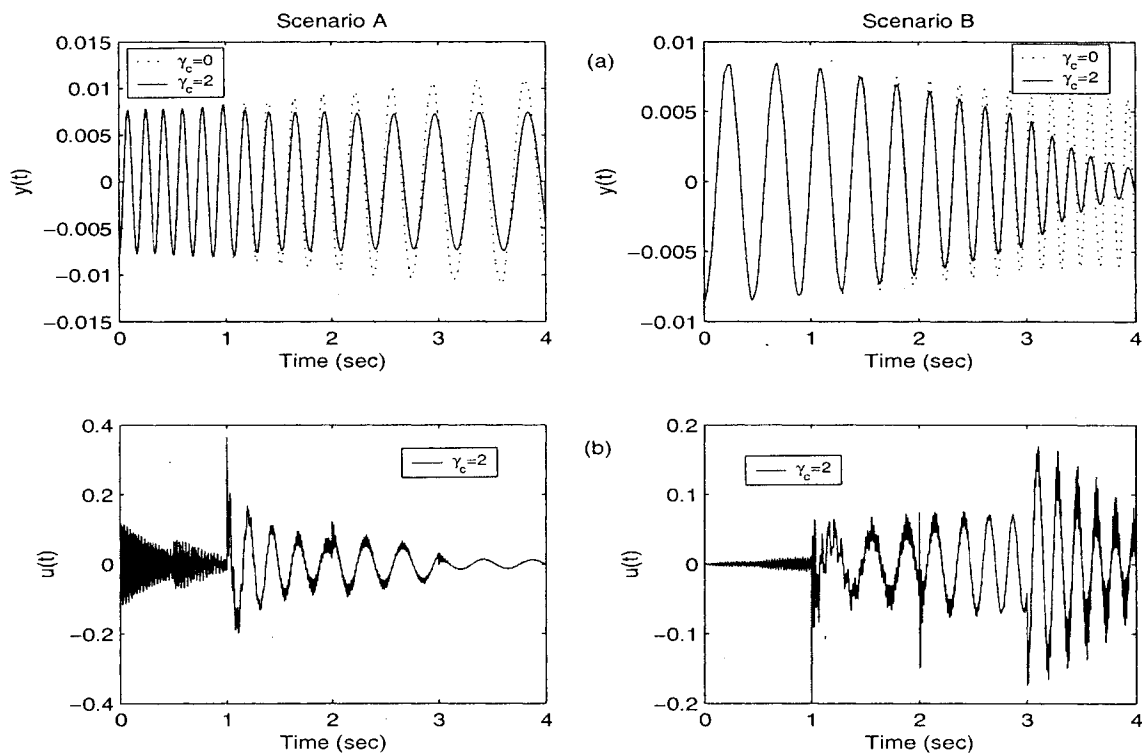


Figure 4.8: State feedback displacement responses at $r_1 = 0.1$ m. (a) Output response with controller ($\gamma_c = 2$) and without controller ($\gamma_c = 0$). (b) Control input $u(t)$ when $\gamma_c = 2$.

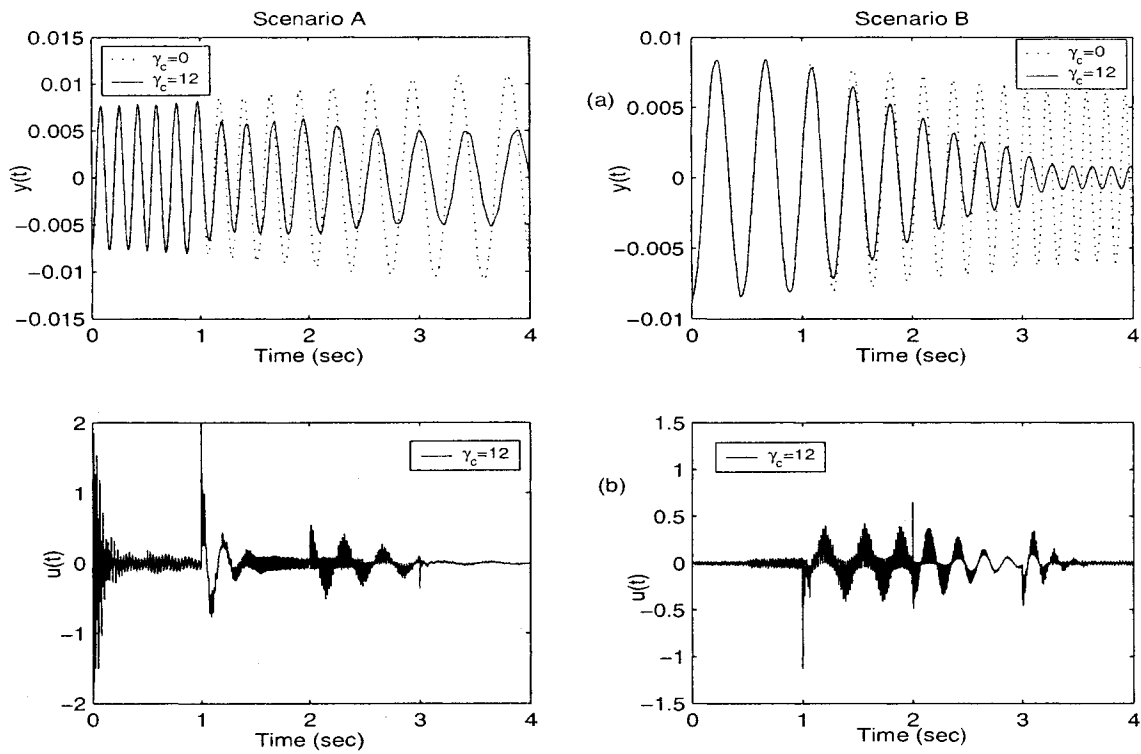


Figure 4.9: State feedback displacement responses at $r_1 = 0.1$ m. (a) Output response with controller ($\gamma_c = 12$) and without controller ($\gamma_c = 0$). (b) Control input $u(t)$ when $\gamma_c = 12$.

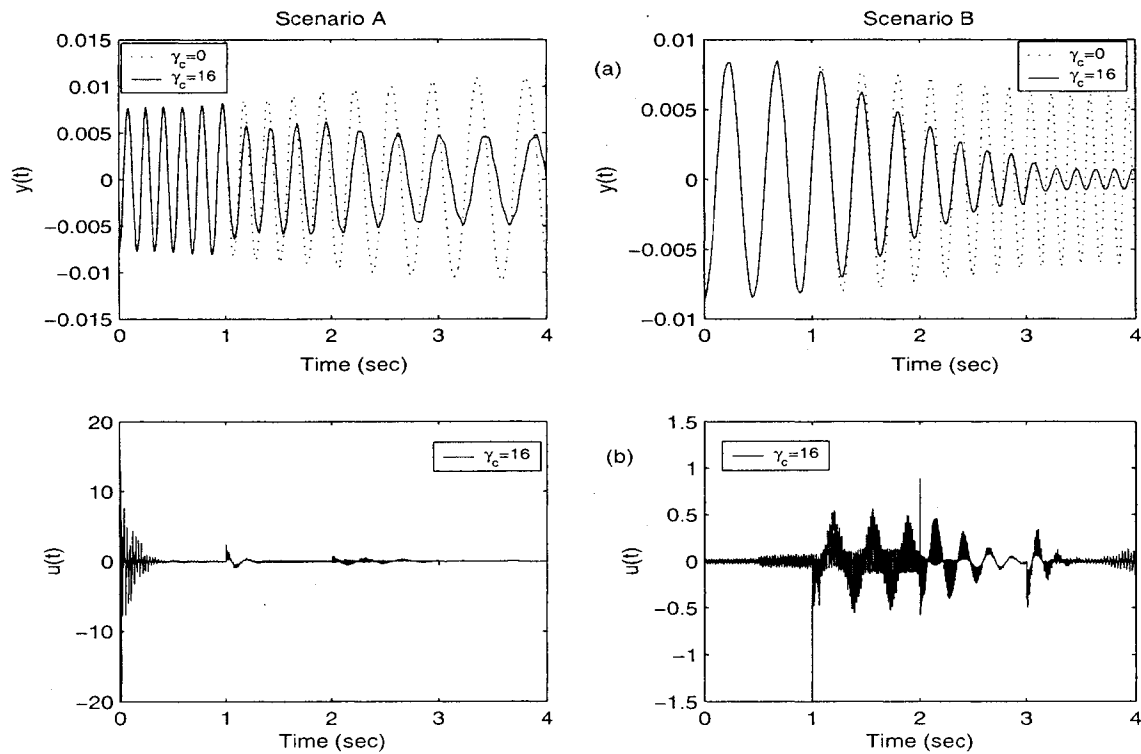


Figure 4.10: State feedback displacement responses at $r_1 = 0.1$ m. (a) Output response with controller ($\gamma_c = 16$) and without controller ($\gamma_c = 0$). (b) Control input $u(t)$ when $\gamma_c = 16$.

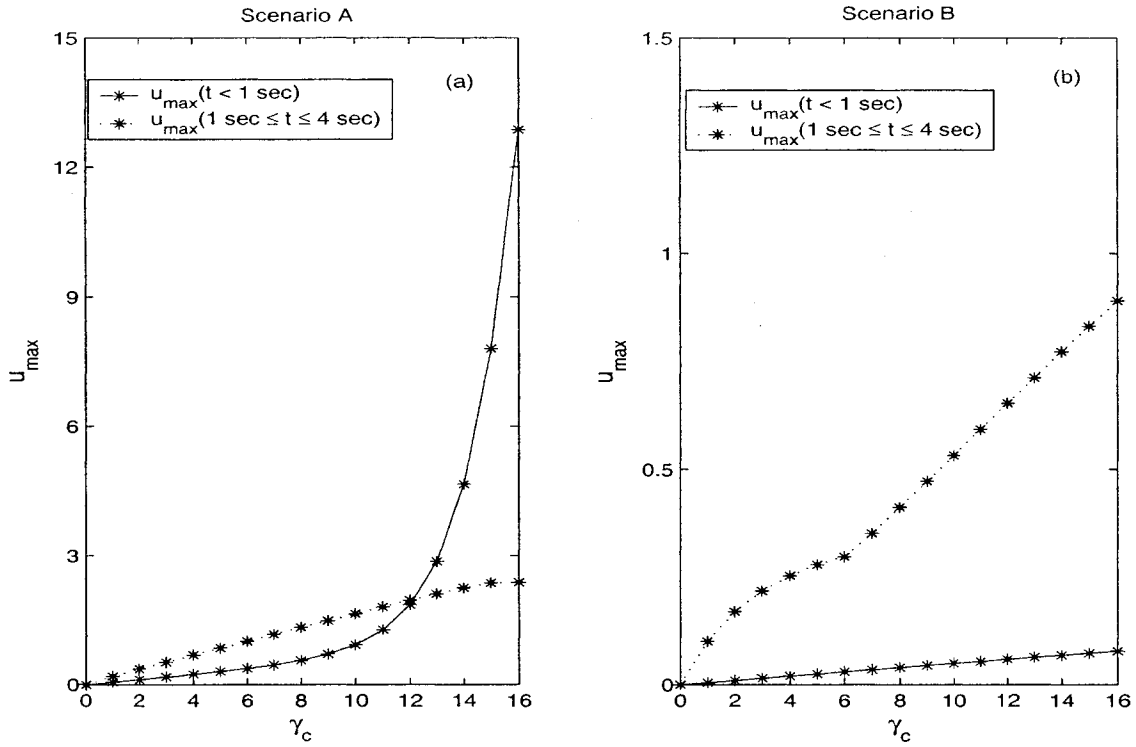


Figure 4.11: Maximum values of control input $u(t)$ for γ_c ranging from 0-16 when $r_1 = 0.1$ m. (a) Scenario A, (b) Scenario B.

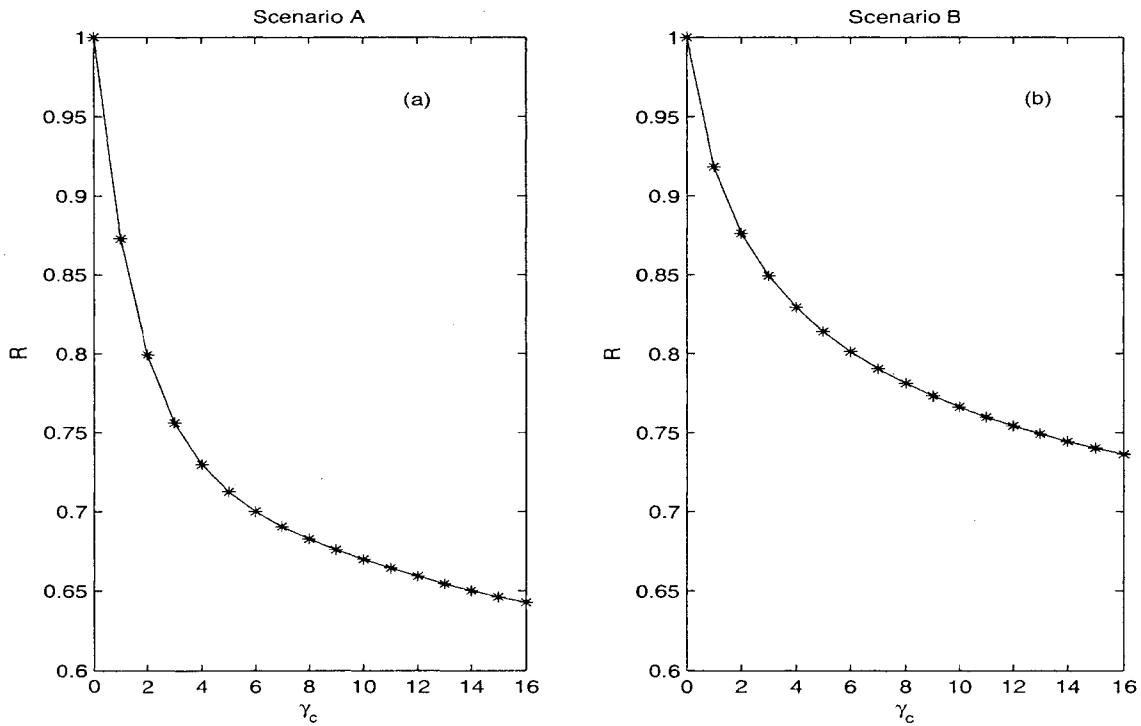


Figure 4.12: R for γ_c 's ranging from 0-16 when $r_1 = 0.1$ m. (a) Scenario A, (b) Scenario B.

From these figures, the following observations are drawn:

- Figures 4.8 to 4.10 show that the controller has little effect on the response during the first second period.
- With the controller, the deflection response in Scenario A decays slowly but in Scenario B, the response decays fast.
- For Scenario A, an increase of the gain makes the response decay slightly fast while it results in a significant increase in the control effort at the beginning. It is also noted that the control effort becomes very small for $t > 3$ sec.
- Figure 4.11 compares the maximum control input for $t < 1$ sec and that for $t \geq 1$ sec. It can be seen that for Scenario A when $\gamma_c = 12$, two curves intersect each other and maximum control input for $t < 1$ sec is smaller and maximum control input for $t \geq 1$ sec is larger when $\gamma_c \leq 12$. While for Scenario B, the maximum control input for $t < 1$ sec is always smaller than the maximum control input for $t \geq 1$ sec for all γ_c 's.
- The measure R in Figure 4.12 shows that the responses for both Scenario A and Scenario B decrease when the γ_c increases.

4.7 Observer Based State Feedback Control

When full states are not available, the state observer is constructed to estimate the system state $x(t)$ from the system output $y(t)$. The system is represented as

$$\dot{x}(t) = A(t)x(t) + B(t)u(t) \quad (4.29)$$

where $x(t)$ is the system state and the output is given by

$$y(t) = C(t)x(t). \quad (4.30)$$

From the basic Luenberger type observer based controller, the estimated system can be represented as

$$\dot{\hat{x}}(t) = A(t)\hat{x}(t) + B(t)u(t) + L(t)(y(t) - \hat{y}(t)) \quad (4.31)$$

where $\hat{x}(t)$ is the estimated state and $\hat{y}(t)$ is the estimated output and given as

$$\hat{y}(t) = C(t)\hat{x}(t) \quad (4.32)$$

and $u(t)$ is the observer-based state feedback control given as

$$u(t) = K(t)\hat{x}(t) \quad (4.33)$$

where the controller gain $K(t)$ is given in Equation (4.25). $L(t)$ is the observer-based feedback gain and it is designed so that $\hat{x}(t)$ approaches $x(t)$ exponentially. Denote the state estimation error by $\tilde{x}(t) = \hat{x}(t) - x(t)$. Subtracting Equation (4.31) from Equation (4.29) yields the state estimation error dynamics

$$\dot{\tilde{x}}(t) = [A(t) - L(t)C(t)]\tilde{x}(t). \quad (4.34)$$

The observer design also utilizes the gradient algorithm in Equation (4.11). For this purpose, the following coordinate transformation is introduced for the state estimation error:

$$\tilde{x}(t) = \Phi(t, kT)\tilde{Z}_k(t) \quad t \in [kT, (k+1)T) \quad (4.35)$$

therefore, the derivative of $\tilde{x}(t)$ will become

$$\dot{\tilde{x}}(t) = \frac{\partial \Phi(t, kT)}{\partial t} \tilde{Z}_k(t) + \Phi(t, kT) \dot{\tilde{Z}}_k(t). \quad (4.36)$$

Substituting Equation (4.3) in Equation (4.36) gives

$$\dot{\tilde{x}}(t) = A(t)\Phi(t, kT)\tilde{Z}_k(t) + \Phi(t, kT)\dot{\tilde{Z}}_k(t). \quad (4.37)$$

Substituting Equation (4.35) in Equation (4.34) gives

$$\dot{\tilde{x}}(t) = [A(t) - L(t)C(t)]\Phi(t, kT)\tilde{Z}_k(t). \quad (4.38)$$

Equating Equations (4.37) and (4.38) gives

$$\dot{\tilde{Z}}_k(t) = -L(t)C(t)\tilde{Z}_k(t). \quad (4.39)$$

From the gradient algorithm (4.11) the transformed state estimation error dynamics becomes

$$\dot{\tilde{Z}}_k(t) = -\gamma_o w_o^T(t) w_o(t) \tilde{Z}_k(t) \quad (4.40)$$

where $w_o(t) = \Phi^T(t, kT)C^T(t)$ and γ_o is a constant observer gain.

Equating Equations (4.40) and (4.39) gives the observer feedback gain $L(t)$

$$L(t) = \gamma_o \Phi(t, kT) \Phi^T(t, kT) C^T(t). \quad (4.41)$$

The estimation error of the state feedback control output response and the observer based state feedback control output response is given by

$$\tilde{y}(t) = \hat{y}(t) - y(t). \quad (4.42)$$

If the system is uniformly observable, the regressor vector $w_o(t)$ is persistently exciting over the time interval $[kT, (k+1)T)$ in the sense that

$$\gamma_1 m_1^2 I \leq P_o^z(t) = \int_{t-\Delta}^t w_o(\tau) w_o^T(\tau) d\tau \leq \gamma_2 m_2^2 I, \quad t \in [kT, (k+1)T) \quad (4.43)$$

where γ_1 and γ_2 are as in Equation (4.9), m_1 and m_2 are two positive constants satisfying as in Equation (4.27).

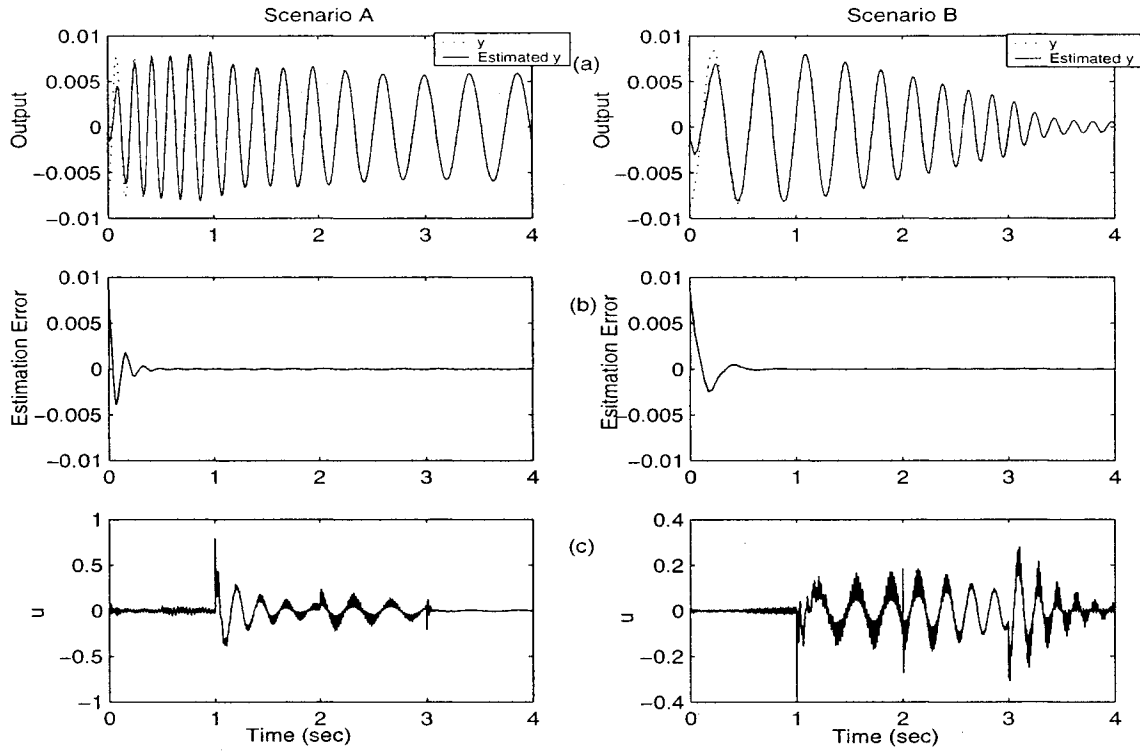


Figure 4.13: Observer based feedback control responses at $r_1 = 0.1$ m. $\gamma_c = 5$ and $\gamma_o = 5$. (a) True output y and estimated output \hat{y} , (b) Estimation error \tilde{y} , (c) control output u .

Figure 4.13 shows the observer based state feedback control deflection output y at $r_1 = 0.1$ m, estimated output \hat{y} , estimation error \tilde{y} and the control input u . The observer gain constant $\gamma_o = 5$ and the controller gain constant $\gamma_c = 5$ are used for this simulation. From the figure it is observed

- The estimated output $\hat{y}(t)$ is decaying and estimation error $\tilde{y}(t)$ converges to zero for Scenario A and Scenario B.
- The estimation error is large until first 0.5 seconds and starts to converge to zero afterwards.
- For Scenario A, the control input u is larger during the period of $1 \text{ sec} \leq t \leq 3 \text{ sec}$. For Scenario B, the control input is larger after 1 second and starts to decay after 3 seconds.
- Higher observer gain constant γ_o reduces the estimation error.

4.8 Summary

In this chapter, a controller design using the Gradient Algorithm was used to suppress the vibration of an axially moving cantilever beam. An advantage of this method over others is that only past and the present information of the time-varying parametric excitations is required to find the control input. The transition matrix was found using Runge-Kutta method. A state feedback controller gain K was designed assuming that all states are available. Also an observer was designed when the only accessible output was the deflection response.

Different controller gain constants γ_c 's were investigated for different output locations. Suitable γ_c was found using the maximum values of the control inputs for the chosen time slots. From the observer design, the estimated error becomes zero as the observer gain constant γ_o increases.

Stability of the system was discussed using the maximum and minimum singular values of the transition matrix. The controllability and the observability grammians for uniform controllability and uniform observability of the system were presented. The closed-loop stability and the convergence rate of the system were also discussed.

Chapter 5

Summary and Future Work

5.1 Summary

- The mathematical model of the lateral vibration of the axially moving cantilever beam is presented. This model is a linear time-varying system. For the computer simulation, the beam axial motion is assumed to have a trapezoidal velocity profile. Deflection and the velocity output responses are sensed at the tip, middle and base locations for the study. Vibration energy is discussed for the beam with and without an end mass. The stability of the system is analyzed using Lyapunov function.
- The use of piezoelectric actuators and their control actions through velocity feedback on the axially moving cantilever beam is presented. Velocity feedback controllers to introduce damping using one output, two outputs and three outputs are considered. The computer simulation indicates that the feedback system is always stable for a lower mode, and not necessarily for higher modes. This is referred to as spillover instability.
- Since one output feedback system with constant gain gives unstable system due to the spillover instability. To overcome the spillover instability problem, three control strategies are proposed. 1. Gain scheduling with two outputs. An on-off gain scheduling is designed

for each of the outputs such that the damping ratios of the “frozen” system are kept positive for all the beam lengths. 2. Varying gains with two outputs. The variable gains can be found using a pseudo-inverse algorithm. 3. Varying gains with three outputs. With three outputs, the variable gains can be determined using a matrix inverse method.

- Another controller design using the Gradient Algorithm is also presented. It is designed to stabilize the system when the open-loop system is neutrally stable or unstable due to parametric excitations, and to speed up the state convergence rate of the closed-loop system. A state feedback controller gain K is designed assuming that all states are available. Also an observer is designed when the only accessible output is the deflection response. Stability of the system is discussed using the maximum and minimum singular values of the transition matrix.

5.2 Future Work

- To determine a proper stability analysis for the control application.
- To apply and study the deflection and velocity feedback control together for the system.
- To apply the control strategies on the experimental setup built in [7]:

Figure 5.1 shows the axially moving cantilever beam and PZT actuator system. The system contains, an axially moving cantilever beam apparatus, a motor control and sensor conditioning circuitry board, and a computer equipped with a data acquisition board. The beam is driven by a gear head DC motor via a set of belt and pulley and a set of pinion and rack. The DC motor, manufactured by DUMORE Co., is 12 V permanent magnet DC motor. The motor gear ratio is 13:1 and rated to run 180 RPM at 1.5 amps with no load and 160 RPM at 6.2 to 7.2 amps with a load of 2.712 Nm. The transmission ratio of the pulley set is 5.25:1. A potentiometer is attached to the pinion shaft. The beam

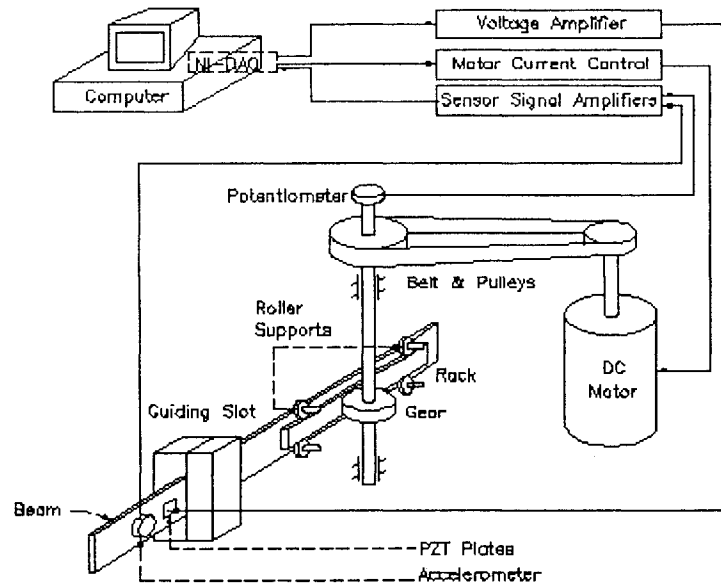


Figure 5.1: Schematic diagram of the axially moving cantilever beam and PZT actuator system

is made of 6061-T6 aluminum alloy. The cross-sectional dimension of the beam is 3.175 mm (thickness) \times 50.8 mm (width). The length of the beam vary from 0.665 m to 1.095 m. The guiding slot is made of Teflon. The clearance of the slot is properly chosen to have a close emulation of a fixed end. The lateral vibration is measured by accelerometer (B & K 4393V). A 4-channel charge amplifier (B & K Nexus2692) is used to condition accelerometer signal. Two axially polarized piezoelectric (PZT) ceramic plates (Sensor Tech) are bonded onto each side of the beam to form a PZT actuator. A high voltage wide band amplifier (Krohn-Nite) is used to drive the actuator. A personal computer is used for control application and data acquisition (DAQ) board, PCI-MIO-16E-4 (National Instruments) are used. LabVIEW is used to interface with the DAQ board.

Bibliography

- [1] B. Tabarrok, C . M. Leech and Y. I. Kim, "On the dynamics of an axially moving beam". *Journal of The Franklin Institutue*, 297(1974), pp. 201-220.
- [2] W. D. Zhu and L. J. Teppo, "Design and analysis of a scaled model of a high-rise, high-speed elevator". *Journal of Sound and Vibration*, 264(2003), pp. 707-731.
- [3] W. D. Zhu and J.Ni, "Energetics and stability of translating media with an arbitrarily varying length". *ASME Journal of Vibration and Acoustics*, 122(2000), pp. 295-304.
- [4] K. Liu, "Identification of linear time-varying systems". *Journal of Sound and Vibration*, 206(1997), pp. 487-505.
- [5] R. E. Bartels, "A numerical scheme for ordinary differential equations having time-varying and nonlinear coefficients based on the state transition matrix". Langley Research Center, Hampton, Virginia NASA/TM-2002-211776, 298(2002), pp. 2-89.
- [6] J. How and J. Deyst, "Virtual work and the derivation of Lagrange's equations". *Lecture Notes (<http://web.mit.edu/16.61/www/>)*, Massachusetts Institute of Technology 2003.
- [7] L. Deng, "Modeling and identification of an axially moving cantilever beam". Masters Thesis, Faculty of Control Engineering, Lakehead University Thunder Bay, Ontario. November 2002.

- [8] A. G. Ulsoy, "Vibration control in rotating or translating elastic systems". *ASME Journal of Dynamic Systems, Measurement, and Control*, 106(1984), pp. 6-14.
- [9] B. Yang and C. D. Mote Jr., "Active vibration control of the axially moving string in the S domain". *ASME Journal of Applied Mechanics*, 58(1991), pp. 189-196.
- [10] W. D. Zhu, C. D. Mote Jr. and B. Z. Guo, "Asymptotic distribution of eigenvalues of a constrained translating string". *ASME Journal of Applied Mechanics*, 64(1997), pp. 613-619.
- [11] W. D. Zhu, B. Z. Guo and C. D. Mote Jr., "Stabilization of a translating tensioned beam through a pointwise control force,". *ASME Journal of Dynamic Systems, Measurement, and Control*, 122(2000), pp. 322-331.
- [12] M. Chen and R. Fu, "An active control design for a class of parametrically excited systems based on the gradient algorithm". *ASME Journal of Vibration and Acoustics*, 120(1998), pp. 727-732.
- [13] W. J. Rugh: *Linear System Theory*. Prentice Hall, Englewood Cliffs, NJ, 1996.
- [14] K. S. Narendra and A. M. Annaswamy: *Stable adaptive systems*. Prentice Hall, Englewood Cliffs, N J, 1989.
- [15] M. S. de Queiroz, D. M. Dawson, C. D. Rahn and F. Zhang: *Adaptive vibration control of an axially moving string*. *ASME Journal of Vibration and Acoustics*, 121(1999), pp. 41-49.
- [16] E. M. Mockensturm, N. C. Perkins and A. G. Ulsoy, "Stability and limit cycles of parametrically excited, axially moving strings". *ASME Journal of Vibration and Acoustics*, 118(1996), pp. 346-351.
- [17] W. D. Zhu, J. Ni and J. Huang, "Active control of translating media with arbitrarily varying length". *ASME Journal of Vibration and Acoustics*, 123(2001), pp. 347-358.

- [18] C. H. Chung and C. A. Tan, "Active vibration control of the axially moving string by wave cancellation". *ASME Journal of Vibration and Acoustics*, 117(1995), pp. 49-55.
- [19] H. Chih-Yu, L. Chien-Chang and G. Lothar "Vibration and sound radiation controls of beams using layered modal sensors and actuators". *Smart Materials and Structures*, 7(1998), pp. 446-455.
- [20] H. Boe, R. Asok and Y. Vigor, "Output feedback linear parameter varying (LPV) L_2 -gain control". *ASME Journal of Dynamic Systems, Measurement and Control*, 125(2003), pp. 485-489.
- [21] V. S. Deshmukh and S. C. Sinha, "Control of dynamic systems with time-periodic coefficients via the Lyapunov-floquet transformation and backstepping technique". *Journal of Vibration and Control*, 10(2004), pp. 1517-1533.
- [22] M. Utsumi, "A new digital algorithm for elimination of spillover". *ASME Journal of Dynamic Systems, Measurement and Control*, 122(2000), pp. 360-364.
- [23] M. S. de Queiroz, D. M. Dawson, C. D. Rahn and F. Zhang, "Adaptive vibration control of an axially moving string". *ASME Journal of Vibration and Acoustics*, 121(1999), pp. 41-49.
- [24] B. K. Elias and P. A. Ioannou, "A switching adaptive controller for feedback linearizable systems". *IEEE Transactions on Automatic Control*, 44(1999), pp. 742-750.
- [25] P. V. Zhivoglyadov, R. H. Middleton and M. Fu, "Localization based switching adaptive control for time-varying discrete-time systems". *IEEE Transactions on Automatic Control*, 45(2000), pp. 752-755.

- [26] Z. Youping, F. Baris and P. A. Ioannou, "Backstepping control of linear time-varying systems with known and unknown parameters". *IEEE Transactions on Automatic Control*, 48(2003), pp. 1908-1925.
- [27] P. Gurfil, "Quantitative L^P stability analysis of a class of linear time-varying feedback systems". *International Journal of Applied Mathematics and Computer Science*, 13(2003), pp. 179-184.
- [28] U. Stobener and L. Gaul, "Active vibration control of a car body based on experimentally evaluated modal parameters". *Mechanical Systems and Signal Processing*, 15(2001), pp. 173-188.
- [29] J. S. Burdess and J. N. Fawcett, "Experimental evaluation of a piezoelectric actuator for the control of vibration in a cantilever beam". *ASME Journal of Systems and Control Engineering*, 206(1992), pp. 99-106.
- [30] K. Liu, "Vibration control of an axially moving cantilever beam using piezoelectric actuators". *Proceedings of the 11th World Congress in Mechanism and Machine Science*, Tianjin, China, (2003), pp. 18-21.
- [31] H. Dunant and S. O. R. Moheimani, "Spatial resonant control of flexible structures - application to a piezoelectric laminate beam". *IEEE Transaction on Control Systems Technology*, 9(2001), pp. 37-53.
- [32] S. Hanagud, M. W. Obal and A. J. Calise, "Optimal vibration control by the use of piezoceramic sensors and actuators". *Journal of Guidance, Control and Dynamics*, 15(1992), pp. 1199-1206.
- [33] H. T. Banks, K. Ito and Y. Wang, "Computational methods for identification and feedback control in structures with piezoceramic actuators and sensors". *Journal of Intelligent Material Systems and Structures*, 4(1993), pp. 469-476.

- [34] L. Chien-Chang and H. Huang-Nan, "Vibration control of beam-plates with bonded piezoelectric sensors and actuators". *Computers and Structures*, 73(1999), pp. 239-248.
- [35] S. M. Yang and Y. C. Liu, "Frequency domain control of flexible beams with piezoelectric actuator". *ASME Journal of Dynamic Systems, Measurement and Control*, 117(1995), pp. 541-546.
- [36] J. D. Jeffrey, J. I. Daniel and G. Ephrahim, "A self-sensing piezoelectric actuator for collocated control". *Journal of Intelligent Material Systems and Structures*, 3(1992), pp. 166-185.
- [37] C. R. Fuller, S. J. Elliot and P. A. Nelson: *Active Control Of Vibration*. Academic Press, Harcourt Brace Company Publishers, London NW1 7DX, 1996.
- [38] D. J. Inman: *Engineering Vibration*. Prentice Hall, Upper Saddle River, NJ, 2001.
- [39] J. E. Slotine and W. Li: *Applied Nonlinear Control*. Prentice Hall, Englewood Cliffs, NJ, 1991.
- [40] H. K. Khalil: *Nonlinear Systems*. Second Edition, Prentice Hall, Englewood Cliffs, NJ, 1996.
- [41] S. Sastry and M. Bodson: *Adaptive Control, Stability, Convergence And Robustness*. Prentice Hall, Englewood Cliffs, NY, 1989.

Appendix A

Proofs of Theorems and Other Calculations

A.1 Proof of Theorem 1

Proof:

If the Lyapunov function is chosen as

$$V(t) = x^T(t)x(t) \tag{A.1}$$

where $V(t) \geq 0$ and the derivative of the function A.1, is given by

$$\begin{aligned} \dot{V}(t) &= x^T(t)\dot{x}(t) + \dot{x}^T(t)x(t) \\ &= x^T(t) [A(t) + A^T(t)] x(t) \end{aligned} \tag{A.2}$$

where $\dot{x}(t)$ is replaced by $A(t)x(t)$ from Equation (2.32). If $\dot{V}(t)$ is negative, that is, if the matrix $[A(t) + A^T(t)]$ is negative definite at each t , then $V(t)$ decreases as t increases. Therefore, $x(t)$ decays exponentially.

End of Proof

A.2 Uniform Exponential Stability

Proof:

For any t_0 , x_0 , and corresponding solution $x(t)$ of the state equation, the inequality (2.39) gives

$$x^T(t) \left[A^T(t)Q(t) + Q(t)A(t) + \dot{Q}(t) \right] x(t) \leq -\nu \|x(t)\|^2 \quad (\text{A.3})$$

where $x^T(t)x(t) = \|x(t)\|^2$. Also from (2.38)

$$x^T(t)Q(t)x(t) \leq \zeta \|x(t)\|^2 \quad (\text{A.4})$$

so that

$$-\|x(t)\|^2 \leq -\frac{1}{\zeta} x^T(t)Q(t)x(t) \quad (\text{A.5})$$

Therefore

$$x^T(t) \left[A^T(t)Q(t) + Q(t)A(t) + \dot{Q}(t) \right] x(t) \leq -\frac{\nu}{\zeta} x^T(t)Q(t)x(t) \quad (\text{A.6})$$

After multiplying by the appropriate exponential integrating factor and integrating from t_0 to t ,

$$x^T(t)Q(t)x(t) \leq \frac{1}{\eta} e^{-\frac{\nu}{\zeta}(t-t_0)} x_0^T Q(t_0) x_0(t) \quad (\text{A.7})$$

Again from (2.38),

$$\begin{aligned} \|x(t)\|^2 &\leq \frac{1}{\eta} x^T Q(t)x(t) \\ &\leq \frac{1}{\eta} e^{-\frac{\nu}{\zeta}(t-t_0)} x_0^T Q(t_0) x_0(t) \end{aligned} \quad (\text{A.8})$$

which gives

$$\|x(t)\|^2 \leq \frac{\zeta}{\eta} e^{-\frac{\nu}{\zeta}(t-t_0)} \|x_0\|^2 \quad (\text{A.9})$$

By taking positive square root of both sides of Equation (A.9), uniform exponential stability is achieved. *End of Proof*

A.3 Determining The Initial Conditions Through Deflection Curve

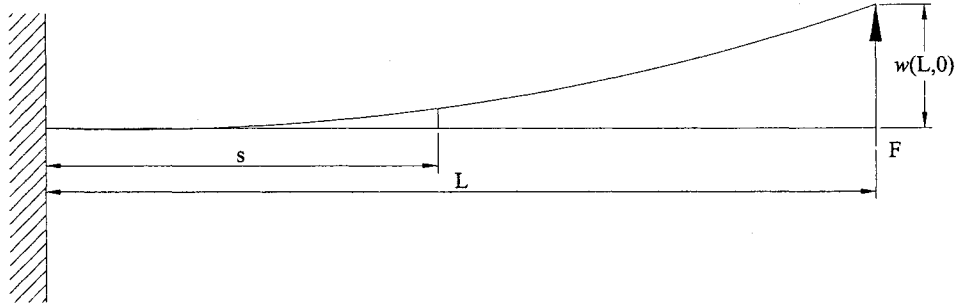


Figure A.1: Deflection Curve

Deflection at location s is given by,

$$\begin{aligned}
 w(s, 0) &= \frac{F}{6EI}(s^3 - 3Ls^2) \\
 &= \frac{F}{6EI}L^3\left[\left(\frac{s}{L}\right)^3 - 3\left(\frac{s}{L}\right)^2\right] \\
 &= \frac{FL^3}{6EI}(\alpha^3 - 3\alpha^2)
 \end{aligned} \tag{A.10}$$

where F is the applied tip force and $\alpha = \frac{s}{L}$. Deflection at location L is given by,

$$w(L, 0) = \frac{FL^3}{3EI} \tag{A.11}$$

from Equation (A.11),

$$F = 3EI \frac{w(L, 0)}{L^3}. \tag{A.12}$$

From the application of mode shapes in Equations (2.2-2.5), the deflection can be written as

$$w(s, t) = \Phi(s, L)q(t) = \frac{1}{\sqrt{L(t)}}\psi_j(\alpha)q(t). \tag{A.13}$$

By choosing a deflection of the tip to be $w(L, 0) = 0.01$ m at $t = 0$ sec, the initial conditions are achieved by

$$q_i(0) = \int_0^L \Phi_i(s, 0)ds. \tag{A.14}$$

A.4 Theorem: Stability of Slowly-Varying System

Proof:

The proof of theorem in section 3.4 (equations 3.27 to 3.29) is presented here.

For each t , let $Q(t)$ $n \times n$ matrix and

$$A^T(t)Q(t) + Q(t)A(t) = -I \quad (\text{A.15})$$

where $Q(t)$ is chosen to be

$$Q(t) = \int_0^\infty e^{A^T(t)\sigma} e^{A(t)\sigma} d\sigma \quad (\text{A.16})$$

If $Q(t)$ satisfies the Theorem, thereby can conclude uniform exponential stability of system (2.32). Detailed proof is given on [13] *Theorem* 8.7 and it shows, the choice of $Q(t)$ is bounded, symmetric and continuously differentiable.

It can be shown that there exists a $\nu \geq 0$ such that

$$A^T(t)Q(t) + Q(t)A(t) + \dot{Q}(t) \leq -\nu I \quad (\text{A.17})$$

using Equation (A.15)

$$\dot{Q}(t) \leq (1 - \nu)I \quad (\text{A.18})$$

and the differentiation of Equation (A.15) with respect to t gives

$$A^T(t)\dot{Q}(t) + \dot{Q}(t)A(t) = -\dot{A}^T(t)Q(t) - Q(t)\dot{A}(t) \quad (\text{A.19})$$

Also this Lyapunov equation has a unique solution

$$\dot{Q}(t) = \int_0^\infty e^{A^T(t)\sigma} \left[\dot{A}^T(t)Q(t) + Q(t)\dot{A}(t) \right] e^{A(t)\sigma} d\sigma \quad (\text{A.20})$$

Since the eigenvalues of $A(t)$ have negative real parts at each t . To derive the boundness of $\|\dot{Q}(t)\|$, the boundness of $\|Q(t)\|$ can be considered. For any $n \times 1$ vector x and any t ,

$$\left| x^T e^{A^T(t)\sigma} \left[\dot{A}^T(t)Q(t) + Q(t)\dot{A}(t) \right] e^{A(t)\sigma} x \right| \leq \left\| \dot{A}^T(t)Q(t) + Q(t)\dot{A}(t) \right\| x^T e^{A^T(t)\sigma} e^{A(t)\sigma} x \quad (\text{A.21})$$

so

$$\begin{aligned}
|x^T \dot{Q}(t)x| &= \left| \int_0^\infty x^T e^{A^T(t)\sigma} \left[\dot{A}^T(t)Q(t) + Q(t)\dot{A}(t) \right] e^{A(t)\sigma} x d\sigma \right| \\
&\leq \| \dot{A}^T(t)Q(t) + Q(t)\dot{A}(t) \| x^T Q(t)x \\
&\leq 2 \| \dot{A}(t) \| \| Q(t) \| x^T Q(t)x
\end{aligned} \tag{A.22}$$

Now for all x , it is true that $\| Q(t) \| \geq x^T Q(t)x$. This will maximize the right side of the equation and gives

$$|x^T \dot{Q}(t)x| \leq 2 \| \dot{A}(t) \| \| Q(t) \|^2 \tag{A.23}$$

similarly by maximizing the left side of the Equation (A.23) knowing that $\| \dot{Q}(t) \| \geq |x^T \dot{Q}(t)x|$, it can be written as

$$\| Q(t) \| \leq 2 \| \dot{A}(t) \| \| Q(t) \|^2 \tag{A.24}$$

Using the bound on $\| Q(t) \|$, the bound β on $\| \dot{A}(t) \|$ can be chosen. To show the lower bound for $Q(t)$, there exists a positive η such that $Q(t) \geq \eta I$ the *Theorem 7.8* in [13],

$$\begin{aligned}
\frac{d}{d\sigma} \left[x^T e^{A^T(t)\sigma} e^{A(t)\sigma} x \right] &= x^T e^{A^T(t)\sigma} \left[A^T(t) + A(t) \right] e^{A(t)\sigma} x \\
&\geq -2\kappa x^T e^{A^T(t)\sigma} e^{A(t)\sigma} x
\end{aligned} \tag{A.25}$$

Since $e^{A^T(t)\sigma}$ goes to zero exponentially as $\sigma \rightarrow \infty$

$$-x^T x = \int_0^\infty \frac{d}{d\sigma} \left[x^T e^{A^T(t)\sigma} e^{A(t)\sigma} x \right] d\sigma \geq -2\kappa x^T Q(t)x \tag{A.26}$$

Therefore,

$$Q(t) \geq \frac{1}{2\kappa} I \tag{A.27}$$

Which gives $\eta = \frac{1}{2\kappa}$.

End of Proof

A.5 First Order Runge-Kutta Method

The transition matrix is found by a discrete first order Runge-Kutta method [38]

$$x_{n+1} = x_n + \frac{\Delta t}{6}(k_{n1} + 2k_{n2} + 2k_{n3} + k_{n4}) \quad (\text{A.28})$$

where, $k_{n1} = f(x_n, t_n)$

$$k_{n2} = f(x_n + \frac{\Delta t}{2}k_{n1}, t_n + \frac{\Delta t}{2})$$

$$k_{n3} = f(x_n + \frac{\Delta t}{2}k_{n2}, t_n + \frac{\Delta t}{2})$$

$$k_{n4} = f(x_n + \Delta t k_{n3}, t_n + \Delta t)$$